

A MODULAR PEBBLE-BED ADVANCED HIGH TEMPERATURE REACTOR

NE-170 Senior Design Project
University of California, Berkeley

Plant and Mechanical Design Group

Ting Fei, Douglas Ogata, Kim Pham, Matthew Solom, Chris Zhao, Cheng Xu

Thermal, Fluid, and Chemical Design Group

Ann Cheng, Chloe Eastridge, Michael Foxe, Ben Reinhart, Jessica Mintz

Beryllium and Radiation Safety Group

Dominic Caron, Kayla Evans, Zack Kline, Darren Johnson, Anh Mai, Christopher Wootton

Structural and Seismic Design Group

Tammy Dhanania, Eric Keldrauk, Anh Mai, Eugene Park, José Rodriguez, Tea Visnjic

Instructors

Per F. Peterson and Bozidar Stojadinovic

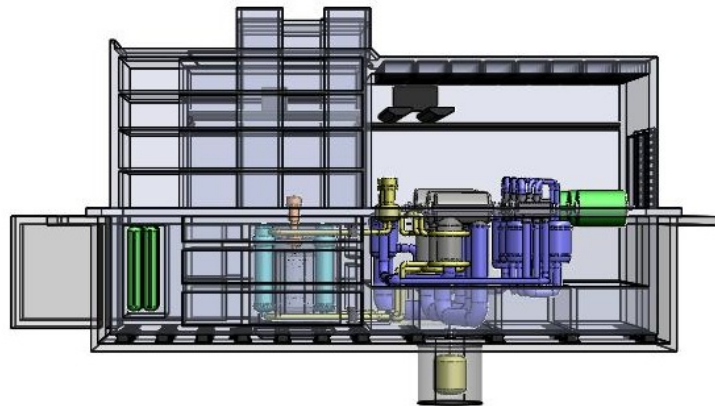
May 16, 2008

Report UCBTH-08-001

Abstract

The Modular Pebble Bed Advanced High Temperature Reactor (PB-AHTR) is a liquid-salt cooled reactor with a nominal thermal power output of 900 MW_{th} and electrical output of 410 MW_e. This report presents the results of a UC Berkeley NE-170 senior design class project to develop a comprehensive plant design for the PB-AHTR, including identifying functional and interface requirements for all of the major reactor and balance of plant systems, developing a physical arrangement for these systems, developing the approach to radiation and chemical safety, identifying functional requirements for the coolant and cover gas chemistry control systems, and developing the major elements of the structural design of a seismically base isolated reactor building, including the analysis and design for aircraft impact. The class worked as a miniature architect-engineering firm,

with students working in one of four different design groups: Plant and Mechanical Design; Thermal, Fluids and Chemistry; Beryllium and Radiation Safety, and Structural and Seismic Design. Chapters 2 to 5 of this report provide the results from the work performed by each of these design groups.



The NE 170 Modular PB-AHTR Final Design

DEDICATION



Christopher Wootton

We dedicate our senior design project to Christopher Wootton, our classmate who died at the very end of the semester, on the morning of Saturday, May 3, 2008. Chris was a member of the Beryllium and Radiation Safety Design Group, and contributed to developing the HVAC zoning design for the plant, described in Section 4.3. We will all miss him.



The NE 170 senior design class, including Christopher Wootton (second from left) watch during demonstration of the CEE Davis Hall shake table facility.

TABLE OF CONTENTS

ABSTRACT	1
DEDICATION.....	2
1. INTRODUCTION TO THE PB-AHTR.....	5
1.1 REFERENCES.....	10
2.0 PB-AHTR PLANT AND MECHANICAL DESIGN.....	12
2.1 POWER CONVERSION.....	14
2.1.1 <i>Physical arrangement</i>	17
2.1.2 <i>Thermal Stress Analysis For Turbine Cross-Over Pipes</i>	19
2.2 PRIMARY LOOP, INTERMEDIATE LOOP, AND SPENT FUEL CANISTERS	22
2.2.1 <i>Reactor Vessel</i>	23
2.2.2 <i>Primary Salt Pumps</i>	24
2.2.3 <i>Intermediate Heat Exchangers</i>	26
2.2.4 <i>Intermediate Loop</i>	27
2.2.5 <i>Spent Fuel Canisters</i>	28
2.3 REACTOR BUILDING AND TURBINE HALL	29
2.4 INTEGRATED DESIGN	34
2.5 REFERENCES	40
3. PB-AHTR FUEL AND CHEMISTRY CONTROL SYSTEMS.....	41
3.1 FUEL HANDLING AND STORAGE SYSTEM.....	41
3.1.1 <i>Sphere unloading and injection</i>	41
3.1.2 <i>Sphere monitoring and characterization</i>	43
3.1.3 <i>Sphere Transfer System</i>	44
3.1.4 <i>Sphere Storage</i>	45
3.1.5 <i>Sphere Replenishment System (SRS) – Fresh Fuel</i>	46
3.2 SALT CHEMISTRY CONTROL SYSTEM	47
3.2.1 <i>Salts and Properties</i>	47
3.2.2 <i>Important Controls</i>	48
3.2.3 <i>Salt Flow in the Primary System</i>	50
3.3 COVER GAS SYSTEM.....	50
3.3.1 <i>Physical Capabilities of the Cover Gas System</i>	50
3.3.2 <i>Argon Leakage and Air Contamination</i>	51
3.2.3 <i>Tritium Recovery</i>	51
3.4 REFERENCES	51
4. PB-AHTR BERYLLIUM AND RADIATION SAFETY	52
4.1 BERYLLIUM AND RADIATION SAFETY APPROACH	52
4.1.1 <i>Medical Surveillance</i>	52
4.1.2 <i>Radiotracer for Beryllium Detection</i>	53
4.1.4 <i>Mixed Waste Management and Disposal</i>	58
4.2 RADIATION SHIELDING AND DECAY HEAT GENERATION	65
4.2.1 <i>Scope and Criteria for Radiation Shielding</i>	65
4.2.2 <i>Depletion Analysis and Determination of the Source Term</i>	65
4.2.3 <i>Fuel Handling Room Shielding</i>	66
4.2.4 <i>Spent Fuel Storage Cell Shielding</i>	68
4.2.5 <i>Thermal Decay Heat Generation Rate</i>	69
4.3 HVAC AND ACCESS CONTROL.....	71
4.3.1 <i>Introduction and Purpose of Zoning</i>	71
4.3.2 <i>Definitions of the PB-AHTR Zones</i>	71
4.4 REFERENCES	74

5. PB-AHTR STRUCTURAL AND SEISMIC DESIGN	76
5.1 INTRODUCTION - SUMMARY OF DESIGN AND INTERFACE REQUIREMENTS.....	76
5.2 STRUCTURAL DESIGN.....	79
5.2.1 <i>Definition of Loading</i>	79
5.2.2 <i>Design of the Base Isolation System</i>	82
5.2.3 <i>Structural Design of Load Bearing Members</i>	83
5.3 PEBBLE SEISMIC TEST (PST) EXPERIMENT.....	86
5.3.1 <i>Theory and Design</i>	86
5.3.2 <i>Description of experimental system:</i>	87

1. INTRODUCTION TO THE PB-AHTR

Advanced High Temperature Reactors (AHTR's) are Generation IV reactors that use high-temperature coated particle fuels, along with a liquid fluoride salt coolant, to achieve high-temperature operation at high power density and low pressure [1.1]. Because these reactors use a chemically inert, low-pressure coolant, they have no stored energy sources (high-pressure or chemically-reactive fluids) to pressurize their containment structures. This, combined with the very high volumetric heat capacity of liquid salts (400% greater than sodium and 25% greater than water), has led to significant interest in the use of salts as coolants for Generation IV reactors.

Work performed previously at UC Berkeley has developed designs for a multiple-reheat helium Brayton cycle for the PB-AHTR [1.2, 1.3], established optimal core inlet and outlet temperatures to allow use of existing ASME Section III materials [1.4], demonstrated the capability to achieve passive decay heat removal and safety [1.5], to design pebble-fueled AHTR's with negative coolant void reactivity and high discharge burn up [1.6], and to recirculate pebbles in liquid-salt cooled cores [1.7]. Based on these results, UC Berkeley's Thermal Hydraulics Research Group has recently proposed a design for a 410-MWe Modular Pebble Bed AHTR (PB-AHTR) reactor design, shown schematically in Fig. 1-1 [1.8].

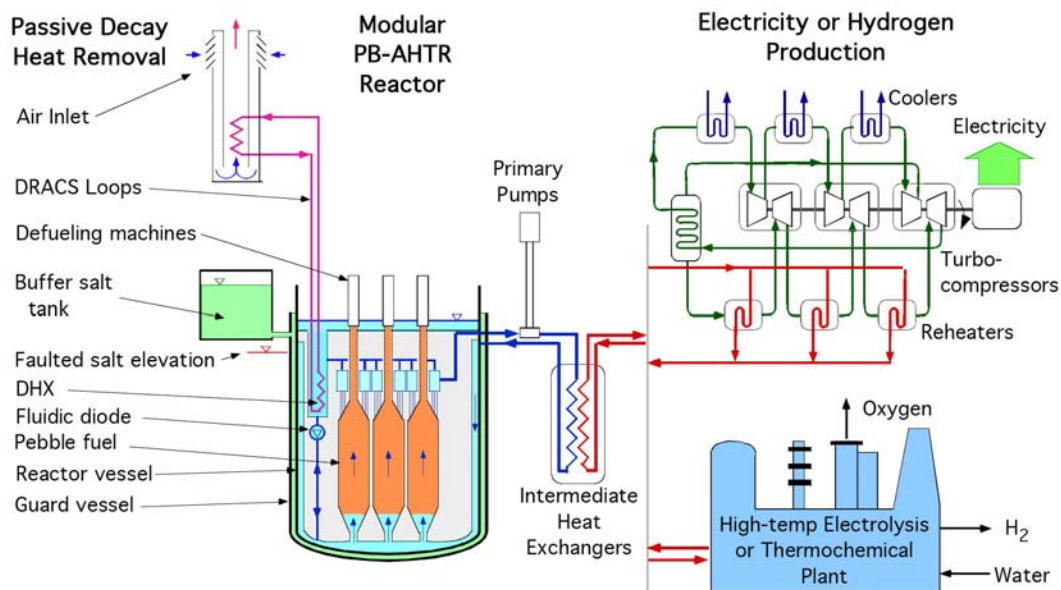


Fig. 1-1 Schematic of the PB-AHTR system.

Because the major reactor and power conversion system design parameters for the PB-AHTR had been defined by these earlier studies, the 22 students in the 2008 NE 170 senior design class decided to work together as a mock architect-engineering firm, to develop an integrated plant design for this Modular PB-AHTR. The senior design class had the following goals:

- Learn how architect-engineering firms design large facilities, including structural design and seismic base isolation
- Develop an understanding of the major design constraints that must be considered in the design of nuclear systems, and make design decisions
- Develop an understanding of how worker health and safety is protected by developing new approaches for managing beryllium safety
- Develop an understanding of how experiments are designed and how they can inform the design process
- Use the skills and tools developed through coursework at UC Berkeley

The class divided itself into four disciplinary design groups, taking advantage of the fact that several of the students have joint majors with either Mechanical or Chemical Engineering, and that some have expertise in Bionuclear Engineering. These design groups and their design deliverables were:

- Plant and Mechanical Design: Plant arrangement drawings for power conversion system and building, primary and intermediate loops, DRACS, spent fuel storage canisters, pebble transfer (rooms), chemistry control (rooms), HVAC and access control (rooms)); stress analysis for power conversion system piping.
- Thermal, Fluid and Chemical Design: Pebble transfer system and fuel storage system design (identifying where rooms go and how large); salt and cover gas chemistry control (rooms).
- Beryllium and Radiation Safety: Beryllium safety requirements and approach, including potential use of radiotracers, efficient coupling with the radiation safety program; define HVAC zones and air handling methods/requirements.
- Structural and Seismic Design: Base isolation system, aircraft impact analysis and feedback to the building design; pebble bed shake testing.

Because the design project involved seismic and structural design of the reactor building, the class was co-taught by Prof. Bozidar Stojadinovic from the Civil and Environmental Engineering Department, and the class included two students from CEE. To further develop their knowledge and background, the class went on field trips to see the seismic base isolation system for the Hearst Mining Building on the UC Berkeley campus (Fig. 1-2), the seismic shake table facility in Davis Hall, and the hot cells and reactor at General Electric's Vallecitos Research Center near Pleasanton, California.

Compared to typical senior design class projects, this project provided the NE 170 students with a unique opportunity to work as a part of a large, interdisciplinary team, in an environment comparable to that encountered in industry, and to work on a realistic design problem. The class faced the challenge of developing an integrated modular reactor structural design that uses seismic base isolation and that could accommodate modern requirements to resist damage from the crash of a large commercial airliner. They also faced the challenges of understanding how the range of different systems needed for a reactor must be integrated together, including how the heating, ventilation and air conditioning (HVAC) system must be designed to control the potential transport of hazardous radioactive and chemical materials. Here the class' field trip to the GE

Vallecitos facility, and design information provided by David Turner at GE Vallecitos for the HVAC system for their hot cells, proved invaluable.

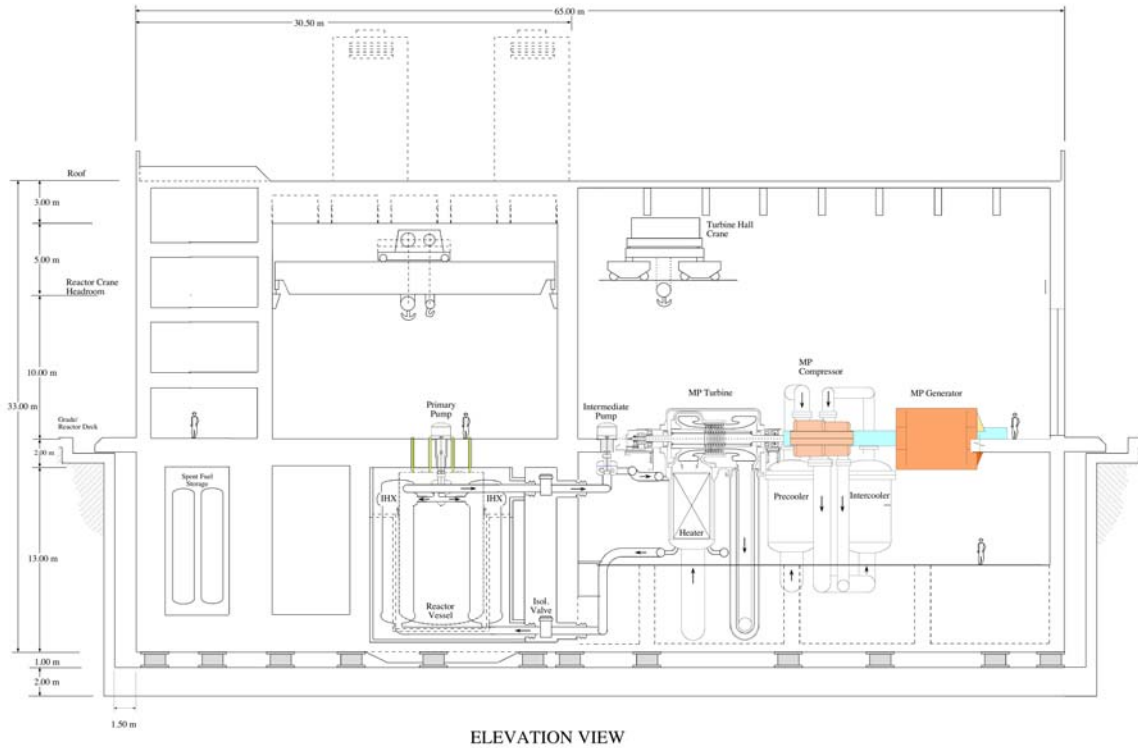


Fig. 1-2 NE 170 senior design class on a field trip to see the seismic base isolation system under the Hearst Mining Building at UC Berkeley.

The class developed a set of two simplified plan and elevation views of the PB-AHTR physical arrangement, shown in Figs. 1-3 and 1-4, as the basis for creating a 3-D model for the plant. In developing the physical arrangement for the building structures, the class received extensive advice from Professors Stojadinovic and Peterson on potential design approaches. The students also received information on the required dimensions for all of the major components in the system, including the reactor (Prof. Per Peterson), the intermediate heat exchangers (Dr. Hyun-jin Lim), and the power conversion system (Dr. Haihau Zhao). Graduate student Max Fratoni made his MCNP neutronics models available, and provided advice on how to perform shielding and decay heat generation analysis.

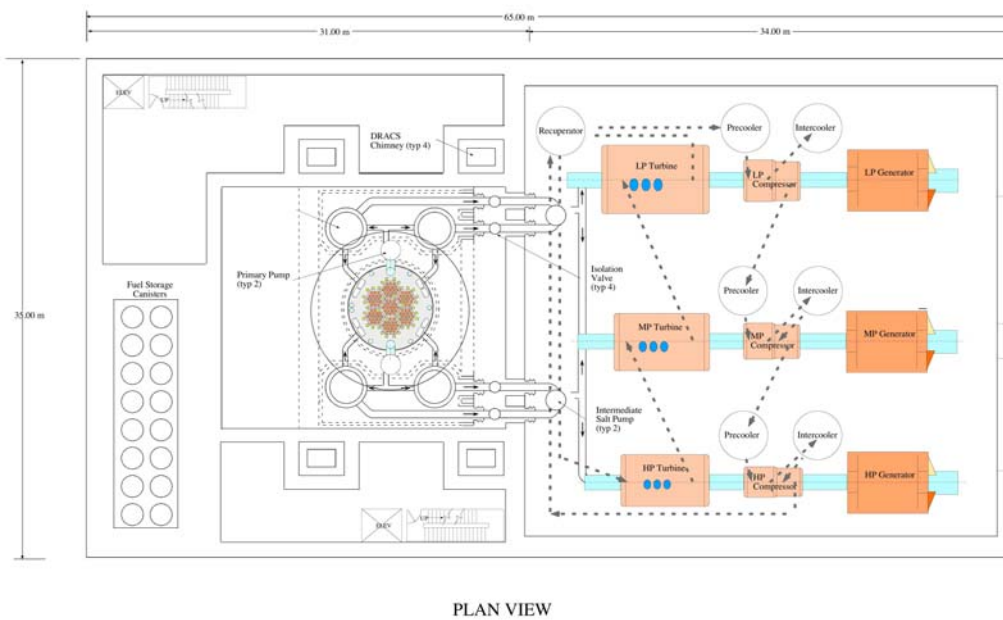
The class used the design of the Pebble Bed Modular Reactor (PBMR) (Fig. 1-5) as a starting point for much of the design work. In particular, the PB-AHTR power conversion system and pebble transfer and storage systems share many features with the PBMR. Likewise, the design of the reactor building for the PB-AHTR was modeled closely from the General Electric ESBWR, where the internal containment structures (or “reactor citadel”) is protected by an external events shell that also provides useful space for housing non-essential systems and components. This was judged to be a highly efficient way to minimize the total building mass and cost, compared to constructing a completely separate external events shell around the building (as with the EPR and AP-

1000), or building the reactor in a below-grade cavity with seismically qualified retaining walls.



ELEVATION VIEW

Fig. 1-3 Elevation view of a preliminary design for the Modular PB-AHTR reactor building.



PLAN VIEW

Fig. 1-4 Plan view of a preliminary design for the Modular PB-AHTR reactor building.

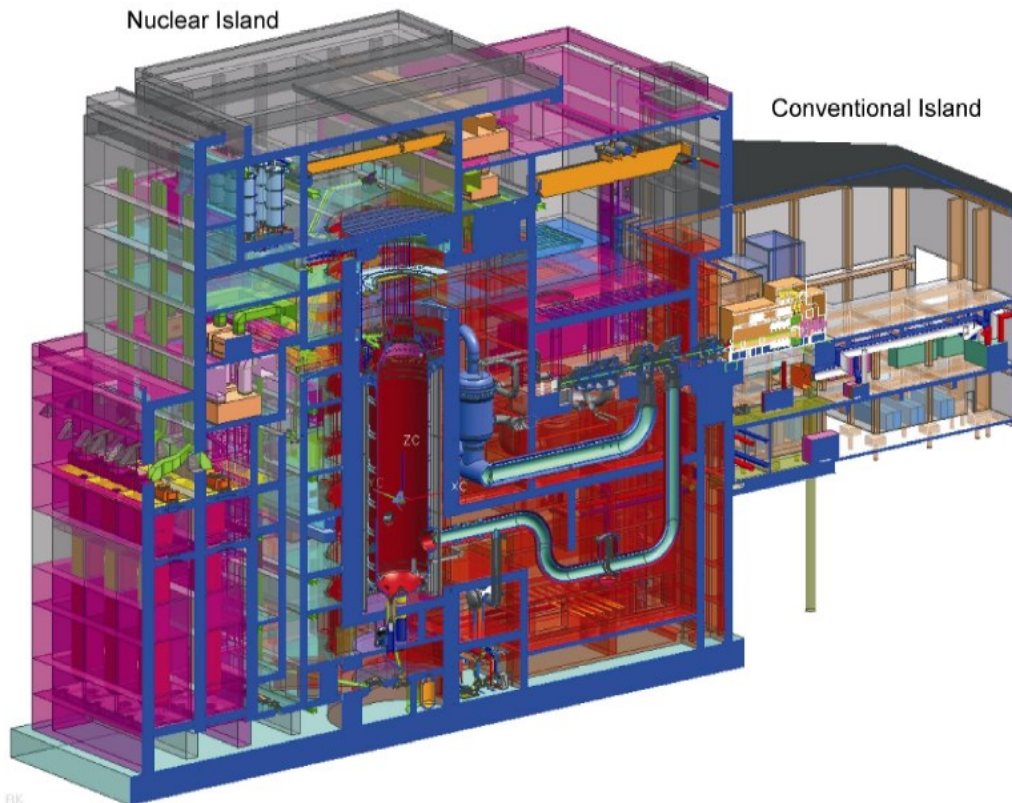


Fig. 1-5 View of the PBMR nuclear and conventional islands. The nuclear island is 63-m high, 37-m wide, and 63-m high with 41 m above the ground. The conventional island holding the generator and electrical equipment is 25-m high, 35-m wide and 37 m long.

The final 410 MWe PB-AHTR design created by the NE 170 class has very attractive features. As shown in Tables 1-1 and 1-2, the total reactor building volume, and the total concrete volume, compare favorably with competing light water reactor and modular helium reactor designs. Likewise, because the 36-m high PB-AHTR reactor building is half the height of these competing reactor designs, construction time is expected to be reduced substantially. Both of these design results suggest that the Modular PB-AHTR may have attractive economics.

The detailed results from the work of each of the student design groups are summarized in the four following chapters. Chapter 2 summarizes the work of the Plant and Mechanical Design Group, Chapter 3 the Thermal, Fluids and Chemistry Group; Chapter 4 the Beryllium and Radiation Safety Group, and Chapter 5 the Structural and Seismic Design Group.

Table 1-1 Comparison of the building volumes of several reactors with the 900 MWt, 410 MWe modular PB-AHTR shown in Figs. 1 and 2 [1.9].

Reactor Type	Reactor Power (MWe)	Reactor & Auxiliaries Volume (m ³ /MWe)	Turbine Building Volume (m ³ /MWe)	Ancillary Structures Volume (m ³ /MWe)	Total Building Volume (m ³ /MWe)
1970's PWR	1000	129	161	46	336
ABWR	1380	211	252	23	486
ESBWR	1550 [†]	132 [†]	166	45	343
EPR	1600	228	107	87	422
GT-MHR	286	388	0	24	412
PBMR	170	1015	0	270	1285
Modular PB-AHTR	410	98	104	40	242

[†] The ESBWR power and reactor building volume are updated values based on the Design Certification application arrangement drawings.

Table 1-2 Comparison of the concrete volumes of several reactors with the 900 MWt, 410 MWe modular PB-AHTR shown in Figs. 1 and 2 [1.9].

Reactor Type	Reactor Power (MWe)	Reactor & Auxiliaries Volume (m ³ /MWe)	Turbine Building Volume (m ³ /MWe)	Ancillary Structures Volume (m ³ /MWe)	Total Building Volume (1000 m ³ /MWe)
1970's PWR	1000	36.7	27.7	10.5	74.9
ABWR	1380	73.9	45.3	22.4	141.7
EPR	1600	62.5	17.8	47.5	127.8
GT-MHR	286	62.9	0	13.3	76.2
Modular PB-AHTR					
Base isolated	-	34.4	17.7	0	
Foundation	-	14.4	7.5		
Total	410	48.8	25.2	15.0	89.0

1.1 References

- 1.1 C.W. Forsberg, P. Pickard, and P.F. Peterson, "Molten-Salt-Cooled Advanced High-Temperature Reactor for Production of Hydrogen and Electricity," *Nuclear Technology* Vol. 144, pp. 289-302 (2003).
- 1.2 P.F. Peterson, "Multiple-Reheat Brayton Cycles for Nuclear Power Conversion With Molten Coolants," *Nuclear Technology*, Vol. 144, pp. 279-288 (2003).

- 1.3 P.F. Peterson and H.Zhao, “Low-Temperature Multiple-Reheat Closed Gas Power Cycles for the AHTR and LSFR,” 2006 International Congress on Advances in Nuclear Power Plants (ICAPP '06), Reno, NV, June 4-8, 2006.
- 1.4 P.F. Peterson and H. Zhao, “A Flexible Baseline Design For the Advanced High Temperature Reactor Utilizing Metallic Reactor Internals (AHTR-MI),” 2006 International Congress on Advances in Nuclear Power Plants (ICAPP '06), Reno, NV, June 4-8, 2006.
- 1.5 A. Griveau, F. Fardin, H. Zhao, and P.F. Peterson, “Transient Thermal Response of the PB-AHTR to Loss of Forced Cooling,” proceedings of Global 2007, Boise, Idaho, September 9-13, 2007, pp. 872-884.
- 1.6 M. Fratoni, F. Koenig, E. Greenspan, and P.F. Peterson, “Neutronic and Depletion Analysis of the PB-AHTR,” proceedings of Global 2007, Boise, Idaho, September 9-13, 2007, pp. 856-865.
- 1.7 P. Bardet, J.Y. An, J.T. Franklin, D. Huang, K. Lee, M. Toulouse and P.F. Peterson, “The Pebble Recirculation Experiment (PREX) for the AHTR,” proceedings of Global 2007, Boise, Idaho, September 9-13, 2007, pp. 845-851.
- 1.8 Philippe Bardet, Edward Blandford, Massimiliano Fratoni, Aurelie Niquille, Ehud Greenspan, and Per F. Peterson, “Design, Analysis and Development of the Modular PB-AHTR,” 2008 International Congress on Advances in Nuclear Power Plants (ICAPP '08), Anaheim, CA, June 8-12, 2008.
- 1.9 P.F. Peterson, H. Zhao, and R. Petroski, “Metal And Concrete Inputs For Several Nuclear Power Plants,” Report UCBTH-05-001, UC Berkeley, February 4, 2005.

2.0 PB-AHTR PLANT AND MECHANICAL DESIGN

The PB-AHTR is a Gen IV nuclear reactor that holds the promise of being the most compact high temperature reactor design today. The Plant and Mechanical Design Group had the responsibility to develop the equipment and building arrangement for the PB-AHTR, in collaboration with the three other NE 170 design groups. The design strategy of the PB-AHTR building was to minimize the concrete volume needed for construction while still satisfying the requirements for shielding, safety, maintenance space and storage space. The Plant and Mechanical Design Group constructed a 3D model of the power plant with the aid of Solidworks CAD software and iterated to identify an optimal physical arrangement for each major component into the building. Figure 2-1 shows the final plant design developed by the group.

Radiation shielding is always the first concern when designing a nuclear power plant. The Plant and Mechanical Design Group consulted with the Beryllium and Radiation Safety Group to determine the minimum wall thickness required for the reactor cavity, pebble transfer and spent fuel storage cells (Section 4.2), in order to help minimize the total building mass. Also, a detailed ventilation zoning plan was developed with the Beryllium and Radiation Safety Group that controls the potential transport of beryllium and radioactive contamination using five separate zones in order to ensure safe operation within the power plant (Section 4.3).

Another key safety concern regards the structural integrity of the building as a whole. The design of the PB-AHTR is one where the entire building is supported upon base isolators for protection against earthquakes. The Structural and Seismic Design Group provided a detailed design for the base isolators and the maximum building weight they can support (Section 5). Special honeycomb structures on the ceiling and floors were also designed in order to reduce the building weight without compromising structural integrity, and to facilitate construction of the building from factory pre-fabricated modules. The building design also locates the reactor primary loop and the Direct Reactor Auxiliary Cooling System in a central reactor “citadel”, which is protected by an external events shield structure consisting of equipment corridors around three quadrants of the building and the turbine hall on the fourth quadrant. Approximately five iterations of consultation with the Structural and Seismic Design Group were performed, to arrive at the final base isolation design shown in Fig. 2-1.

Due to the compact geometry of the building, physical arrangements of the major components and their piping also became a challenge. A 3D model of the power conversion systems was created using component and pipe dimensions provided by Dr. Haihau Zhao at Idaho National Laboratory. This power conversion system design is derived from the PBMR power conversion system, which has been designed by Mitsubishi, and the design of the major components (turbines, compressors, generators, recuperator) has been adapted for the PB-AHTR. By using these 3D models, we determined exactly where the power conversion system components should optimally sit inside the turbine hall and their corresponding piping arrangements (Fig. 2-2). The Plant and Mechanical Design Group also performed thermal stress analysis on the pipes connecting the three turbines to ensure that thermal stresses caused by warming from room temperature to operating temperature are within allowable stresses. One design

iteration consultation was made within the group to increase the vertical length of these pipes, was required to achieve a design with an acceptable stress level.

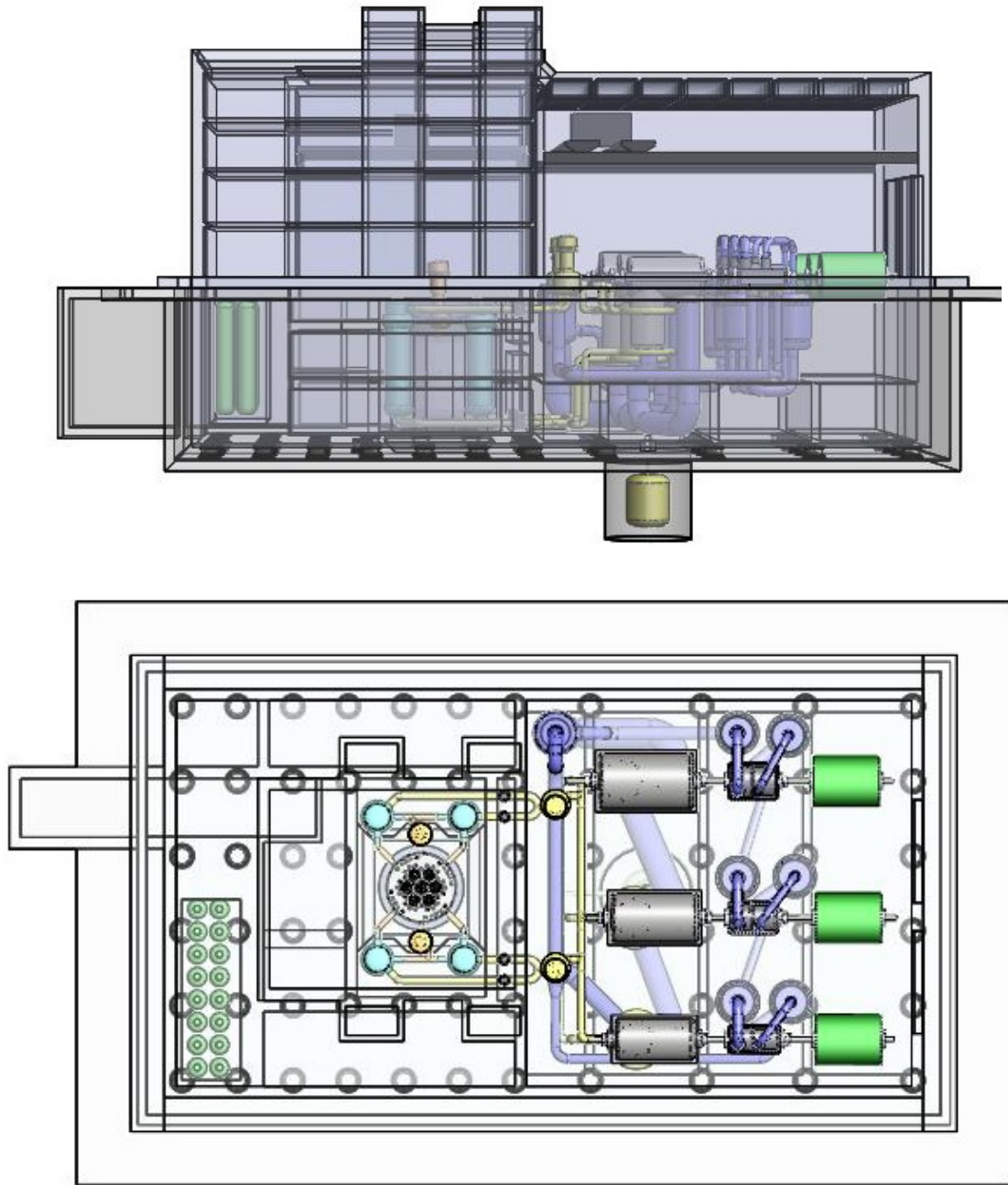


Fig. 2-1 PB-AHTR 3-D power plant model.

Lastly, we want to make sure that there is enough space left in the building for smaller equipment, such as the HVAC, pebble transfer, and salt chemistry control systems. We interfaced with the other design groups and arrived at an integrated design model that fits the criteria of each group satisfactorily. We have pinpointed the locations of all the major components and left enough room for minor components that would be

added during later detailed design of the PB-AHTR. The PB-AHTR reactor building is able to house every necessary component to provide a high power density while still remaining safe, light, and cost effective to compete in the nuclear renaissance of the Gen IV reactor designs.

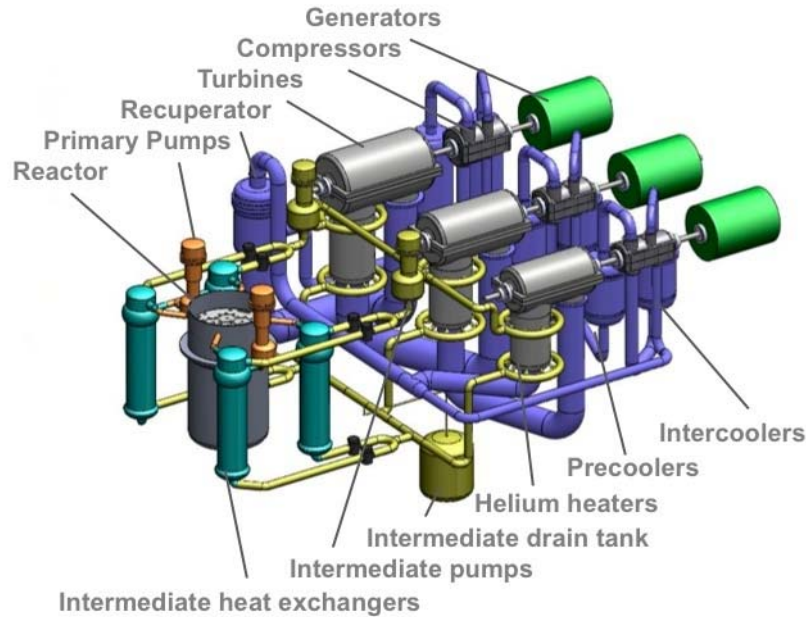


Fig. 2-2 The Modular PB-AHTR primary loop, intermediate loop, and power conversion system designs created by the Plant and Mechanical Design Group.

2.1 Power conversion

PB-AHTR uses a multiple-reheat Brayton cycle as shown in Fig. 1-1. The power conversion system (PCS) uses helium as the working fluid, while the primary and intermediate coolants of the system are liquid fluoride salts. The PCS consists three trains of power conversion units, which are very similar to the PCS design developed by Mitsubishi Heavy Industries for the Pebble Bed Modular Reactor (PBMR). As the result of using a closed gas Brayton cycle, the net power conversion is estimated to be 46%.

The power conversion components were modeled in SolidWorks, 3-D modeling software, based on component and pipe dimensions provided by Dr. Haihua Zhao at Idaho National Laboratory (INL) and summarized in Table 2-1. Though the design parameters and the plant schematics initially provided to the group were helpful in the creation of the 3D design of the power conversion system, many details were adjusted in order to realize the complete power conversion system. The group coordinated these design changes with Dr. Zhao to assure that the final equipment arrangement would still meet the functional requirements for the power conversion system.

Table 2-1 Turbo-machinery design parameters for the high, medium and low expansion stages of the 900-MWt PB-AHTR conversion system, with comparisons to the 400-MWt PBMR power conversion system (credit H. Zhao, INL).

	PBMR	PB-AHTR HP Stage	PB-AHTR MP Stage	PB-AHTR LP Stage
General Parameters				
Rotational Speed (rpm)	6000	3600	3600	3600
Helium mass flow (kg/s)	193	308.9		
Turbine				
Inlet/outlet temperature (°C)	900/503	675/495	675/495	675/495
Inlet/outlet pressure (MPa)	9.00/2.81	10/5.65	5.65/3.19	3.19/1.81
Inlet pipe OD/ID (m)	0.68/1.58	0.68/1.50	0.90/2.00	1.10/2.45
Outlet pipe OD/ID (m)	0.68/1.58	0.68/1.50	0.90/2.00	1.10/2.45
Specific speed (-)	0.88	0.66	0.67	0.80
Specific diameter (-)	2.74	3.21	3.11	2.86
Number of blade stages	14	10	7	6
Length of bladed region (m)	1.94	1.66	1.35	1.36
Diameter of bladed region (m)	1.48	1.77	2.07	2.43
Length of turbine case (m)	4.30	6.20	6.90	7.50
Diameter of turbine case (m)	4.62	3.62	4.15	4.78
LP and HP Compressors				
LP Inlet temperature (°C)	~26°C	30	30	30
LP Inlet pressure (MPa)	2.81	5.42	2.94	1.60
HP Inlet pressure (MPa)	5.03	7.37	4.00	2.17
HP Outlet pressure (MPa)	~9.00	10.	5.42	2.94
LP Inlet pipe OD/ID (m)	0.70/1.00	0.51/0.72	0.73/1.06	
LP Outlet pipe OD/ID (m)	0.80/1.10		0.84/1.15	
HP Inlet pipe OD/ID (m)	0.50/0.75		0.52/0.78	
HP Outlet pipe OD/ID (m)	0.58/0.82		0.61/0.86	
LP Spec. speed (-)	1.76	1.40	1.39	1.32
HP Spec. speed (-)	1.85	1.57	1.42	1.46
LP/HP spec. diameter (-)	1.99/2.20	2.45/2.42	2.33/2.38	2.25/2.23
LP Number of blade stages	17	12	8	5
HP Number of blade stages	19	17	10	7
LP Length of bladed region (m)	1.64	0.85	0.65	0.47
LP Dia. of bladed region (m)	1.00	1.27	1.47	1.70
HP Length of bladed region (m)	1.30	1.12	0.76	0.62
HP Dia. of bladed region (m)	0.90	1.18	1.37	1.58
LP/HP Length of compressor case (m)	4.69	1.96/2.15 ¹	1.94/1.96	1.96/2.00
LP/HP Dia. of compressor case (m)	3.16/2.60	2.19/2.03	2.53/2.35	2.92/2.72
Recuperator				
Vessel diameter (m)	4.60 ²	3.5		
Vessel height (m)	~9.0 ^b	6.0		
Precooler				
Vessel diameter (m)	2.85	3.4	3.4	3.4
Vessel height (m)	~7.5	5.0	5.0	7.0
Intercooler				
Vessel diameter (m)	2.85	3.4	3.4	3.4

¹ Each compressor has its own vessel.

² The PBMR has two recuperator vessels.

	PBMR	PB-AHTR HP Stage	PB-AHTR MP Stage	PB-AHTR LP Stage
Vessel height (m)	~7.5	5.0	5.0	5.0
Heater				
Vessel diameter (m)	N/A	3.0	3.2	3.4
Vessel height (m)	N/A	4.0	4.5	5.0
Salt inlet/outlet pipe diameter (m)	N/A			
Generator				
Length (m)	6.10	5.6 ³	5.6	5.6
Diameter (m)	4.64	4.3	4.3	4.3

Many features in the equipment and the physical arrangement for this 410-MWe PB-AHTR power conversion system are similar to the 168-MWe PBMR design, but the specific dimensions of the PB-AHTR equipment are different. For example, the three PB-AHTR turbines are each individually smaller than the single PBMR turbine since the pressure difference, the inlet temperature, and the temperature difference are all comparatively lower in the PB-AHTR turbines. There is one important difference between the two designs. In the PB-AHTR conversion system no gearbox is needed for the power train because the higher helium flow rate in the PB-AHTR design allows an optimal specific speed at 3600 rpm, compared to 6000 rpm for the PBMR power conversion system.

Table 2-1 presents most of the design parameters used by the group to develop the 3D model. The table also includes corresponding PBMR parameters for comparison to identify some of the advantages and disadvantages of PB-AHTR design. In addition, some of the design parameters were scaled from the already available PBMR design, which is satisfactory for developing some component models leading to our initial physical arrangement. Several iteration followed to obtain correct spacing between the power conversion trains for access by the turbine hall crane to remove large equipment (principally the turbine casing covers) out to a maintenance building that will be located next to the turbine hall, and to increase the vertical length of the pipes connecting the turbines to achieve acceptable thermal stress levels.

While the PB-AHTR PCS has more components than PBMR, the PB-AHTR has one less recuperator vessel than the PBMR, since multiple reheat stages reduce the required size of the recuperator heat exchangers. In addition, the secondary inlet and outlet of the PB-AHTR recuperator have only one piping connection, which includes inlet and outlet pipes in an annular arrangement. In other words, the PB-AHTR recuperator carries inlet and outlet flows using two concentric pipes. The cold secondary inlet is carried in the outer annulus, and the hot outlet is carried within the inner pipe. Figure 2-3 shows the SolidWorks model of a recuperator used in PB-AHTR design, and a side view of a PBMR recuperator⁴ with details and flows. Figure 2-3 does not show the exact 3D model for PBMR recuperator, but the two designs are very similar in the figure except the PB-

³ The generator power is assumed to scale with its volume.

⁴ The PBMR recuperator drawing is obtain from pg 64 of the PBMR NRC report revision 4. The figure is only used for system comparison.

AHTR has an annular connection on top instead of the two separate connections used for the PBMR recuperator.

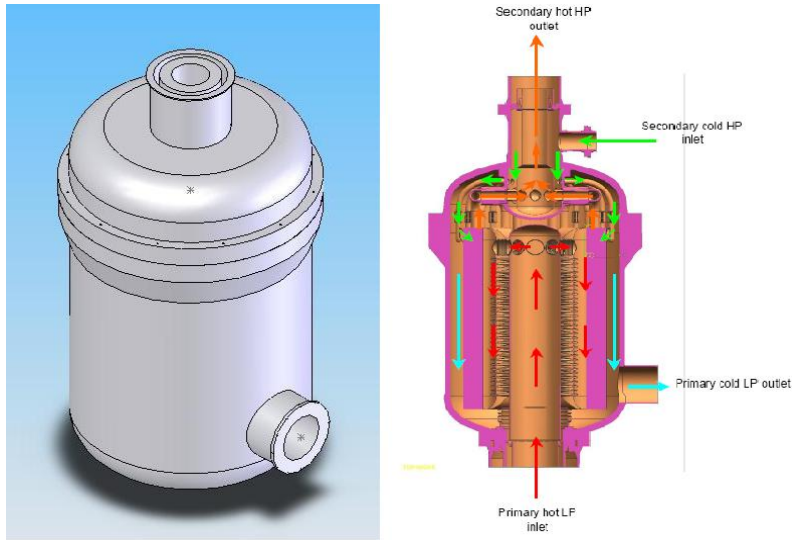


Fig. 2-3 (L) PB-AHTR recuperator model developed in SolidWorks with annular type of secondary pipe connection on top. (R) PBMR recuperator model with some internal details, pipe connections, and fluid flow directions.

Table 2-2 outlines the design assumptions used to determine the required thickness of the PB-AHTR turbine and compressor casings, relative to the values for the PBMR pressure boundary. The compressor casings followed the basic pressure dependent scaling based on thin wall shear stress approximation assuming that the dimensions of the

components are much greater than the desired thicknesses $\left(\sigma_{\theta\theta} = \frac{Pr}{t}\right)$ and $\left(\sigma_{zz} = \frac{Pr}{2t}\right)$. The expected yield strength for the compressor casing material is 139 MPa, which allows a safety factor of 3 or 4. However, the turbine, the intercooler, and precooler thicknesses were designed with constant pressure boundary thicknesses, which do not take into account the estimated yield strength of steel. With 10 MPa pressure at the inlet, and an assumed 5m diameter, the steel yield strength is expected to be 500 MPa.

2.1.1 Physical arrangement

Because there are three trains of power conversion system, the physical arrangement in the turbine hall is crucial for determining the overall size of the building, which houses both the reactor primary system and the power conversion system. Locating both the reactor and the PCS inside a single base isolated building provides the advantage that no high-temperature piping needs to pass across the seismic base isolation gap (Section 5.2). The physical arrangement of the PCS needs to be compact in order to minimize the building size, which in turn leads to reduced concrete volume and a lower building mass.

On the other hand, the PCS arrangement must provide adequate space for maintenance activities, which encourages having the three trains as far apart as possible, because to maintain or to repair any component in the power conversion system requires accessibility and space for assisting equipment and personnel. In addition, the

arrangement needs to accommodate all the pipes that connect different equipment, especially the large diameter pipes that go in and out of turbines. Fig. 2-4 provides an overview of primary and secondary system arrangement with all pipe connections, and it shows the upper floor of the turbine hall showing system locations and pipe connections.

Table 2-2 Design summary for the thickness of the PB-AHTR power conversion system pressure boundary

Power Conversion Trains*					
Total mass = 2748 metric tons					
Total volume = 437.02 m ³					
Components	Turbine	Compressor	Intercooler and Precooler	Recuperator	Generator
High Pressure (HP)	5 cm	9 cm	4 cm	5 cm	3.3 m
Medium Pressure (MP)	5 cm	7 cm	4 cm		3.3 m
Low Pressure (LP)	5 cm	5 cm	4 cm		3.3 m
Assumed materials	SA508	SA508	SA508	SA508	Cast Carbon Steel

* pipes were not calculated in the total mass and volume

The optimal spacing between each power train was determined to be 6.7 meters between the low and medium pressure trains and 6.0 meters between medium and high pressure trains, to provide sufficient space so that the turbine hall crane can be used to move the turbine casing covers to one of the two exit doors for transfer to a maintenance building that will be located next to the turbine hall. Among all the power conversion components, the low-pressure turbine casing is the largest with a width of 4.78 meters. A spacing of 6.7 meters ensures the accessibility of maintenance work during normal plant operation in the future. In addition, for each power generation train, the separation distances between major components was selected to allow structural ribs for the turbine hall foundation to pass between the turbine and compressor pipes, and between the compressor pipes and the generator pedestals, to reinforce structural integrity of the building foundation and carry gravity loads down to the seismic base isolators. Hence, the turbine shaft length had to be increased by 1 m compared to the initial design to compensate for the extra length created by the turbines and to satisfy the building structural design criteria. In addition, the pre-cooler and intercooler elbows on the top of the compressors were shortened about 1 meter downward to eliminate potential interferences during turbine casing cover removal.

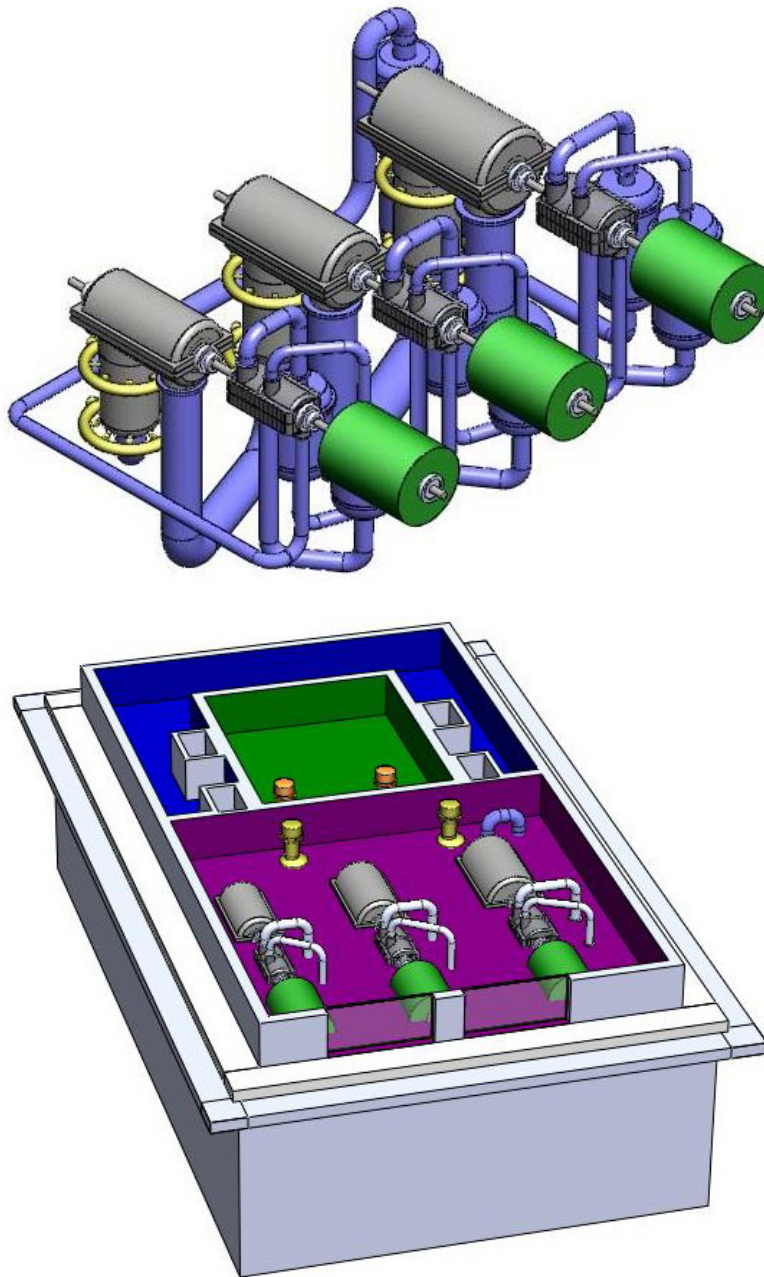


Fig. 2-4 (T) Secondary system arrangement and pipe connections. (B) Upper floor of turbine hall with system locations

2.1.2 Thermal Stress Analysis For Turbine Cross-Over Pipes

The piping between the turbines in the PB-AHTR consists of an outer pipe that acts as the pressure boundary and is cooled by a bypass flow from the compressor, and an insulated inner hot pipe that acts as a duct to transfer hot flow from the higher-pressure turbine outlet to the heaters for the next expansion stage. Thermal stress analysis was performed for the outer pipe that connects HP turbine to MP turbine, because this pipe

has the largest diameter of all of the cross-over pipes between the turbomachinery. The cross-over pipe has the shape shown in Fig. 2-5.

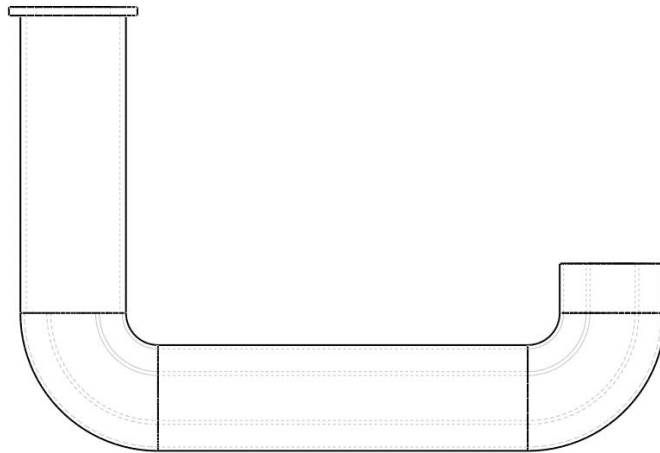


Fig. 2-5 Cross-over pipe geometry between the HP and MP turbines.

This cross-over pipe has three segments: two vertical and one horizontal. The pipe is installed at room temperature, so when it reaches operating temperature (the compressor outlet temperature of 100°C) thermal expansion will take place. The top of each vertical pipe is assumed to be rigidly constrained where it attaches to the bottom of the turbine casing. When thermal expansion takes place, the pipe expands downward freely because the bottom is unconstrained. A free expansion will not create thermal stress inside pipes. The horizontal portion is partially constrained, and it will expand horizontally due to temperature difference. When it expands, it will cause the two vertical pipes to bend. The two vertical pipes are displaced from their initial position. This means that the horizontal pipe exerts a shear force and moment on the vertical pipes, which will create stress inside the vertical pipe. The vertical pipe also exerts back a compressive force on the horizontal pipe, and causes it to bend. So the thermal expansion of the horizontal pipe creates thermal stress in all three parts.

To estimate the thermal stress inside the pipe, first a one-dimensional model was developed to simplify the problem and understand the effects of different design variables on the thermal stress. This simplified model also helps to understand which design parameters have the largest effect on stresses in the cross-over pipes. In this model, shown in Fig. 2-6, a shear stress F corresponds to a displacement V_{\max} , and it also creates a moment that tries to rotate the vertical pipe. To balance this moment, there must be moments inside the pipe. The maximum stress is related to the moment by:

$$\sigma_{\max} = \frac{Mc}{I} \quad (2.1)$$

where c is the distance between the center of the pipe to the outermost location of the beam (the pipe outside radius in this case), and I the moment of inertial of the pipe. The moment M is equal to force times distance, so the maximum moment is Fh , where h is

the height of the pipe, the maximum distance. The maximum stress is related to the shear force. The shear force is related to the maximum displacement.

$$V_{\max} = \frac{Fh^3}{3EI} \quad (2.2)$$

where E is the Young's Modulus of the pipe material.

$$V_{\max} = 0.5\alpha\Delta TL \quad (2.3)$$

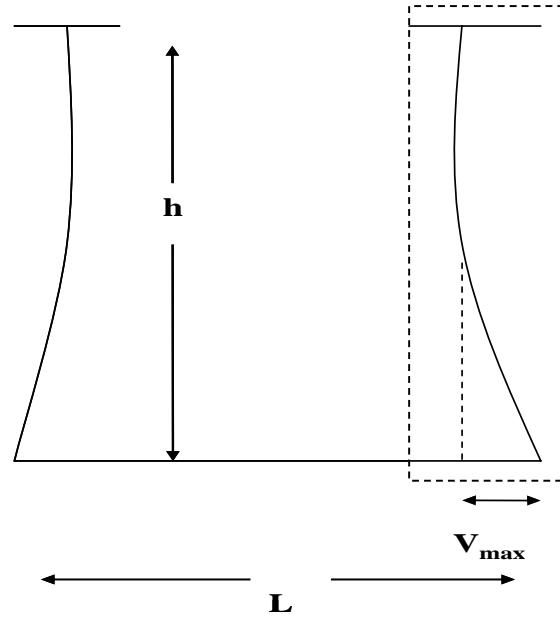


Fig. 2-6 Simplified model for thermal stress computation

where α is the thermal expansion coefficient. ΔT is the temperature difference between operational temperature of the pipe and the room temperature. L is the length of the horizontal pipe. Equating (2.2) and (2.3), F can be solved and σ_{\max} can be calculated from F .

$$F = \frac{1.5\alpha\Delta TL EI}{h^3} \quad (2.4)$$

$$\sigma_{\max} = \frac{Mc}{I} = \frac{Fhc}{I} = \frac{1.5\alpha\Delta TLEc}{h^2} \quad (2.5)$$

In this case, $\alpha = 1.7E-6/^{\circ}C$, $\Delta T = 800K$, $L = 12m$, $h = 9.5m$. c is taken to be the outer radius of the pipe which maximizes the stress, so c is 1.2m, and $E = 2 \times 10^{11}$ Pa. Plug in all these numbers into the equation (2.5), the predicted stress is 65 MPa. The allowable stress is 180 MPa, so the thermal stress is only about one third of the allowable stress.

There are several assumptions made in this estimation. First, the two vertical pipes are modified to have the same heights. If they have different heights h_1 and h_2 , then the displacements of these two pipes are no longer equal, and

$$V_1 = A_1 \alpha \Delta T L = \frac{F h_1^3}{3EI}$$

$$V_2 = A_2 \alpha \Delta T L = \frac{F h_2^3}{3EI}$$

$$\frac{A_1}{A_2} = \frac{h_1^3}{h_2^3} \quad (2.6)$$

The shear forces F on either side have to be equal to balance each other. A_1 and A_2 give the fractions of expansion to either direction. Thermal stress is proportional to A/h^2 , so the stress of the shorter pipe is proportional to $A_2/h_2^2 = A_1/h_1^2 * h_2/h_1$ and is always smaller than the stress of the longer pipe since h_2 is smaller than h_1 . A_1 takes a new value other than 0.5. Using $A_1 + A_2 = 1$, we get $A_1 = h_1^3 / (h_2^3 + h_1^3)$. h_2 is about half of h_1 , so A_1 is about 0.9. The new stress is about 117 MPa and is still smaller than the allowable stress.

Two vertical pipes also exert forces on the horizontal pipe. These forces tend to compress the pipe, so the displacement V_{\max} is smaller, but this contraction is much smaller than the thermal expansion, so it is neglected in this estimation.

Also, in this estimation, the bending of the horizontal pipe is ignored. Bending of the pipe will reduce the maximum displacement V_{\max} , so the thermal stress should also be reduced. This means that the calculation above is an over estimation of the stress.

To provide a more accurate prediction of the thermal stress, MATLAB was used to solve the beam equations exactly for the three pipe elements; the stress is smaller than the estimated stress. In the three plots shown in Fig. 2-7, pipe one is the long vertical pipe, pipe two the horizontal pipe, and pipe three the short vertical pipe. The blue line and the red line represent the maximum thermal stress at each end of the pipe. From the plot above, the maximum stress occurs at the bottom of the long vertical pipe. The maximum stress at this point is about 90MPa, which is very similar to the result of the previous estimation.

2.2 Primary Loop, Intermediate Loop, and Spent Fuel Canisters

The primary loop, shown in Fig. 2-8, consists of the reactor vessel, primary salt pumps, intermediate heat exchangers, intermediate loop isolation valves, and the associated piping. Also described here are the spent fuel canisters. The primary loop takes the heat generated by fission in the reactor and transfers it through a liquid flibe-based salt to the intermediate salt in the intermediate heat exchangers. These components are described below.

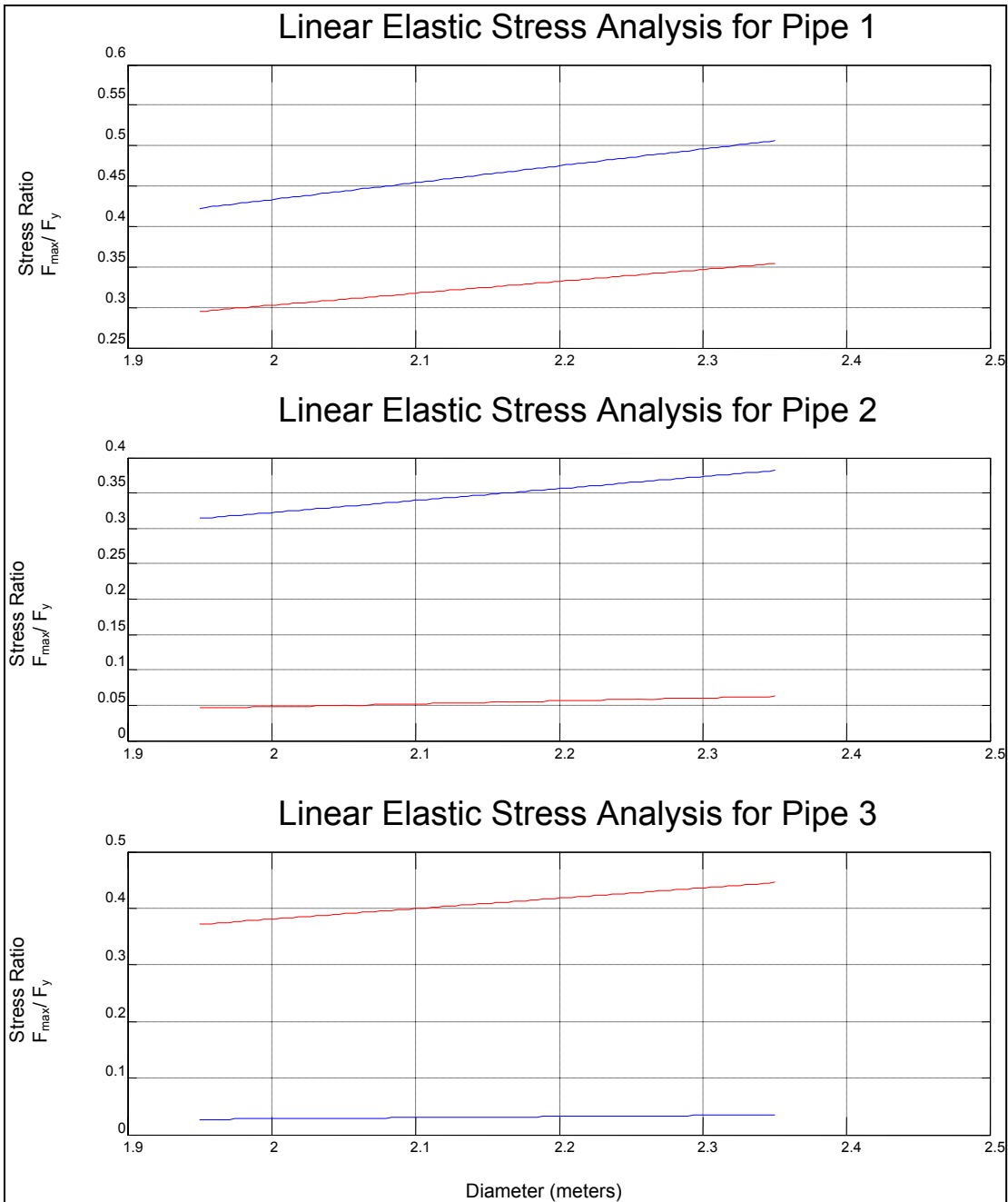


Fig. 2-7 Thermal stress analysis from matlab simulation

2.2.1 Reactor Vessel

The reactor vessel (Fig. 2-9) has an outer diameter of 6.0 m and a height of 10.6 m. The detailed model of the reactor vessel was developed previously in SolidWorks by Manolis Dimotakis in UC Berkeley Thermal Hydraulics Laboratory, shown in Fig. 2-9. The reactor vessel fits concentrically into a reactor cavity that has a diameter of 7.0 m and 0.5 m of space below the vessel to accommodate thermal expansion. As with the Molten Salt Breeder Reactor (MSBR) design, the primary loop equipment is not

insulated, and instead the reactor and IHX cells have insulating liners. As discussed in Section 4.3 (HVAC and Access Control), the cell is inerted with nitrogen and has a heating system. The cell walls are also insulated with a cooling system under the insulation, similar to that used in the original MSBR design, in order to keep the concrete within acceptable temperature limits. The pebble defueling machines, pebble insertion machines, and control rod drives were not modeled in the current configuration because they do not affect the overall physical arrangement. Locations for these components were identified in collaboration with the Thermal, Fluids and Chemistry Group (Chapter 3).

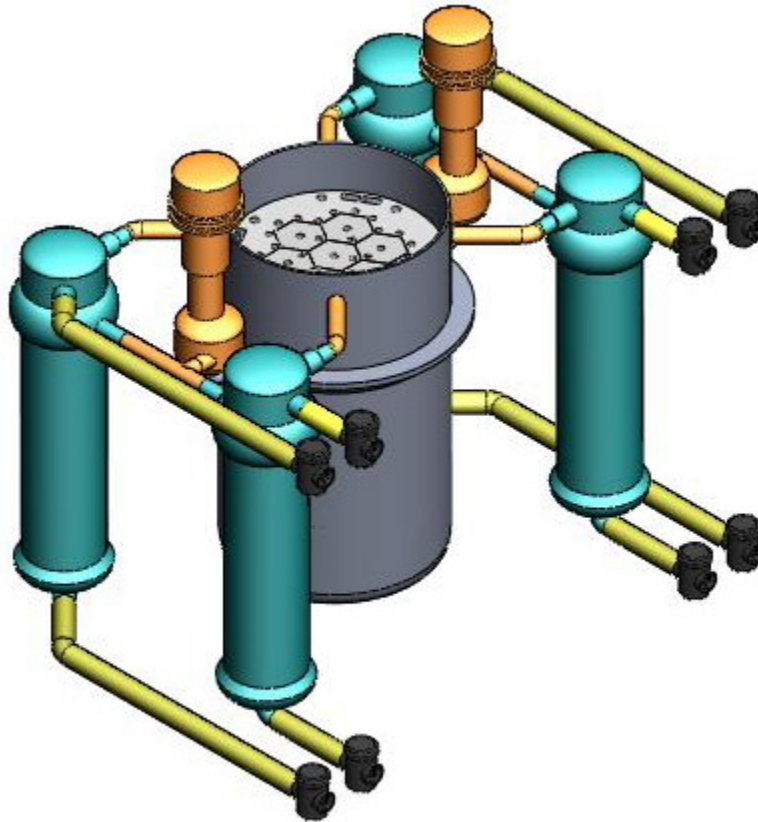


Fig. 2-8 PB-AHTR Primary Loop Model

2.2.2 Primary Salt Pumps

The primary salt pumps are derived from designs originally developed for the Molten Salt Breeder Reactor (MSBR) program in the 1970's. The motor sits on top, in a different compartment than the pump, separated by concrete shielding but connected by a coupling assembly approximately 3 m long. Salt enters the bottom through 0.40 m inner diameter piping and exits the side of a seal bowl near the bottom. The seal bowl allows the use of a cantilevered centrifugal pump and avoids the need for any salt-lubricated bearings. Each of the two primary salt pumps provides flow to two of the four intermediate heat exchangers (IHX's). Each of the pump casings was modeled in

SolidWorks as a hollow shell 2.5 cm thick, except for the motor. The motor was modeled as a solid block.

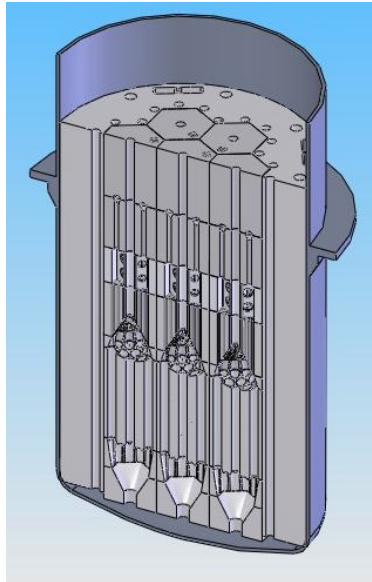


Fig. 2-9 PB-AHTR reactor vessel models detailed model previously developed

It should be noted that the primary salt pumps share their motor model with the intermediate salt pumps. The intermediate pump model, however, has a shorter coupling assembly and a larger seal bowl. This is due to the larger diameter intermediate piping and a lower separation requirement. Both the primary and intermediate pumps are shown for comparison in Fig. 2-10.

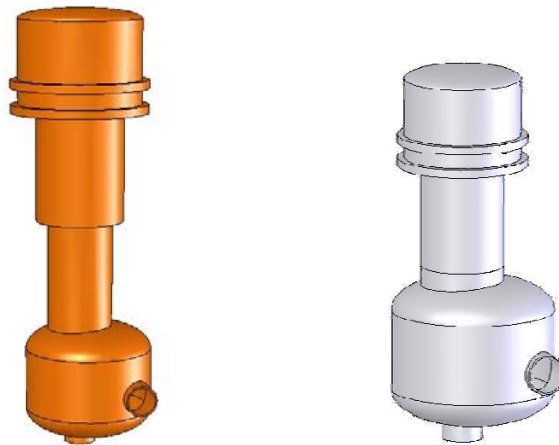


Fig. 2-10 PB-AHTR primary salt pump model (left) and intermediate salt pump model (right)

2.2.3 Intermediate Heat Exchangers

The Intermediate Heat Exchangers (IHX's) were modeled based upon a detailed design and dimensional information provided by Dr. Hyun-Jin Lim in the UC Berkeley Thermal Hydraulics Laboratory, as shown in Fig. 2-11. These heat exchangers are mounted in IHX cavities in the reactor cell, on bearings that permit the IHX's to move to accommodate thermal expansion of the primary salt piping. This allows the primary salt pipes to be designed to take short paths from the IHX to the reactor vessel and to the primary pumps. There are four of these vertically mounted cross-flow type heat exchangers, with a single primary salt pump and a single intermediate salt pump servicing groups of two IHX's. The hot primary salt enters through the side near the top in a 0.40-m inner diameter pipe and flows down in tubes with an average length of 8.54 m, returning to the top and exiting the side at a height above the entrance. Cold intermediate salt enters the bottom of the IHX in a 0.55-m inner diameter pipe and is directed to flow on the shell side through a disk and donut baffle system to the top of the IHX and exits the side at the same height as the primary outlet. The vertical configuration allows the tube bundle to be pulled upward by the reactor hall crane into a transfer cask, allowing replacement with a new tube bundle if required.

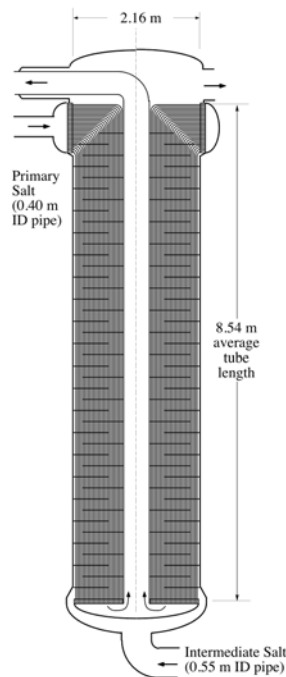


Fig. 2-11 IHX Design by Dr. Hyun-Jin Lim

Each IHX was modeled as a hollow shell 2.5 cm thick. The total height of each IHX as modeled is 10.65 m, excluding the intermediate inlet pipe on the bottom. The inlet pipe has a sharp elbow immediately below the bottom of the IHX vessel as a space saving feature, as shown in Fig. 2-12.

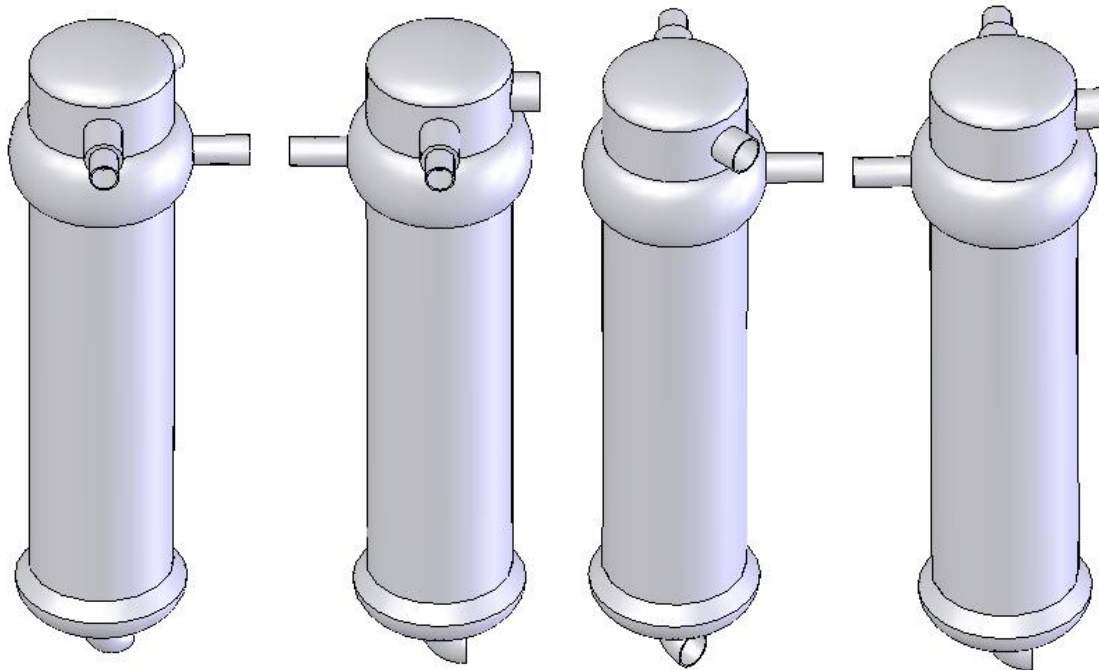


Fig. 2-12 IHX models

Two of the IHX vessels angle their intermediate loop connections at 45° relative to the other two vessels. This prevents their intermediate loop piping from interfering with the other IHX as it passes by.

2.2.4 Intermediate Loop

The intermediate salt loop Fig. 2-12 was necessary to transfer the heat from the primary loop to the power conversion system and to provide isolation between the primary salt loop and the high-pressure helium in the PCS. To increase the radiation safety, isolation valves were placed at locations of penetrations between Zones 2 and 4 as discussed in detail in Section 4.3. The intermediate loop piping is insulated outside the IHX cavities. Because the hot flow exits from the tops of the IHX's and the cold flow enters the bottoms of the IHX's, the intermediate loop can also remove decay heat via natural circulation flow, and this flow also helps prevent freezing of the intermediate loop under shutdown conditions, although these lines are also heat traced and are designed to allow drainage to a drain tank.

The drain tank is placed at the lowest point of the intermediate salt loop, which requires an extension below the base isolators. The restriction of the extrude through the base isolation provided another criteria that determines the radial size of the drain tank. Also, given that the building is allowed to oscillate during seismic-like events with a predicted maximum displacement of 0.82 m (Section 5.2), adequate radial clearance space of 2.5 m and 1.0 m above and below the tank is implemented between the tank and concrete side walls. The drain tank's volume is based on the intermediate salt loop calculation of 44.32823 m³. Thus, the 5 cm diameter drain line extends from the intermediate loop to a drain tank with 4.0 m radius and a height of 4.8 m below the base isolators. Due to a lower threat imposed by immediate physical access below the turbine

hall compared to the reactor and IHX's cavities, the extrusion required by the drain tank is not designed to limit physical access.

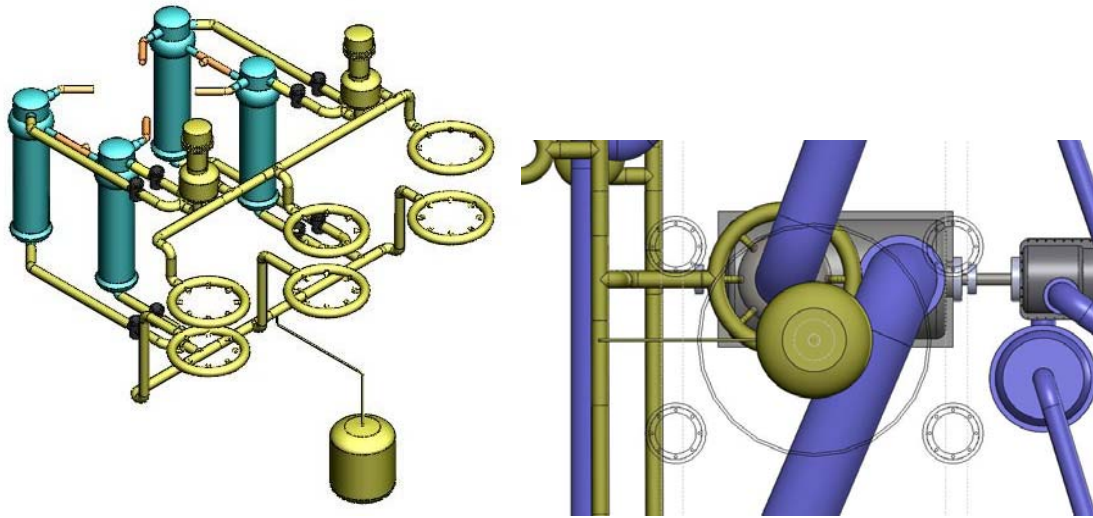


Fig. 2-12 (L) PB-AHTR intermediate salt loop (R) Intermediate salt loop drain tank is situated beneath medium-pressure turbine.

Because the intermediate salt loop uses a relatively small pipe diameter (compared to the helium piping of the PCS), the computer model incorporates several turns and adjustments. The main concerns for the computer model were to connect the four inlets from four heat exchangers, to distribute the flow to three turbines' helium heaters, and then to accept flow from the three heaters and distribute it back into four pipes for the intermediate heat exchangers. Simple pipe intersections were modeled at the inlet of the intermediate salt pumps to combine two incoming salt flow and feed it into one of the two intermediate salt pumps. Helium heater distribution rings (Fig. 2-13) were created to fit around the heater vessel under each turbine, with eight inlets with equal spacing of 45° at approximately 1 m from the bottom of the turbine casings and eight outlets protruding at 45° from the curved bottom portion of the heater.

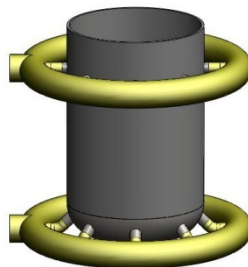


Fig. 2-13 Helium heater feeder rings

2.2.5 Spent Fuel Canisters

The 16 spent fuel, core off-load, and inert graphite sphere storage canisters are provided for in-building storage, as discussed in greater detail by the Thermal, Fluids and Chemical Design Group in Section 3.1.4. As shown in Fig. 2-14, these canisters were

modeled in SolidWorks as cylindrical vessels with a diameter of 1.6 m and a height of 10 m with 30 cm to 50 cm spacing from the walls of the spent fuel cell and equal spacing of 1.9 cm throughout the total length of the cell at 16 m. Details of shielding design for the spent fuel storage cell are given by the Beryllium and Radiation Safety Group in section 4.2.4.

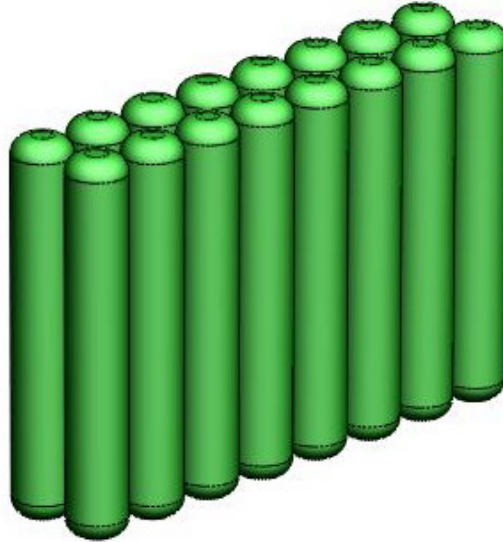


Fig. 2-14 Spent fuel canisters model

2.3 Reactor Building and Turbine Hall

The PB-AHTR reactor building and turbine hall was modeled in 3-D in Solidworks, based upon preliminary 2-D elevation and plan views sketched in Canvas (Figs. 1-3 and 1-4). The general configuration of equipment and the building was recommended by Professors Peterson and Stojadinovic. Throughout the process of designing and modeling the building, two main priorities were to minimize the volume and mass of concrete used and to optimize the building design and configuration in a way that met the design constraints of the other design groups. In particular, the Seismic and Structural Design Group provided recommendations for the thickness of major building elements needed to meet strength requirements (Section 5.2).

One of the first challenges for the building design was to minimize the mass of concrete in a way that took into consideration radiation shielding requirements, defined by the Beryllium and Radiation Safety Group (Section 4.2), to provide the necessary halls, hallways and rooms needed for equipment, and to provide appropriate isolation and access control between the building HVAC zones (Section 4.3). In essence, we removed concrete where it was not needed, while meeting the design requirements of the other design groups.

Table 2-3 Changes in wall and floor thicknesses from original to final values.

	Old Thickness (m)	New Thickness (m)
Floor between dry cask loading and 1st upper floor	0.4	0.9
Floor between spent fuel storage cell and 1 st upper floor	1.4	1.9
Dry cask loading floor	1.5	1
Reactor vessel bottom	0.5	1
IHX cavity bottom	1.5	1
1 st floor of turbine hall	2.5	0.5
Roof of turbine hall	2	0.5
Between 1 st and 2 nd upper floors	0.9	0.4
Between 3 rd and 4 th upper floors	0.9	0.4
Between 2 nd and 3 rd upper floors	0.8	0.3
Between reactor vessel cavity/fuel handling room and reactor citadel highbay space	1	2

Table 2-4 PB-AHTR building mass and volume.

	Mass (kg)	Concrete Volume (m ³)
With base mat and base isolators:	75,870,002	30,348
With base isolators only:	53,746,338	21,499
W/out base mat and isolators:	53,451,638	21,381
Before honeycomb structure and before thinning of walls and with base mat and isolators:	81,093,750	32,438
Before honeycomb structure and thinning of walls and w/out base mat and isolators:	58,693,750	23,478
Turbine hall with isolators and base mat:	31,948,038	12,779
Reactor Side with isolators and base mat:	43,921,964	17,569
Turbine hall w/out isolators and base mat:	20,221,280	8089
Reactor Side w/out isolators and base mat:	33,370,980	13,348

*Density of Concrete = 2500 (kg/m³)

The width of the building was changed from 38 m to 35 m, and the height of the building was changed from 30.5 m to 33 m during the course of the design project. The

original cavity for the fresh fuel room was divided into 2 levels, and the same was done for the cover gas control system cavity. A structural system of transverse (N-S) ribs was also created on the inside of the top and bottom floors of the turbine hall in order to reduce concrete mass as well as to provide room for the power conversion unit pipe systems. Base isolators were then located under these N-S ribs. Throughout the iterative design process with the other design groups, several changes in rib structure and isolator arrangement were made on the bottom floor of the turbine hall to accommodate the PCU piping systems, including a shift of one rib 2 m to the right, another 3.2 m to the right, and the deletion of another rib completely.

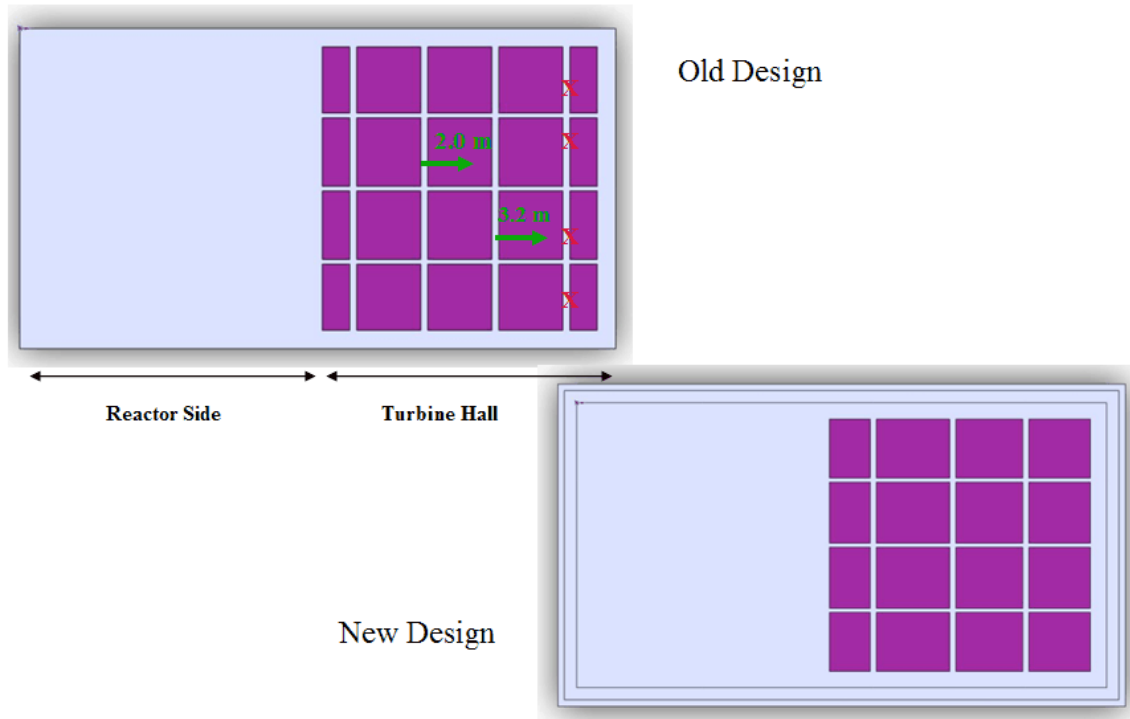


Fig. 2-15 Turbine hall floor rib structure, where the transverse N-S ribs are the primary load carrying members, and the E-W ribs are primarily for bracing.

The design of the reactor building located the reactor primary loop and reactor cavity, which provides the reactor's containment function, inside a "citadel" structure as shown in the section views in Figs. 2-16 to 2-19. The citadel structure is protected by an external events shell created by the equipment hallway system on the north, west and south sides and by the turbine hall on the east side. The Seismic and Structural Design Group selected acceptable wall thicknesses for this external events shell from the dynamic response evaluation of the structure's displacements and accelerations of an impulse load generated by a 500 ton mass, colliding at 200 m/s (450 mph), over a time period of 0.25 seconds in order to (Section 5.2.1.2). But the Seismic and Structural Design Group did not perform detailed analysis of the local, inelastic response of the external event shell or the DRACS chimneys to the deposited aircraft impulse, which would have required a more in depth analysis to confirm the design of an appropriate structural reinforcing system.

In order to allocate adequate operation spaces and enforce radiation safety protections, several below grade spaces were partitioned into smaller corridors while the four above grade levels still remain available for placement of additional equipment not considered in this conceptual design effort (e.g. motor control centers, battery rooms, heating and ventilation equipment and ducting, cooling water systems, remote shutdown panels, etc.). More importantly, the Spent Fuel Handling and Fresh Fuel Handling systems as well as for primary salt and cover gas chemistry control were designated inside the building with the collaboration with the Thermal, Fluid, and Chemical Design group.

With maintenance consideration of IHX's tubes, a noticeable side extrusion is designed to permit extraction of the tubes by lifting into the Reactor Highbay Space and dropping into a designated partition, which enables the movement of the tubes outside the building. This side extrusion could also serve as a service pathway to the Spent Fuel Storage Cell. The maintenance pathway has a height of 12.0 m and width of 4.0 m.

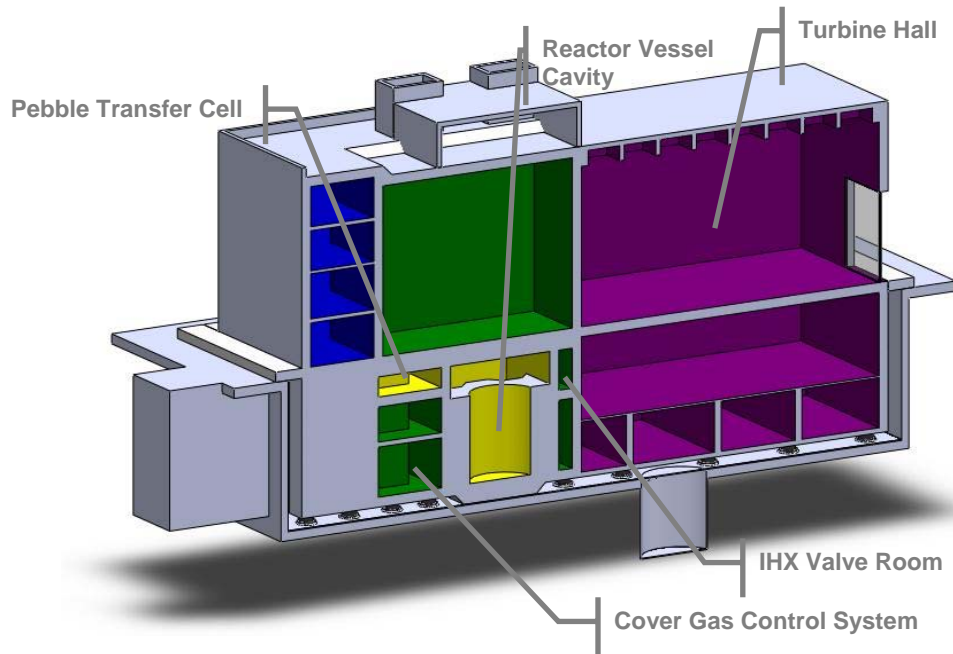


Fig. 2-16 Section view of building 16 m from the north side.

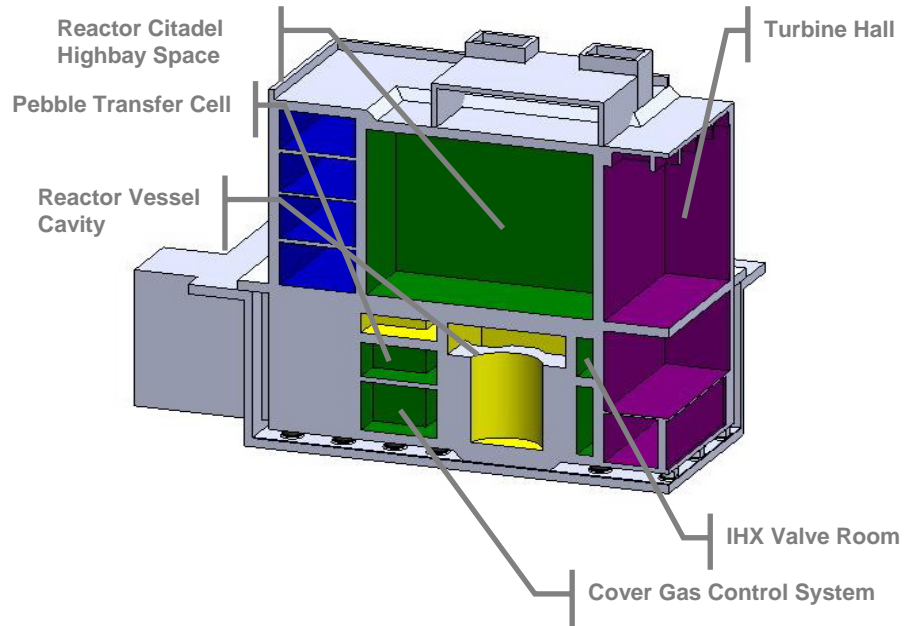


Fig. 2-17 Reactor side section view 16m from west end.

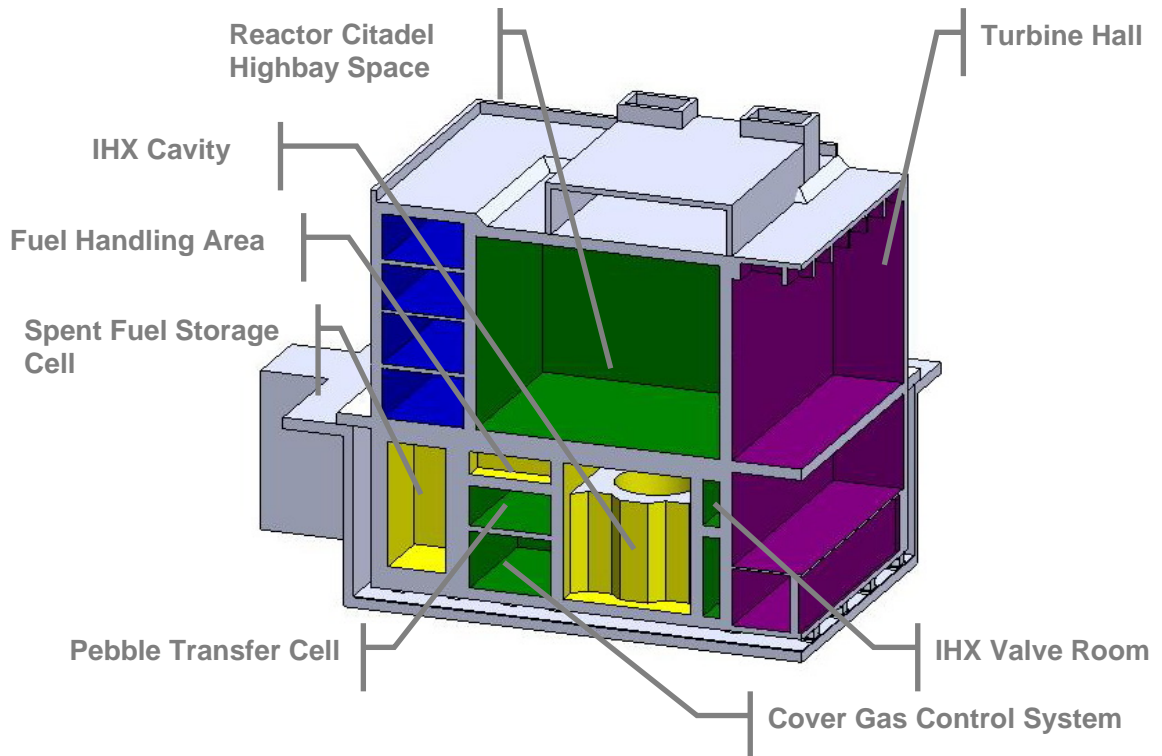


Fig. 2-18 Reactor side section view 24m from west end

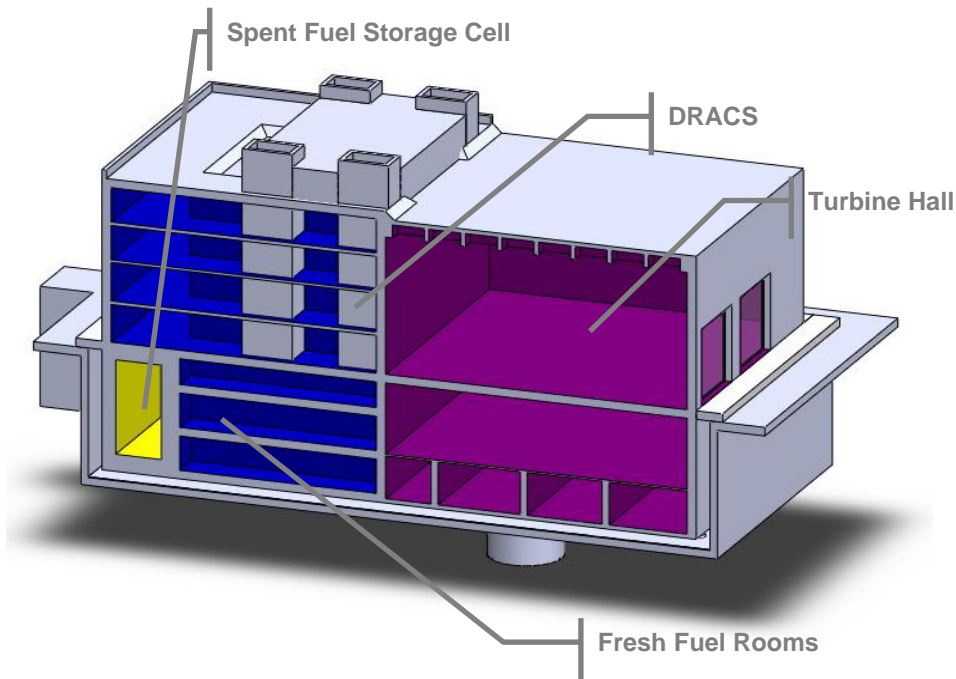


Fig. 2-19 Reactor side section view 33m from west end.

Based on the detailed design by the Seismic and Structural Design Group (Section 5.1), the entire building sits on 61 base isolators which themselves sit on a base mat foundation that resembles a moat, as shown in Fig. 2-20.

2.4 Integrated Design

With a stringent criterion on building space for the three power conversion trains, pipe connections became more compact and component arrangements led to revisions of the original design drawings. The integrated design served as a unifying step between the plant schematics (Figs. 1-3 and 1-4) and component designs. Many conflicts between plant schematic and component designs were noticeable in the integrated 3-D design. The 3-D modeling for the integrated design in SolidWorks helped to pinpoint overlooked details, interferences, and other problems with different design dimension and arrangement assumptions.

To assist in overall component arrangement and to provide adequate access to allow modifications, the major components of the power cycle were separated and assembled to fit comfortably with small tolerances as outlined in Fig. 2-21. The structure depicts the increase of tolerances from each level to the next. In other words, the lowest items in the hierarchy represent the components with the smallest design tolerance errors and larger dimensional errors were accrued as the components were fitted together at higher levels. The details of the accrued errors must be addressed in additional design and construction processes. Furthermore, the dimensions for the lowest level of the hierarchy were accurate according to design assumptions and scaling, whereas the items on the next level of the hierarchy contain the inaccuracies from the lower level and the added requirement of separations distances in accordance to component placements and pipe connections.

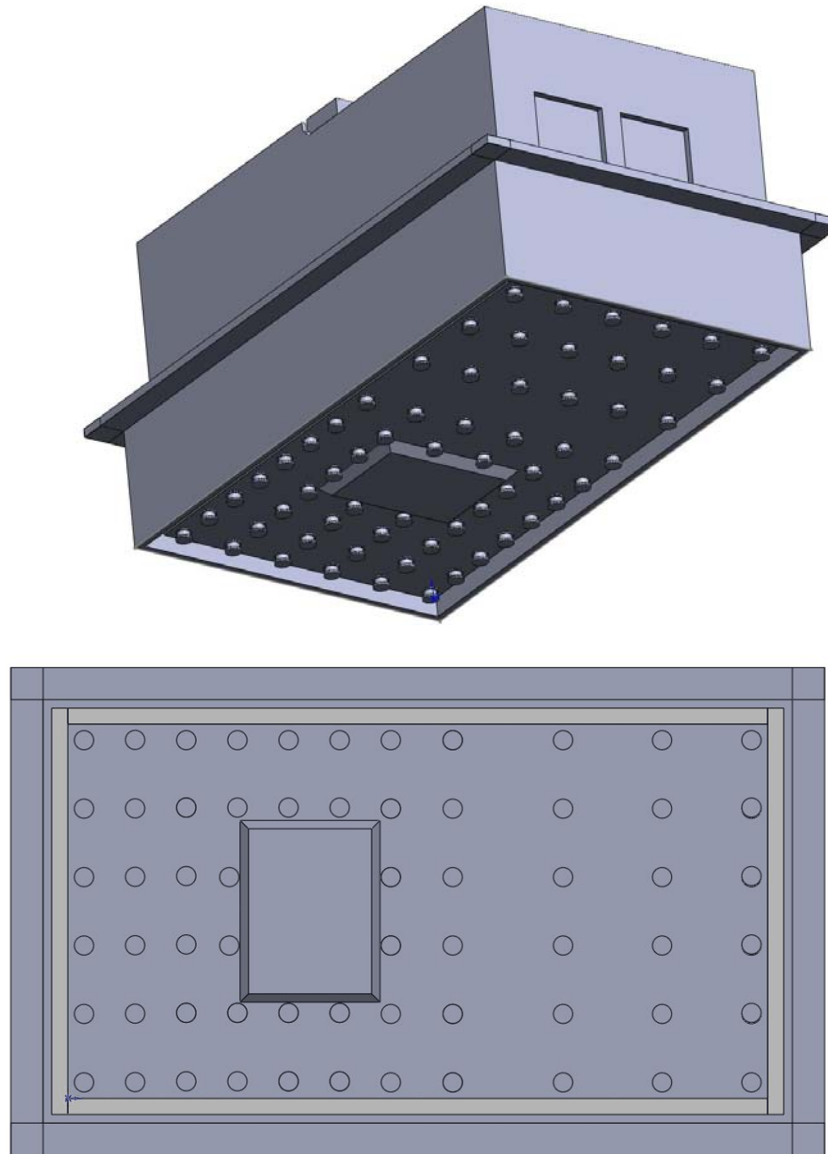


Fig. 2-20 PB-AHTR base isolators arrangement in a cutaway view from beneath (top) and a plan view (bottom).

The final assembly was divided into three major assemblies: the primary and intermediate salt loops (Section 2.1), the power conversion system (Section 2.2), and the building (Section 2.3). These components were placed at the highest level of the hierarchy due to their measurements and fitting method. To elaborate, most connections between these components do not fit perfectly with each other. The differences between connections were as large as 1.0 m. Also due to the errors and incomplete design information for the major components, certain component placements were determined visually with the aid of the design software and basing on the construction of other parts rather than analytically.

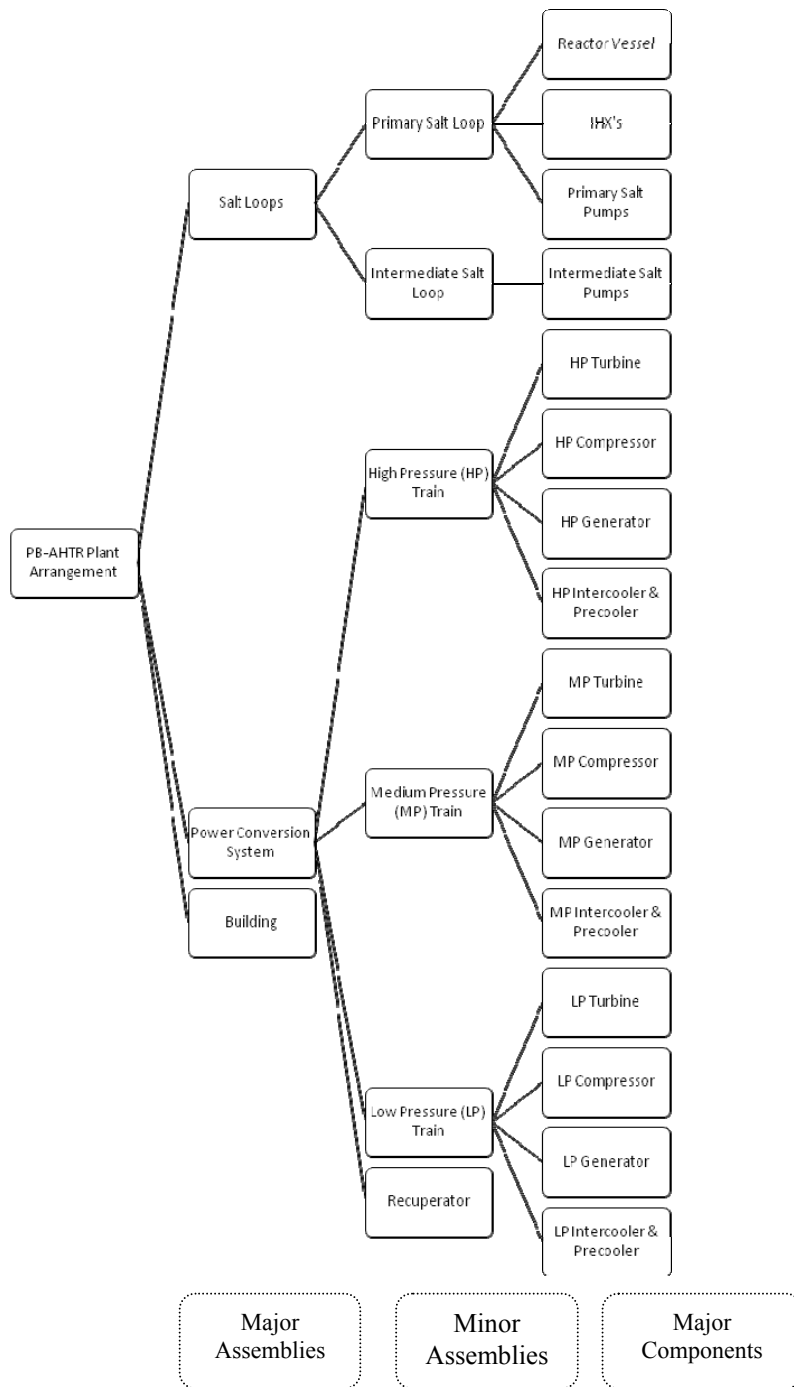


Fig. 2-21 Design Tolerance Hierarchy

Two major components were placed visually rather than having a specified reference frame. Though the reactor vessel fits concentrically inside the reactor cavity, the primary salt loop is based on approximate locations of the Intermediate Heat Exchangers (IHX's) relative to the reactor vessel.

Another visual estimate for location was performed for the recuperator due to the various connections and the constricted space in the corner of the turbine hall. The plant schematic calls for about 1 m to 1.5 m clearance from the walls; however, due to the required pipe to the high pressure power train and the large diameter pipe connecting to the low pressure turbine, the recuperator was placed more closely at 0.5 m to 1.0 m from the building walls. Additionally, the annular pipe connection between the recuperator and the HP turbine has to bend such that it does not interfere with the intermediate salt pump. Vertically, the reference between the recuperator and the PCS is the level of the LP intercooler and precooler. A summary of the references used to match the assemblies is provided in Fig. 2-22. The lines connecting each element denote the primary connections between each major assembly.

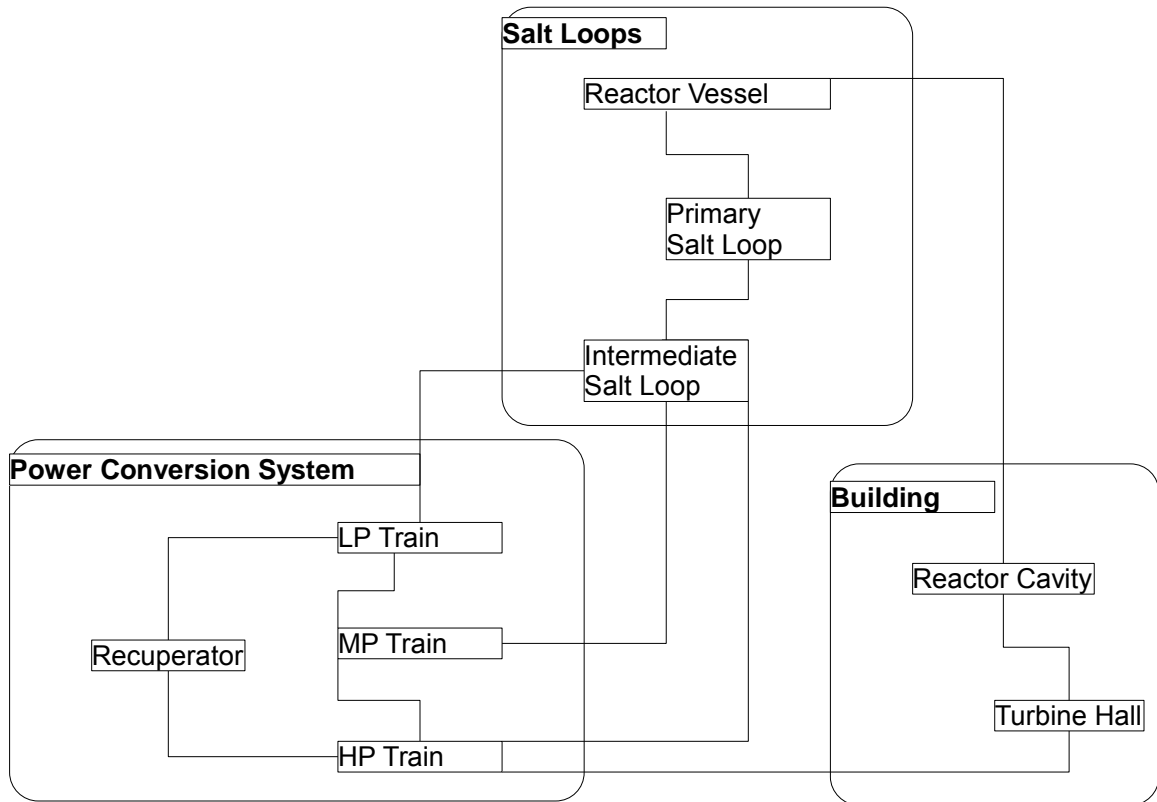


Fig. 2-22 Main references between major assemblies.

Notable references that determine the overall arrangement of major assemblies were the matching between the building, the power conversion system, and the salt loops. The importance of this function was to determine the most appropriate placements for the major assemblies vertically and horizontally.

The reference between the building and the power conversion systems was the top surface of the bottom half of the compressor casing. More importantly, the power conversion systems were aligned such that the compressor casing faces adjacent to their respective turbines and the bottom compressor surfaces were on the same planes. Thus, the pressure stages were aligned vertically and horizontally. The reference between the building and the primary salt loop was the base of the primary salt pump, which sits on the bottom surface of the Reactor Citadel Highbay Space. As a result, with the reactor vessel in the reactor cavity and the primary salt loop fitted with the building, the salt loops were situated vertically and horizontally.

Pipe connections in the integrated design served as the minimum separation distances between connecting elements. Although pipe elbows allowed spatial freedom for pipe connections, they also set the minimum separation distances between components due to their required length (Table 2-5). The designs were made in segments in order to connect the components in a relatively defined space where the diameters attempt to match the components' diameters (Table 2-6). However, the pipe connections between turbines and the connections between the recuperator and the LP turbine were designed to be constant diameter rather than adhering to the given parameters in order to simplify placements and connections. On the other hand, the connections to and from the intercoolers and the precoolers were based on the model parameters of the different pressure stage compressors. Additionally, due to the more detailed modeling of the compressor casing, the intercoolers were assumed to be at 90 degrees from the shaft and the precoolers were positioned at 45 degrees from the center of the compressor casings. To reiterate, for most connections, the pipe lengths were determined analytically, but manual adjustments were to ensure the proper pipe connections.

Table 2-5 Pipe elbow designs

Major Assemblies	Minor Assemblies	Connection Descriptions	Design Criteria (m)	Angle (°)	Diagram
Power Conversion	Power Trains (HP/MP/LP)	Turbine connections	2.00	90	
		Intercooler/Precooler connections	1.00	90	
	Recuperator	HP Turbine connection	1.0	90	
		HP Turbine split connection	1.50	45	
		HP Precooler split connection	1.0	90	
		LP Intercooler connection	1.0	90	
		LP Turbine connection	2.0	90	
Salt Loops	Primary Salt Loop		0.50	45	
	Intermediate Salt Loop	He Heater connections	0.25	45	
		Salt Pump Connections	0.25	90	
		Drain line connection	0.5624	90	

Table 2-6 Pipe design diameters

Major Assemblies	Minor Assemblies	Description of Connections		Innermost Diameter (cm)	Outermost Diameter (cm)	Thickness Inner/Outer (cm)	Annular
Power Conversion	Power trains (HP/MP/LP)	Turbine Connections	HP to MP	90	200	5/ 5	Yes
			MP to LP	110	245	5/ 5	Yes
	Compressor Connections (HP/MP/LP)	Inlets	From Intercooler	73	83	5	No
			From Precooler	52	62	5	No
		Outlets	To Precooler	84	94	5	No
			To other components	61	71	5	No
	Recuperator	HP Connection		550	700/6	17.5/ 20/6	Yes
		HP Turbine		68	150	5/ 5	Yes
HP Compressor		61	71	5	No		
LP Turbine		110	245	5/ 5	Yes		
LP Intercooler		840	940	5	No		
Salt Loops	Primary Salt Loop	Intermediate salt connections		55	60	2.5	No
		Primary salt connections		40	45	2.5	No
	Intermediate Salt Loop	He Heater feeder connections		25	30	2.5	No
		Salt pump connections		55	60	2.5	No
		Drain line connections		5	10	2.5	No

Model pipe connections and measurements between major components were made with the aid of computer design software in order to determine proper or best estimate pipe lengths. Priorities were given to the large diameter pipes, which connected the turbines. Smaller diameter pipes were designed to minimize diagonal arrangements, which were often more manageable to define than diagonal pipe lengths. Due to current arrangement propositions, vertical pipes were designed with better tolerances since diagonal pipes were not required vertically unlike pipes in the horizontal plane.

2.5 References

Peterson, P. F. Personal Communication. Jan. – May 2008.

Peterson, P. F. NE170 PB-AHTR 2008 Project Overview Slides. Jan 2008.

Documents Control Centre for PBMR (Pty) Ltd., NRC Technical Description of the PBMR Demonstration Power Plant. Document No. 016959, Rev 4., 2006.

Lim, H.J. Personal Communication. Jan. 2008.

Dimotakis, M. Personal Communication. Jun 2008.

ORNL Report 4812, pp. 222, August 1972.

Zhao, H. Personal Communication. Jan. 2008.

3. PB-AHTR FUEL AND CHEMISTRY CONTROL SYSTEMS

The Fluids, Thermal and Chemical Design (FTCD) group's work focused on developing descriptions, functional requirements, and identifying locations for the PB-AHTR systems for handling pebble fuel and for controlling the chemistry of the primary salt and its cover gas. This chapter discusses this design work.

3.1 Fuel Handling and Storage System

The Modular PB-AHTR has a fuel handling and storage system (FHSS) that includes 7 defueling machines located on top of the reactor vessel, a transfer system that sorts pebbles by burn up level and either recycles pebbles to one of 7 pebble injection machines or transfers the pebbles to one of several storage tanks and replaces the pebble with a fresh pebble. Table 5-1 provides summarizes the major design parameters for the FHSS.

The major subsystems of the FHSS are similar in design and function to those of the PBMR, but because the Modular PB-AHTR pebbles are half the diameter, the PB-AHTR fuel handling equipment is smaller and more compact. Likewise, because the PCA's provide additional moderation of neutrons, the PB-AHTR fuel has approximately twice the energy production per unit of storage volume compared to the PBMR, reducing the required fresh fuel and spent fuel storage volume.

This chapter describes major components and functions of the FHSS.

3.1.1 Sphere unloading and injection

The PB-AHTR FHSS has the following subsystems that deal with loading and unloading the pebbles:

Core Loading Subsystem CLS. The CLS includes of 7 sphere injection machines. The sphere injection machines transfer the pebbles from the atmospheric pressure gas environment of the Sphere Circulation Subsystem into a flow of cold primary salt entering one of the seven PCA's.

Core Unloading Subsystem CUS. The CUS includes of 7 sphere defueling machines. The sphere defueling machines transfer spheres from the 7 core defueling chutes to the Sphere Circulation Subsystem. The CUS also recovers broken and damaged pebbles, including pebbles worn down to minimum diameter, and graphite debris and transfers these materials to the High-level Waste (Broken Sphere) Handling Subsystem.

Fuel Handling Control Subsystem FCS. The FCS collects and processes data from instrumentation in the FHSS, and generates the control signals to activate the sphere injection and unloading machines, Instrumentation and Distribution Block valves, pneumatic transfer valves, and other components of the FHSS. The FCS instrumentation is also used for pebble accounting by the International Atomic Energy Agency to apply safeguards to the PB-AHTR fuel.

Table 3-1 PB-AHTR pebble transfer system design parameters.

Reactor power	900 MWth
Pebble diameter	3.0 cm
Typical energy generation by a pebble	0.32 MWth-day
Number of passes through outer PCA	6
Number of passes through center PCA	1
Volume of pebbles in core	
Defueling chutes	0.88 m ³
Upper pebble plenum	2.70 m ³
Core channels (18 per PCA)	8.60 m ³
Lower pebble plenum	2.70 m ³
Total volume	14.88 m ³
Pebble packing density	0.60
Total number of pebbles in core	630,000
Normal residence time of pebble in one pass	32.5 days
Residence time of pebble defueling chute	1.93 days
Pebble recirculation interval	
Normal for full core	4.5 sec
Normal each defueling/injection machine	31.2 sec
3-day core defuel/refuel, minimum for each defueling machine	3.0 sec
Number of pebbles used in 5 years ^a	5,060,000
Volume of spent pebbles produced in 5 yr ^a	120 m ³
Number of 1.6-m dia., 8.0-m high, 16.0 m ³ storage canisters needed for spent pebbles	8

^a For 100% capacity factor.

Core Loading During Commissioning and Start-Up: The PB-AHTR primary loop equipment is uninsulated, and is located in an insulated reactor cavity or “furnace,” similar to the design used previously for the MSRE and MSBR. Prior to start up the PB-AHTR reactor cavity and primary loop equipment is preheated using the Cavity Thermal Control Subsystem to uniform temperature of 550°C. The Pebble Channel Assemblies are loaded with inert graphite spheres when installed. Primary salt is introduced into the reactor vessel, loading it to the level where the primary pump impellers are submerged, and primary salt circulation can occur. The Primary Salt Inventory and Chemistry Control Subsystem then operates to clean contamination introduced by the fluxing of oxide films from the metal surfaces of the primary loop. After salt purification is completed, the FHSS is operated to remove the graphite spheres and introduce a mixture of graphite and fuel spheres into the core. The initial fuel loading has reduced enrichment

compared to the steady-state fuel loading. As a part of the initial start up, periodic subcritical multiplication measurements are made to verify core neutronics are as required.

Fig. 3-1 shows an isometric view of what these types of system look like for the PBMR [3.1]. Note though that the PBMR loads at the top and unloads at the bottom which is opposite of the PB-AHTR.

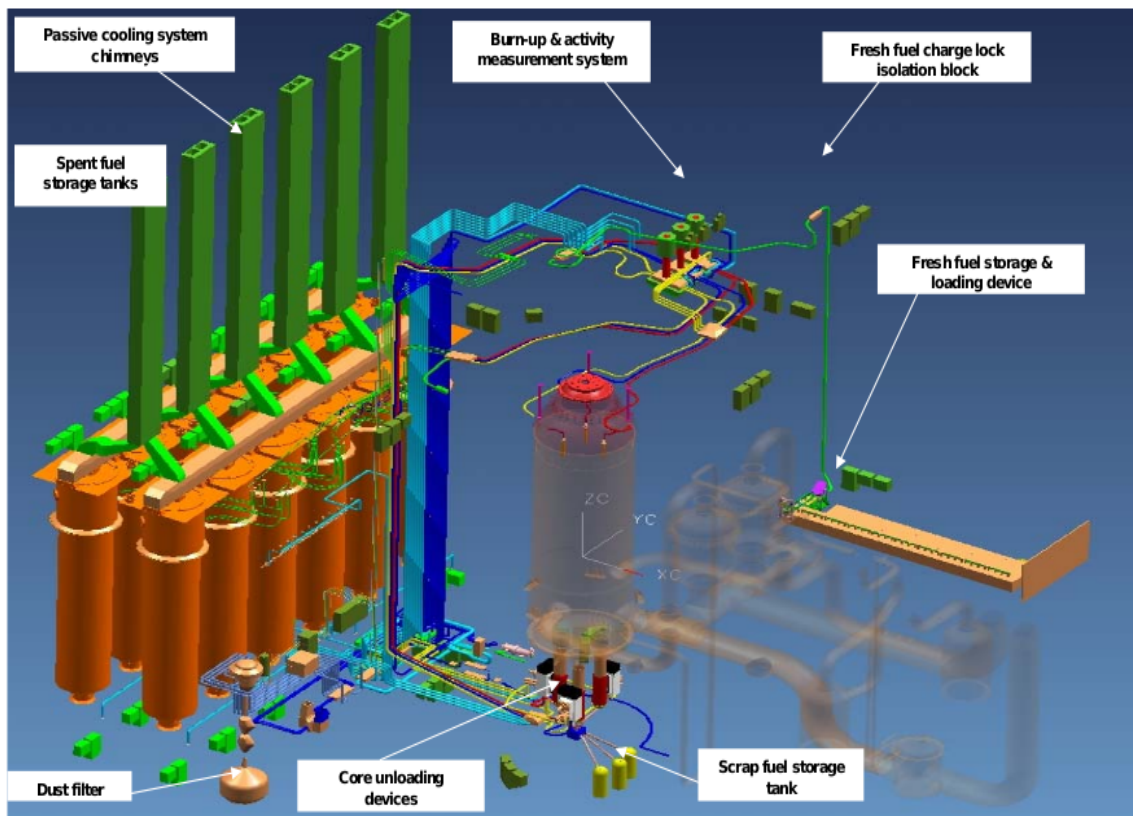


Fig. 3-1: Fuel Handling System for the PBMR [3.1]

3.1.2 Sphere monitoring and characterization

This system for sphere monitoring and characterization for the PB-AHTR is essentially the same as that for the PBMR. The dose-rate of the spheres will first be measured by the Activity Measurement System (AMS), which will also categorize the sphere as either graphite or fuel. The AMS will use an ionization chamber. The spheres will then be scanned by the Burn-Up Measurement System (BUMS), as shown in Fig. 3-2, which will categorize the spheres as either graphite, low-burn-up, high-burn-up (used or spent). The BUMS will use a high-purity germanium detector with cryogenic refrigeration system; a Digital Signal Processor (DSP) based burn-up analysis system; and a photon collimator.

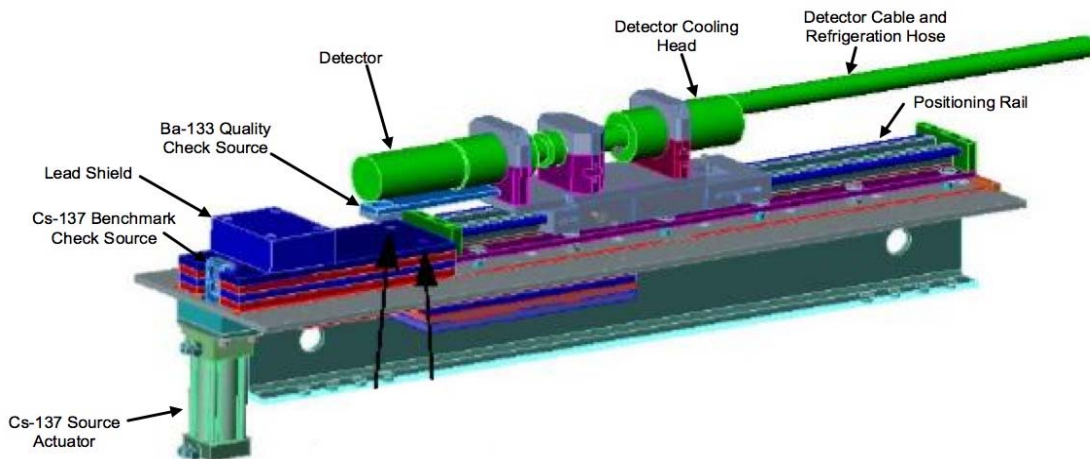


Fig. 3-2: The Burn-Up Measurement System Detector Assembly (from PBMR design [3.1])

3.1.3 Sphere Transfer System

As shown schematically in Fig. 3-3, spheres are unloaded from the top of the core by means of the Core Unloading Device (CUD). The CUD will also leave behind in a trap any sphere that is damaged or has worn down sufficiently. The spheres are then transferred to the chemistry facility where the spheres are cleaned of any residual beryllium. The spheres are then passed on to the AMS to determine if they are fuel or graphite, and then to the BUMS to determine the burn-up of the fuel. The Transfer Block then uses remotely operated valves to direct the sphere either back to the core via the Core Loading Device located at the bottom of the core, or to spent fuel storage depending on its current burn-up. Also the Transfer Block will accept fresh fuel from the fresh fuel line. The design of the Sphere Transfer System is modeled very closely to that of the PBMR, however, there are some important differences. The pebbles float in the molten salt, so the pebbles are extracted from the top of the core, which consequently affects the manner in which the damaged and worn spheres are separated in the CUD. The spheres are approximately one-half the diameter of the PBMR spheres, which will decrease the size of all transfer pipes and transfer equipment; and the BUMS will have to account for the decrease in fuel per sphere. Pebbles will be transferred in Argon as opposed to Helium, with pneumatic transfer being used where pebbles must be lifted to higher elevations.

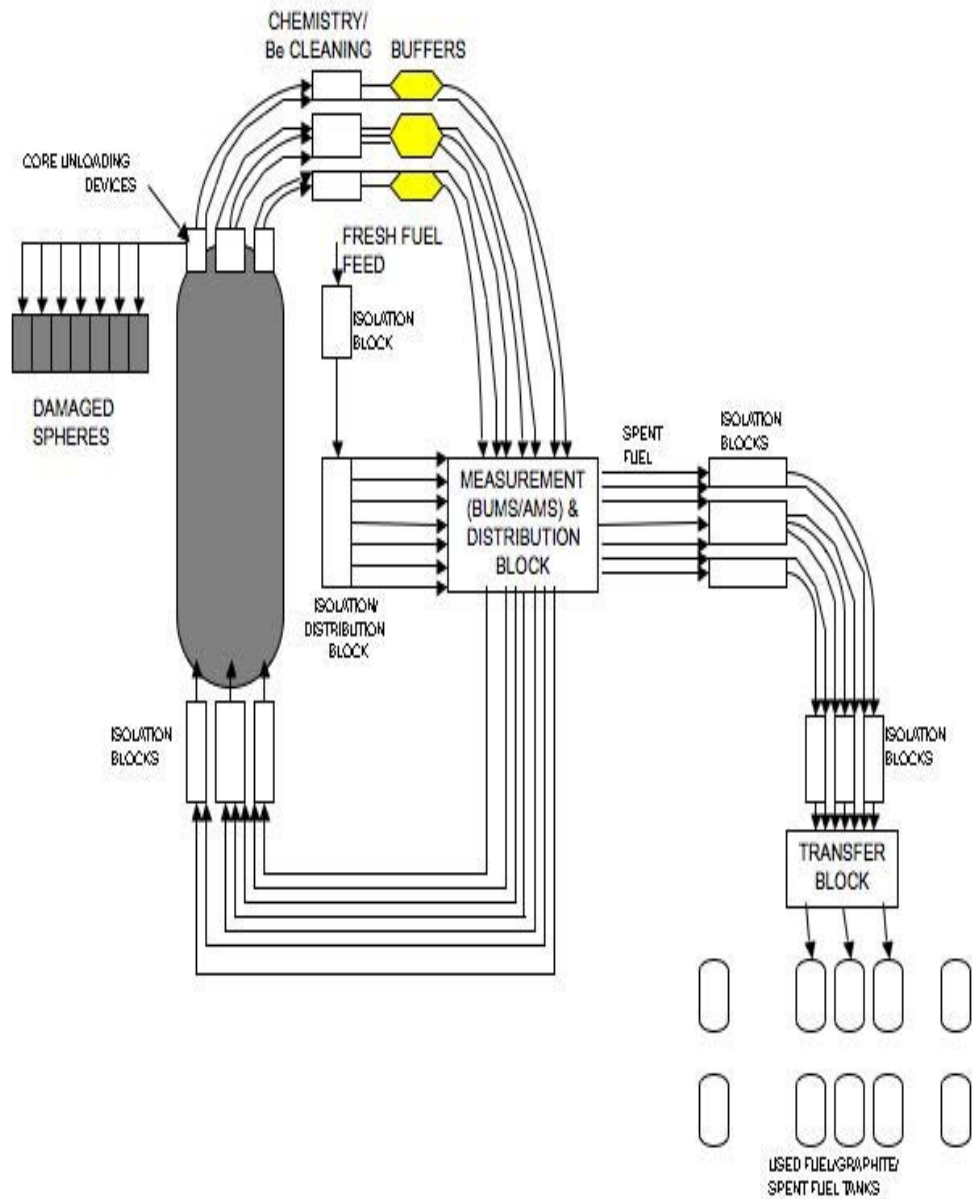


Fig. 3-3: Fuel Handling and Storage System

3.1.4 Sphere Storage

Sphere Storage Subsystem SSS. The SSS consists of 14 storage canisters, each with a storage volume of 16.0 m³ as described in Table 5-1, located in a shielded and cooled enclosure below grade, next to the reactor citadel. The SSS is sized to provide sufficient volume to store 5 years of spent fuel resulting from operation at a capacity factor of 100%, to store one full core offload of pebbles, to store one full core volume of inert graphite pebbles, and to provide an additional 25% excess storage capacity. The sphere inlet systems in the storage tanks are designed so that the maximum distance a sphere will fall, before bouncing, is less than 2 m. This is done with a series of stair steps as the

pebbles fall into the storage tanks. Each storage tank also has a sphere unloading machine that allows spheres to be removed from the tank and returned to the Sphere Circulation System.

High-level Waste (Broken Sphere) Handling Subsystem HLWHS. The HLWHS transfers broken spheres and other debris from the defueling machines to a damaged sphere container.

Used Sphere Canister Loading and Unloading Subsystem USCS. The USCS provides the capability to transfer spheres to and from the Sphere Storage Subsystem to dry cask transport and canisters. The USCS consists of a crane and a shielded cavity where transport and storage casks can be lowered, and a system to load and unload the transport and storage casks. The USCS is also used to receive canisters for shipments of fresh deep-burn transmutation fuel, and to transfer the deep burn fuel spheres to shielded storage in the Sphere Storage Subsystem.

3.1.5 Sphere Replenishment System (SRS) – Fresh Fuel

The Sphere Replenishment System (SRS) is designed to hold one year's supply of fresh fuel on-site or equivalently, 1,012,000 spheres. Fresh fuel spheres consist of low-enriched uranium oxycarbide fuel (10.4% ^{235}U) covered with pyrolytic carbon and silicon carbide. The spheres have a diameter of 3.0 cm. The fresh uranium spheres are stored in a total of fifty 50-gallon metal drums. The SRS is located close to the reactor citadel, in a ground-floor hallway also near the pebble handling cell and spent fuel storage cell. This optimizes access to the reactor, and its location inside the reactor building also enhances security for the fresh fuel. Within the fresh fuel storage room, machinery is in place to transfer the fresh spheres to the automatically load the spheres into the valve box of the Fuel Handling Control System, and from there to the seven sphere injection machines, which are designated as part of the Core Loading Subsystem (CLS). Figure 3-4 shows this SRS area for the PBMR.

Deep burn transmutation fuels are brought into the facility differently, using the same transfer cask system used for removal of spent fuel, due to the higher radiation levels for recycled fuels containing transuranics like Am-241.

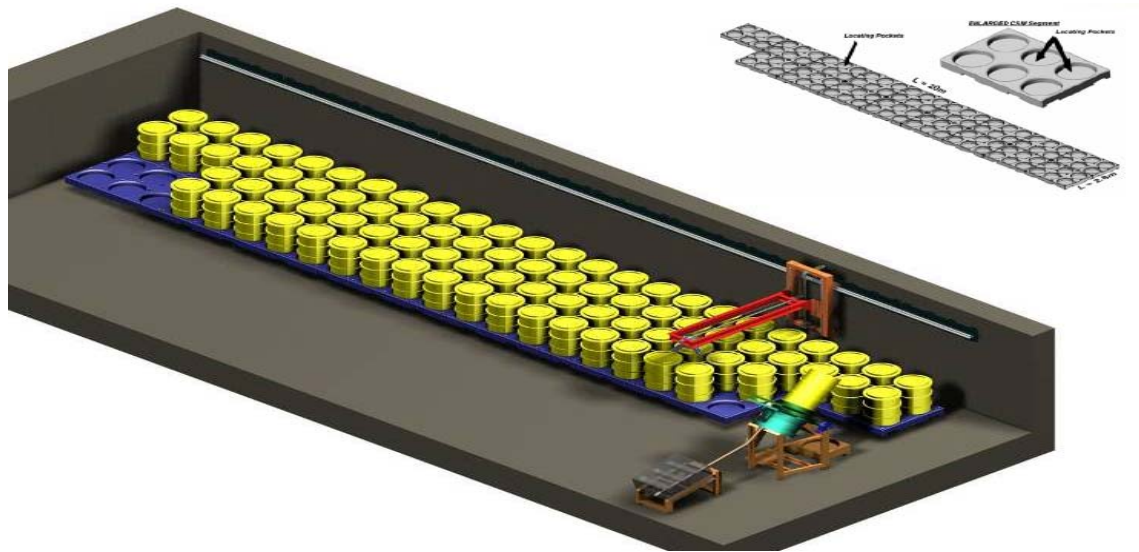


Fig. 3-4 Sphere Replenishment System (taken from the PBMR [3.1])

3.2 Salt Chemistry Control System

In the reactor vessel, the enriched uranium fuel pellet spheres will be cooled by a liquid salt primary coolant. This has a number of operational advantages compared to helium, including improved heat transfer, higher power density, and low pressure operation. In this section, candidates for liquid salt in this reactor are reviewed, and the functional requirements for the primary salt chemistry control system are specified.

3.2.1 Salts and Properties

The types of salts being investigated to act as the liquid for this pebble bed reactor are mainly fluoride salts because of their high compatibility with the graphite fuel spheres and excellent stability under neutron irradiation. The liquid fluoride salt that immerses the fuel spheres also protects the fuel from a chemical attack by air. The salts can, however, also chemically react slowly with contaminants like air and water, possibly resulting in destructive corrosion. The reactor vessel itself and the pipes used to transport the salt throughout the primary and secondary systems must therefore be clad an exceptionally corrosion-resistant alloy, Hastelloy N, which can also withstand the operating temperatures of the reactor. Still, a chemistry control system is required to remove potential contaminants and to control the salt fluorine potential to assure that very low corrosion rates are maintained.

Candidate fluoride salts for nuclear applications include lithium fluoride, sodium fluoride, beryllium fluoride, zirconium (IV) fluoride, and rubidium fluoride. The “pure” salts such as NaF, however, have the disadvantage of extremely high melting points. This

problem can be alleviated by using a mixture of salts. Although an impurity will increase the melting point range of any given substance, the overall melting point of the resulting mixture has the potential to be greatly reduced. Therefore, considering more complex binary or ternary fluoride salts is advisable.

Some examples of these possible salt mixtures and some of their properties are given in Table 3-2.

Table 3-2 Possible Fluoride Salts and Mixtures for the Molten Reactor Coolant (Standard States)

Salt	Melting Point (°C)	Density (kg/m ³)	Heat Capacity (kJ/(kg°C))	ρC_p (kJ/(m ³ °C))
Pure LiF	848	2640	-	-
Pure RbF	795	3200	-	-
Pure BeF ₂	545	1986	-	-
Flibe (Li ₂ BeF ₄)	459	1940	2.34	4540
58% NaF, 42% ZrF ₄	500	3140	1.17	3670

The thermophysical properties of many of these fluoride salts are very similar to those of water. In the case of the PB-AHTR, flibe is selected as the primary coolant due to its acceptable melting temperature and excellent neutronics properties. Because the beryllium in flibe is toxic, the Beryllium and Radiation Safety Design Group's work has focused on developing the beryllium and radiation safety approach for the PB-AHTR.

3.2.2 Important Controls

As with any real engineering system, unintended and unwanted side effects can occur that can have destructive consequences if left untreated. As mentioned previously, fluoride salts can become corrosive when contaminated by contact with air or water vapor, and other contaminants in the salt can result from neutron capture reactions and broken fuel spheres and graphite dust. The Thermal, Fluid and Chemistry Design Group developed a set of functional requirements for the chemistry control system to address these potential sources of primary salt contamination, and worked with the Plant and Mechanical Design Group to identify space where this equipment would be located. The detailed design of this equipment would occur later in the PB-AHTR development process, based on the functional requirements listed below.

Oxygen Removal and Fluorine Potential Control

The ingress of air or water vapor can result in the contamination of the salt with oxygen, which creates corrosive conditions. This creates the requirement to control oxygen in the salt. For this purpose, the chemistry control system will remove a side-stream flow from the primary loop. This flow will be processed with an HF/H₂ purge to remove oxygen contaminant. In this purge, hydrogen fluoride gas is bubbled through the salt along with hydrogen gas which chemically reacts with the oxygen to produce water vapor, and replaces oxygen with fluorine. The fluorine potential is then reduced by contacting the salt with beryllium metal.

Tritium Removal

The primary salt will have some initial content of lithium-6, and additional Li-6 will be generated by neutron reactions with beryllium. This Li-6 can capture a neutron to produce tritium in a ${}^6\text{Li}(n,\alpha){}^3\text{H}$ reaction. This tritium must be removed through a sparging the salt flow with helium. The cover gas system discussed in the next section can be designed to remove tritium in this way.

Rubidium Decay Product Removal

A rubidium salt, RbF, may be added to the salt to act as a radioactive tracer for beryllium safety, as being studied by the Beryllium and Radiation Safety Design Group. This may have an additional consequence: naturally occurring radioactive ${}^{87}\text{Rb}$ beta minus decays into ${}^{87}\text{Sr}$ and strontium fluoride (SrF_2) may be insoluble in the molten salt. Additional experiments will have to be carried out to observe and control for this effect in the reactor system if the rubidium salt was chosen.

Other Contaminants

Fourth, a system must be in place to remove other contaminants from the salt, including particulates such as graphite dust and larger pebble pieces from broken spheres. For this, a non-reactive metal such as nickel should be used to design a filter that will be remove particulates coming from the primary system to the chemistry control system. Additional filtering equipment may be needed in the primary loop, and the defueling machines will need to be designed to remove and recover broken pebble pieces that are too large to be carried to the filter system by the primary coolant.

Lastly, methods are also required to clean and purify the buffer salt, the intermediate salt, and the salt for the direct reactor auxiliary cooling system (DRACS) loops. These components will have identical functions as those described in the previous paragraphs for the primary system. Depending upon the rate of diffusion of tritium through the various heat exchangers, these loops may also need tritium recovery and control.

3.2.3 Salt Flow in the Primary System

In the primary system, the chemistry control system should be sized so that the primary salt is processed approximately once per week. Since about 40 m³ of total inventory must be processed in that time, a calculation can be performed to determine the approximate sizing of the pipes in which the molten salt must flow at a velocity of 1-2 m/s.

$$\text{Volumetric flow rate } Q = \frac{40,000 \text{ L}}{\left(\frac{7 \text{ d}}{\text{week}}\right) \left(\frac{86400 \text{ s}}{\text{d}}\right)} = 66 \text{ mL/s} = 6.6 \times 10^{-5} \text{ m}^3/\text{s}$$

$$\text{Cross sectional area } A = \frac{Q}{v}$$

$$\pi R_{\text{pipe}}^2 = \frac{6.6 \times 10^{-5} \text{ m}^3/\text{s}}{1.5 \text{ m/s}}$$

$$R_{\text{pipe}} = \sqrt{\frac{6.6 \times 10^{-5}}{\pi(1.5)}} \text{ m} = .0037 \text{ m}$$

For strength reasons, the actual diameter of the chemistry control system piping will be larger, between 0.025 and 0.050 m inside diameter as determined by detailed pipe stress analysis.

3.3 Cover Gas System

The cover gas over the primary is generally an inert gas fills the gas space of the primary loop, below the reactor vessel cover and in the pump seal bowls, which prevents the primary salt from chemically reacting with air and other contaminants. The cover gas control system in this design will use argon (Ar), a noble gas that is cost-effective for this plant because it can be bought from a company that extracts it from air. This inert gas will also be used for pneumatic transfers in the sphere transfer system and in the spent fuel storage canisters.

3.3.1 Physical Capabilities of the Cover Gas System

The cover gas control system will provide argon for:

1. The primary vessel (pump, seal bowls)
2. The pebble transfer system
3. Spent fuel storage canisters

4. Seals for control rods and pump shafts

The machine that regulates the flow of argon gas through these systems must have certain physical capabilities. Most importantly, the gas must be pumped into and through the system. For this, a large centrifugal pump or other pump type suitable for this task must be engineered at a stable location. There must also be a filter to clean and a heat exchanger present to cool any extracted gas.

3.3.2 Argon Leakage and Air Contamination

Since some argon will inevitably leak back out into the environment, there must be an argon replenishment system available outside the reactor building to replace any escaped gas. Potential leak paths for argon, such as the seals for the primary pump shafts, will be equipped with a clean argon purge flow to prevent any migration of radioactive material or beryllium out of the primary loop.

3.2.3 Tritium Recovery

As discussed earlier, a tritium recovery system must also be present in the cover gas cleanup process. The tritium would most likely be recovered by sparging the primary salt with helium or argon. Tritium diffusion through heat exchangers may also be recovered at the cooler points along the gas cycle, using possibly an intermediate salt gas stripping system and/or tritium recovery from the power conversion system helium flow.

3.4 References

- 3.1 Documents Control Centre for PBMR (Pty) Ltd. NRC Technical Description of the PBMR Demonstration Power Plant. Document No. 016959 rev 4. 2006.

4. PB-AHTR BERYLLIUM AND RADIATION SAFETY

The PB-AHTR uses materials that can create potential hazards to workers. As a nuclear reactor the PB-AHTR will have radiation hazards, but chemicals used in the facility, particularly the beryllium that is a component in the primary salt, also create potential hazards. The use of beryllium in the coolant provides several major advantages, due to its ability to provide a negative void reactivity coefficient for the core, to facilitate high discharge burn up of the fuel, and to provide excellent heat transfer capability. Because the PB-AHTR will require a radiation safety program in any case, this design project studied how the management of beryllium hazards could be best integrated in with the management of radiation hazards.

4.1 Beryllium and Radiation Safety Approach

4.1.1 Medical Surveillance

The use of beryllium in the liquid salt coolant poses potential safety concerns. There are several potential adverse health effects from beryllium exposure that must be carefully controlled and monitored for. Chronic beryllium disease (CBD) primarily affects the lungs and has a very slow onset. The most common signs and symptoms include an unexplained cough, fatigue, weight loss, fever and night sweats, although CBD is known to affect different people in different ways, making it often difficult to diagnose. Also, CBD can only develop in workers who have developed beryllium sensitization, which is an allergy to beryllium. This allergy can be tested for through a beryllium lymphocyte proliferation test, or BeLPT. Beryllium exposure can also elevate a worker's risk of contracting lung cancer and if there is skin exposure, skin disease can develop in the form of a rash [4.1]. Due to the adverse health effects, the current exposure limits according to the Occupational Health and Safety Administration are set at $2 \mu\text{g}/\text{m}^3$ as the 8 hour TWA, $5 \mu\text{g}/\text{m}^3$ as the ceiling exposure that should not be exceeded for more than 30 minutes and $25 \mu\text{g}/\text{m}^3$ as the peak exposure never to be exceeded. These current safety standards however are currently under debate due to the fact that recently obtained data suggests that the $2 \mu\text{g}/\text{m}^3$ as the 8 hour TWA may not be adequate in preventing CBD. Therefore, it has been recommended that the $2 \mu\text{g}/\text{m}^3$ as the 8 hour TWA be changed to $0.2 \mu\text{g}/\text{m}^3$ as the 8 hour TWA [4.2].

Based on experience in other industries that use beryllium, there are several exposure controls that should be put in place to maximize the personal protection for every worker. The first are several engineering controls, such as proper ventilation in each zone, enclosing processes, using vacuum systems in machining operations, minimizing the number of workers who have access to each zone and implementing mandatory personal sampling techniques for monitoring exposure. Using good work practices can also help prevent beryllium exposure. Good work practices include good cleaning practices, like using HEPA vacuums, not leaving exposed film or dust after water dries if a mop was used to clean up a spill and not using compressed air to clean machine parts. Also, never eating, drinking, smoking or applying cosmetics in the work station is advisable. Workers should change into work uniform before entering the work areas and store work uniforms in a covered uniform bin between shifts. Workers should also shower and change into street clothes prior to leaving the premises. Respiratory protection is also advisable in

potentially contaminated zones considering that recent data has shown that exposures to beryllium even at levels under the $2 \mu\text{g}/\text{m}^3$ PEL may have caused CBD in some workers. According to NIOSH, supplied-air respirators equipped with 100-series filters (either N-, P-, or R-type) that have a full face piece operated in a pressure-demand or positive pressure mode should be used for activities where beryllium dust may be present [4.3]. Giving workers the proper training for working with beryllium, in addition to radiation and radioactive materials, is also necessary. This includes supplying the workers with a copy of the materials safety data sheets for beryllium, giving them the facts about diseases caused by beryllium and how to protect themselves, and teaching workers how to use protective equipment appropriately. Finally, employers should send beryllium-exposed workers to a trained physician to be evaluated for beryllium sensitization or for the presence of CBD at least once a year [4.4].

4.1.2 Radiotracer for Beryllium Detection

4.1.2.1 Prospect of Radiotracer

With beryllium being toxic to humans, beryllium monitoring is essential to ensure the safety of the workers who could potentially be exposed to beryllium. Direct methods for detecting beryllium often take days for lab work before results are obtained. Using a radiotracer for detection purposes would allow real time detection of beryllium contamination. Real time beryllium monitoring would improve safety of workers, and is therefore a worthwhile endeavor to consider.

Beryllium in the liquid salt can go into the vapor above the salt and condense into particulates in the air, particulates that need to be monitored. Beryllium may also be released if leaks occur in chemistry control piping, and during maintenance activities on primary loop components. The radiotracer of choice would be a neutron activation product that would act as a gamma emitter. Activation would occur due to the salt being in the reactor core and exposed to the neutron flux. Potential candidates that would be chemically stable in the primary salt and generate useful activation products include sodium fluoride and rubidium fluoride.

4.1.2.2 Limitations

There are various limitations to using a radiotracer as a detection method for beryllium. Because the radiotracer decays over time, a neutron flux is required to produce the radiotracer, and thus the inventory of the radiotracer will drop when the reactor is not operating. Only the salt in the primary loop will be exposed to the neutron flux. All salt in storage will not have the activated tracer. The radiotracer will decay with time. Once beryllium escapes from the primary loop, the ability to detect it will diminish with time, as the activity of the radiotracer will decay. Buildup of beryllium on surfaces over long times will not be detectable by the tracer, and must be checked for by other methods.

4.1.2.3 Detection

To determine the concentration of tracer needed in the salt to permit detection of beryllium, it is required to calculate the neutron capture rate in the primary salt,

concentration of the radiotracer in the liquid and vapor phases, and the gamma emission rate from the radiotracer.

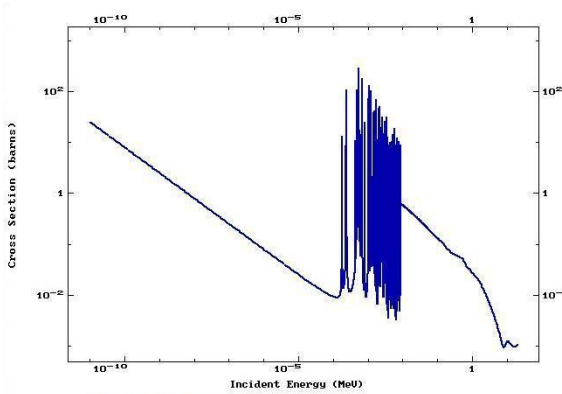


Fig.1 Rubidium-85 cross section

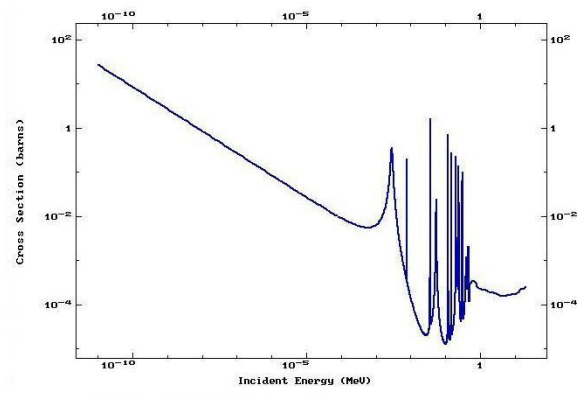


Fig.2 Sodium-23 cross section

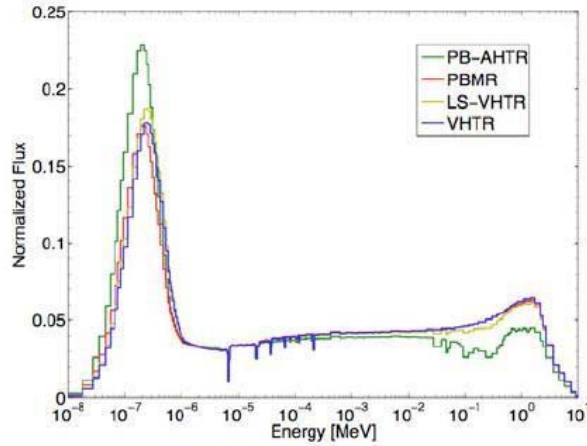


Fig.3 PB-AHTR flux shape

Fig. 4-1 Microscopic cross sections for the two radioisotopes under consideration, as well as a plot of the reactor flux.

In order to calculate the production rate, the cross section for each element [4.5] needs to be integrated over the range of neutron energies in the reactor core [4.6], to get a normalized cross section. Once that value is obtained, the calculations follow.

Table 4-1 Parameters used in the radiotracer analysis.

	Na-23	Rb-85	units
microscopic cross section	0.1089	0.1324	b
Reactor flux [4.6]	8.00E+14		n cm ⁻² s ⁻¹
Flibe density	1963		kg m ⁻³
	1.963		g cm ⁻³
Flibe molar mass	99		g/mol
Flibe molecular density	1.19E+22		molecule cm ⁻³
Beryllium atom density	1.19E+22		at. cm ⁻³
Natural abundance	1	0.722	
radiotracer density (1% of salt)	1.19E+20	8.59E+19	at cm ⁻³
total salt inventory	32.6		m ³
salt in core	5.6		m ³
mass flow rate	905.9		kg/s
time in core (per cycle)	12.15		s
total time (per cycle)	70.72		s
Activity of tracer	1.78E+09	1.56E+09	Bq cm ⁻³
beryllium molar mass	9		g/mol
beryllium atom mass	1.49452E-23		g/at.
beryllium density	0.178		g cm ⁻³
	5.62		cm ³ g ⁻¹
vol of 0.2µg beryllium (10% threshold)	1.12E-06		cm ³
corresponding activity (in salt)	2.00E+03	1.76E+03	bq
branching ratio of gamma	1	0.09	
gamma ray activity (in salt)	2.00E+03	1.58E+02	gammas/s
ratio of vapor pressures to Be	0.1	0.1	
gamma ray activity in vapor	2.00E+02	1.58E+01	gammas/s

Sodium being the best choice for a tracer, showing a promising figure of 200 gammas emitted per second in vapor-phase salt containing 0.2 µg of beryllium. The sodium activation product has a half life of 15 hours. Those figures are for one tenth the limit for beryllium concentration for one cubic meter of air. Sodium-24 emits 2 gamma rays at 100% branching, one at 2754 keV and one at 1369 keV. The primary method for detection of these gamma rays would be a germanium detector to resolve the

characteristic gamma ray. At 2.7 MeV a germanium detector has an efficiency of about 6% and at 1.7 MeV an efficiency of about 18% [4.7]. The efficiency of the detectors will vary depending on size and other factors, but their efficiencies will not vary too far from these approximate values. The other factor in detection is the solid angle the detector takes up. This value is dependent on the geometry of the system designed to detect the radiation. Such systems might include a filter to pick up the beryllium particulates in the air and placed next to a detector to measure counts. Another system could be compressing air into a chamber and having it right next to a detector to detect the beryllium particulates in the air. In any case the solid angle in such case shouldn't be below much beyond 10% solid angle coverage. Measuring the 1369 keV gamma an expected counts from your detection would be 3.6 counts per second or 216 counts per minute. Such a count rate is a detectable level, and to detect the full $2\mu\text{g}$ of beryllium concentration is possible even considering the generalizations made in the analysis.

4.1.2.4 False Positive Research

The possibility of having a false positive detection is within reason for this kind of detection method. Fission products could leak from the fuel into the salt, and if any have a characteristic gamma decay of 1369, that has potential to create a false positive. Of all the fission products and neutron capture isotopes with characteristic gamma ray energy of 1368.63 ± 1 keV none of them had branching ratios of significant magnitude [4.8]. The probability of such density getting to anywhere near that of the radiotracer is essentially zero, and so is the likelihood of having a false positive.

4.1.2.5 Assumptions

It was assumed that the resonance capture probability was zero in the calculation of the cross sections for sodium and rubidium. This assumption gives a cross section that is smaller than the actual one would be, meaning that the tracer is easier to detect than calculated here.

The shape of the flux was approximated to seven linear portions to make calculations easier. This changed the value of the cross section very slightly.

An assumption was made in the calculation of the flibe density. With the addition of 1% tracer to the salt, the density of flibe would be slightly different than the one used in the calculation.

The reactor flux is an approximate value. The actual operation flux might be different by a slight percentage.

4.1.3 Beryllium Control

Due to beryllium's high toxicity, one of the main goals of the safety systems must be to prevent exposure to respiratable particles for both plant personnel and the public. In order to ensure public and safety and compliance with regulations, the hazardous material must be isolated by distance (from the biosphere) and physical barriers, contained in a manner as to prevent its release or misuse, and handled only by trained persons [4.9].

Any releases to the environment must be monitored, and local ecosystems should be tested periodically to determine the impact of any external releases.

In order to ensure that the failure of a plant system does not cause potentially-beryllium-contaminated air to leak into occupied areas or into the outside atmosphere, the ventilation system (and cover gas control system) must establish flow paths and, by the differences in HVAC Zone air pressures, leak paths which cause air from areas of “lower contamination” to flow (or leak) to areas of “higher contamination”.

Large amounts of molten beryllium-containing salt will be continually present within the primary reactor cooling loop and in out-of-loop processing and inventory. The salt is to be contained within the piping system in a (mostly) sealed, shielded room with an inert atmosphere and isolated heating/ventilation system (HVAC Zone 1). There should be no human entry to the reactor room under normal circumstances.

In the primary salt pumps, the control rod channels and in the salt chemistry control system, molten salt comes into contact with an inert argon gas atmosphere (HVAC Zone 0). At operating temperature, the primary coolant salt will evaporate into the gas phase and the gas must be circulated and stripped to prevent vapors from entering the aforementioned equipment. The gas exiting Zone 0 will contain some quantity of vaporized beryllium-containing salt, so the gas must be cooled below 650K (to precipitate vapors) and filtered before being compressed and recirculated.

Equipment which has contact with the primary coolant, the vapor space above the primary coolant, or the graphite/fuel spheres (salt chemistry control equipment, cover gas control equipment, and fuel handling and storage system) should be considered to have a high probability of bearing beryllium contamination and the rooms containing this equipment may need to be considered “high hazard areas” which should not be entered during normal operation and only rarely for maintenance/repair. Entry would then require full protective gear with high-filtration respirators. Ventilation for these rooms (HVAC Zone 2) must come from the lower-hazard areas (e.g., from above the refueling deck) and the exhaust from the high-hazard area and must include a cooling/filtering stage to precipitate any beryllium-containing vapors and collect any airborne dust which may be released due to leaks or mechanical failure.

Some areas, such as airlock/dust-off cells and maintenance hatches through which material crosses the high/low hazard boundary should be treated as “quarantine areas” in which there is a reasonably high probability that objects contaminated with beryllium will be present. The potentially-contaminated object could then either be cleaned of all surface dust or sealed in an airtight container (which would then be cleaned) before moving the object out into low contamination areas. Other temporary quarantine areas may be required above the refueling deck during primary loop equipment maintenance work. These rooms/chambers may require a separate ventilation system (operating at a higher relative airflow rate) due to the high likelihood of dust being disturbed during movement, and the air should exhaust into the “high hazard” rooms.

Some hatches and doorways may be designed such that they connect directly to a “transfer vessel” which operates as a sealed “high hazard” area to move contaminated

equipment through “low hazard” space to another location for work or decontamination or disposal.

Occasionally, containers of coolant salt will also be moved through handling/loading areas (HVAC Zone 3) and/or small amounts of encapsulated salt will be transferred to containers for transportation/disposal. Workers would likely only need dust masks, goggles, and coveralls to work in these “low hazard” areas to allow the ease of movement and communication afforded by lighter personal protective gear.

Within human-occupied space, all beryllium-containing salts will be in solid form, either as suspended particles or as surface dust or coatings. Airborne dust will either settle onto surfaces or be drawn into the HVAC system and trapped in filters. A high air-changeover rate will ensure that airborne dust does not linger for significant periods, but the settled dust may still pose a hazard if disturbed or picked up by contact transfer. Surfaces should be monitored for beryllium contamination regularly (through chemical and radiometric detection) and any room found to hold significant contamination should be cleaned thoroughly and retested. One such chemical detection method, as described by Taylor and Sauer [4.10] (shown below), indicates the presence and amount of any beryllium or beryllium-containing compounds by a surface swipe-test.



Fig. 4-2 Chemical detection method of Taylor and Sauer [4.11].

4.1.4 Mixed Waste Management and Disposal

4.1.4.1 Handling, Transporting and Disposal of Beryllium Waste

The PB-AHTR, like future fusion power plants, uses beryllium due to its very favorable nuclear properties. Beryllium waste can be recycled and residual waste can be handled in similar fashion as low level radioactive waste. However, special precaution must be taken when dealing with Be powder or dust to prevent it from becoming airborne

because of its toxicity and health effects. Inhaling a small amount of beryllium dust or contact by skin could cause serious health hazards later on. Beryllium contaminated wastes must be labeled, managed and disposed in accordance with federal, state and local requirements. Low level radioactive wastes are separated by isotope and those with half life of 90 days or less is managed by storage to allow them to decay in place, whereas low level wastes that do not must be stored and then transported a disposal site. Low level waste contaminated with beryllium would be classified as mixed waste. Figure 4-3 shows a process diagram for the approach for managing such mixed waste the Lawrence Berkeley National Laboratory.

Overview of Mixed Waste Process

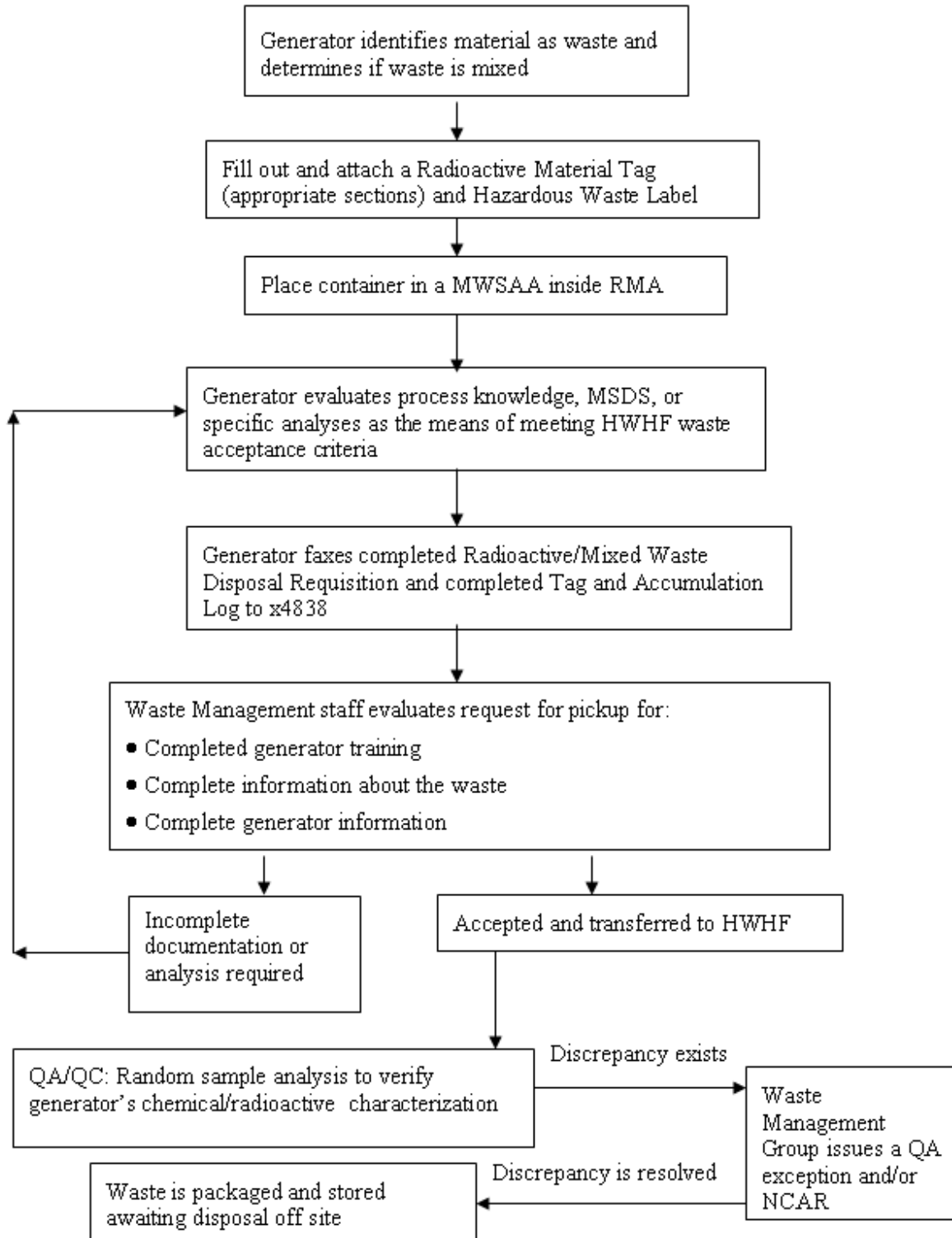


Fig. 4-3 Overview of mixed waste process [4.12].

4.1.4.2 Policy Cost and Impact due to Presence of Beryllium

Difficulty in managing and detecting beryllium dust and airborne beryllium at nuclear power plant site can raise the cost. When working with Be, a quick sampling and on site analysis is required so that there will not be a loss of operational time. This would require laboratory technicians to do the samplings and that an on-site Be analysis and Health Physics laboratory be provided to manage beryllium. As a result, this would add additional cost to building this type of plant. Much can be learned from the JET facility located in the UK, which uses beryllium components in fusion experiments. The JET facility also managed tritium. Figure 4-4 and Figure 4-5 below show that the total overall operating cost of Be-analysis and air and surface contamination monitoring at JET over the 10 years (1995-2004) period averaged 252,000 pounds or \$382,000 per year. If the PB-AHTR produces 410 MWe with an average capacity factor of 90%, this would add \$0.12 per MWhr to the electricity production cost, which is very small.

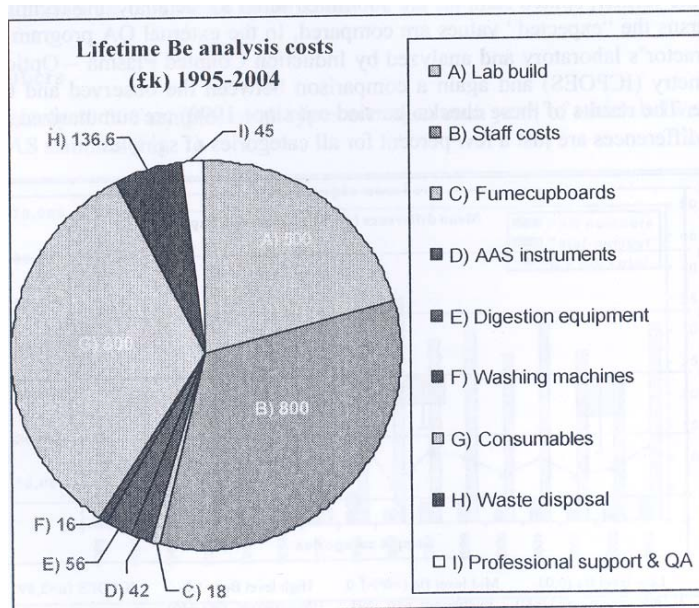


Fig. 4-2 Be analysis laboratory lifetime (ten years) running costs [4.13].

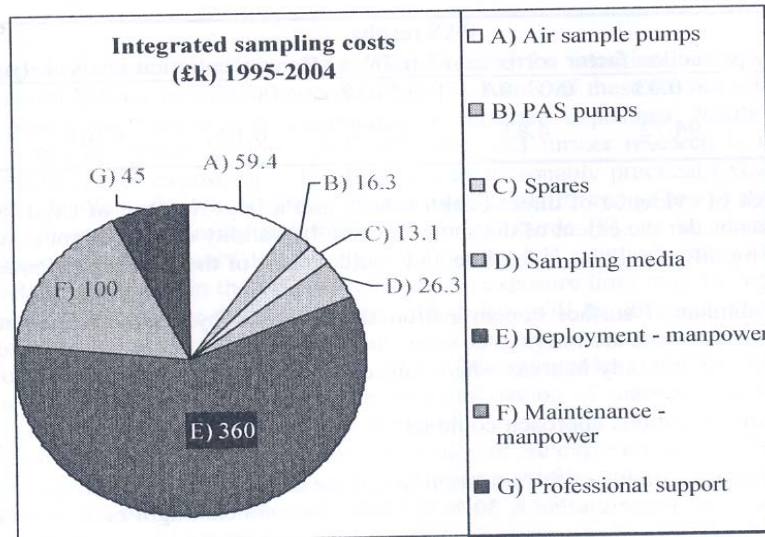


Fig. 4-5 Integrated (ten years) air and surface contamination sampling costs [4.14].

4.1.4.3 Beryllium Sampling and Methods

4.1.4.3.1 Air Samples

In the United States, procedures for using filter samplers to detect and measure beryllium and other metals in workplace atmospheres has been well standardized and published by National Institute for Occupational Safety and Health (NIOSH) and the Occupational Safety and Health Administration (OSHA) [4.15]. For personal monitoring of workplace air sample, a portable battery powered sampling pumps that pull air at a desired flow rates through the samplers can be used. These pumps are also effective for detecting radioactive contamination, and thus their use can contribute to both chemical and nuclear safety. The sampling pump is placed within the workers' personal breathing zones to provide best estimates of workers' exposures. Such pumps are likely to be used in Zone 2 of the reactor building in the equipment areas below the refueling deck, and during maintenance activities above the refueling deck when primary loop equipment is maintained, as well as in the hot machine shop when primary loop equipment is worked on. Area sampling is also possible [4.15] and will be used in Zone 2 to detect airborne beryllium and radioactive contamination. The Beryllium and Radiation Safety Group has studied methods to add a radioactive tracer to the primary salt, so that this air monitoring equipment would be able to alarm on radiation if primary salt beryllium were to become airborne. The NIOSH and OSHA methods describe "total" air samplers consisting of closed-faced sampling cassettes housing mixed-cellulose ester (MCE) membrane filters [4.15]. Table 2 shows the sampling methods for beryllium in workplace atmospheres.

Table 4-2 Governmental and consensus standard methods for sampling beryllium aerosols in workplace atmospheres [4.15].

Method(s)	Aerosol Fraction(s) Sampled	Filter Type(s) Used
NIOSH 7102 & 7300	“Total”	Membrane
OSHA ID-125G & ID-206	“Total”	Membrane
HSE 29/2 (UK)	Inhalable	Membrane
BIA 6015 (Germany)	Inhalable	Membrane
INRS Fiche 003 (France)	Inhalable	Quartz Fiber
ISO 15202-1	Inhalable or Respirable	Membrane or Fibrous
ASTM D7035	“Total,” Inhalable or Respirable	Membrane or Fibrous

4.1.4.3.2 Surface Samples

There are two well known methods of surface sampling to assess contamination and prevent dermal contact. They are “wet” sampling techniques and dry sampling techniques. “Wet” sampling techniques are generally preferred because for collection efficiency but there are instances where dry sampling techniques are required [4.15]. The NE 170A/B class toured the GE Vallecitos Nuclear Center this year, and learned that they use dry sampling techniques to detect potential contamination in the equipment and work areas. Table 4-3 shows the standardized procedures for wet and dry sampling produced by various organizations. Much more information about “wet” and dry sampling can be found in OSHA and NIOSH web pages.

Table 4-3 Standardized sampling procedures for collecting beryllium dust samples from surfaces [4.15].

Method(s)	Sampling Media/Device	Substrate(s) Sampled	Comments
OSHA ID-125G & ID-206	“Wet” or “dry” filter or wipe	Smooth surfaces, dermal samples	Alcohol wipes widely used
NIOSH 9100 & 9102	“Wet” wipe	Smooth surfaces, dermal samples	Individually packaged wipes
ASTM D 6966	“Wet” wipe	Smooth surfaces	Individually packaged wipes; ASTM E 1792 wipes acceptable for Be sampling
ASTM E 1216	Adhesive tape	Smooth surfaces	May damage fragile surfaces
OSHA Technical Manual	Patch samples, hand rinsates	Dermal samples	Various protocols; may sample clothing, gloves, etc.
NIOSH 2600, 3601, 9202 & 9205	Patch samples, hand rinsates	Dermal samples	Developed for sampling pesticides, metalworking fluids, etc.
ASTM D 5438	Modified upright vacuum cleaner	Floors	Sampling from carpets
ASTM E 1973	Sampling cassette with collection nozzle	Rough, porous, uneven surfaces	“microvacuum” Pb dust sampling (withdrawn standard)
ASTM WK4996 (work item)	Sampling cassette with collection nozzle	Rough, porous, uneven surfaces; fragile surfaces	“microvacuum” dust sampling for metals (under development; to replace ASTM E 1973)

4.1.4.4 Analysis

Beryllium samples are prepared and analyzed in the on-site analytical laboratory using beryllium dissolution techniques that have been published [4.15]. Standardized instrumental analytical methods for beryllium are based on atomic spectrometric techniques. The two most widely used instrumental methods for determining beryllium in extracts from workplace samples are graphite furnace atomic absorbance spectrometry (GFAAS) and inductively coupled plasma atomic emission spectrometry (ICP-AES) [4.15]. Table 4-4 shows the sample preparation and Table 4-5 shows the analysis of beryllium samples collected.

Table 4-4 Governmental and consensus standard procedures for preparation of beryllium samples obtained in workplaces [4.15].

Method	Sample Type(s)	Acid Mixture	Digestion Method(s)
NIOSH 7102	Air filter	Nitric & Sulfuric	Hot plate
NIOSH 7300	Air filter	Nitric & perchloric	Hot plate or microwave
NIOSH 7302	Wipe	Nitric & perchloric	Hot plate or microwave
OSHA ID-125G	Air filter, wipe, or bulk	Nitric, sulfuric, & hydrochloric	Hot plate
OSHA ID-206	Air filter, wipe (smear tab), or bulk	Hydrochloric, nitric	Hot plate
HSE 29/2 (UK)	Air filter	Nitric & Sulfuric	Hot plate
INRS Fiche 003 (France)	Air filter	Nitric & hydrofluoric	Hot plate or microwave
ASTM D7035	Air filter	Various options	Hot plate or microwave
ISO 15202-2	Air filter	Various options	Hot plate, microwave, or ultrasound

Table 4-5 Governmental and consensus standard methods for atomic spectrometric analysis of workplace beryllium samples [4.15].

Method	Instrumental Technique	Estimated Method Detection Limit ($\mu\text{g Be/sample}$)
NIOSH 7102	GFAAS	0.005
NIOSH 7300	ICP-AES	0.005
OSHA ID-125G	ICP-AES	0.013
OSHA ID-206	ICP-AES	0.0072
EPA 7091	GFAAS	0.005
EPA 200.7	ICP-AES	0.008
EPA 200.8	ICP-MS	0.001
EPA 6010B	ICP-AES	0.005*
EPA 6020	ICP-MS	0.0005*
ASTM D7035	ICP-AES	0.009
ISO 15202-3	ICP-AES	Not evaluated

4.1.4.5 Beryllium Detection Methods and On Site Monitoring

It is very important to be able to monitor beryllium particles in real-time and have an alarm system to warn humans. Table 4-6 shows the requirements for a new real-time beryllium monitor [4.13]. A real-time monitoring of Be in the air instrument has been developed for DOE/Y-12 and has shown promising results [4.13]. The Beryllium and Radiation Safety Group has also studied the use of a radioactive tracer to aid in real-time detection of beryllium.

Table 4-6 Requirements for a new real-time beryllium monitor [4.13].

No	Description of Requirement
1	Digital output display in $\mu\text{g Be}/\text{m}^3$
2	Minimum detection level $0.05 \mu\text{g}/\text{m}^3$ (or best available)
3	Measurement range 0.05 to $1,000 \mu\text{g}/\text{m}^3$
4	Fifteen-min or less response time
5	Measurement accuracy $\pm 10 \%$ (or best available)
6	Low drift for stable and reliable readings
7	Capability to log/store, and download data to other computer
8	Operation in 0-95 %relative humidity
9	Operation at 32-100°F temperature range
10	Indication that the monitor is working
11	Transportable size for field measurement
12	Corrections for common interferences
13	Correction for carryover from the previous sample

4.2 Radiation Shielding and Decay Heat Generation

4.2.1 Scope and Criteria for Radiation Shielding

As part of the radiation safety measures to be implemented for the Modular PB-AHTR, sufficient shielding must be provided for all radiation sources in the plant. This section addresses shielding for radiation sources outside of the core, as shielding for the reactor vessel has already been designed. Of primary concern are the fuel handling room and spent fuel storage cell.

Acceptable radiation dose rates for areas within the plant vary with frequency of access. For areas accessed on a daily basis, the shielding is designed to minimize the equivalent dose rate to 5 mrem/h (50 $\mu\text{Sv}/\text{h}$). Areas accessed on an infrequent basis need only to limit the equivalent dose rate to 50 mrem/h (500 $\mu\text{Sv}/\text{h}$) [4.16].

4.2.2 Depletion Analysis and Determination of the Source Term

The kernel size for the Modular PB-AHTR is to be determined and a detailed depletion analysis does not yet exist. Earlier, a 2400 MWth Integral PB-AHTR was designed with a lower power density than the Modular PB-AHTR studied in this report, which used 425 μm diameter fuel kernels inside 6 cm diameter fuel pebbles (compared to the 3 cm diameter pebbles used here), permitting an energy generation of 1.30 MWd/pebble [4.17]. Depletion analysis for the Integral PB-AHTR has been performed and was done so using ORIGEN2, V2.2 [4.18]. Here, the Integral PB-AHTR depletion data has been adapted to the Modular PB-AHTR design by maintaining the carbon-to-heavy metal atom ratio and the discharge burn-up constant between the two designs [4.19]. This allows the decay heat and gamma radiation levels of the Modular PB-AHTR pebbles to be calculated based on the earlier simulations for the Integral PB-AHTR design.

Compared to the Integral PB-AHTR, the Modular PB-AHTR uses 3 cm diameter fuel pebbles and relocates half of the graphite volume to the pebble channel structures. In order to preserve the carbon-to-heavy metal atom ratio, a Modular PB-AHTR fuel pebble must be loaded with approximately twice the heavy metal per unit volume as an Integral PB-AHTR fuel pebble. Based on this criterion and the pebble volume (the ratio of the pebble radii raised to the third power), the mass of heavy metal in one Modular PB-AHTR fuel pebble is one fourth that of an Integral PB-AHTR fuel pebble. If the discharge burn-up is to be the same for the Integral and Modular designs, then it is required that there be 2.519 g heavy metal (equivalent to 2.837 g $UC_{0.5}O_{1.5}$ at 10% initial enrichment) per Modular PB-AHTR fuel pebble. Taking the ratio of the latter number to the mass of a 425 μm fuel kernel, it is determined that one Modular PB-AHTR fuel pebble contains 6720 425 μm fuel kernels. To adjust the ORIGEN output from the original Integral PB-AHTR design calculations to a per pebble basis for the Modular design requires multiplication by the number of 425 μm fuel kernels per pebble.

Using the ORIGEN2 cross-section libraries written by Massimiliano Fratoni for the Integral PB-AHTR, calculations were made to determine the photon spectra and thermal decay heat generation rates at times of interest [4.20]. For both quantities, cumulative totals were taken over all three of ORIGEN's nuclide segments (activation products, actinides and daughters, and fission products). Photon emission rates were kept separated into the eighteen average energy groups provided by ORIGEN. Gamma radiation is the only source for which shielding was considered; alpha and beta radiation will be stopped within the fuel pebble.

4.2.3. Fuel Handling Room Shielding

The fuel handling room must provide shielding for fuel pebbles of various stages of burn-up and decay time. The overall radiation source strength is a function of the number of pebbles present, the extent of the burn-up of each, and the time that each has had to decay after moving out of the reactor core. In turn, the number of pebbles present is a function of the pebble residence time in the fuel handling cell, where pebbles are monitored and then transferred, over a certain total residence time, either back to the core or into a fuel storage canister. Specific operating conditions fix the recirculation interval and residence time, and therefore the number of pebbles present is also fixed, as given in Table 4-7.

Table 4-7 Modular PB-AHTR operating condition parameters [4.21].

	Normal Operation	Three Day Defuel
Pebble recirculation interval	4.5 s	0.43 s
Pebble residence time in fuel handling room	30 min	6 min
Pebble decay time in defueling chute, or following reactor shutdown, before entering fuel handling room	1.9 d	1.0 d
Number of pebbles in fuel handling room	400	840

The exact geometry of the pebble transport system within the fuel handling room is currently unknown. Likely source geometries, in particular pebbles in a transport pipe and pebbles collected together on a planar surface, were considered instead. In both cases, all pebbles were assumed to have entered the fuel handling room fully depleted and having decayed (by residence in the defueling chute or following shutdown of the reactor prior to defueling) for the minimum pebble decay time prescribed in Table 4-7. The pebble activity was assumed to remain constant throughout the time spent in the fuel handling room. These assumptions allowed the source strength to be described by the ORIGEN output and the source geometries to be treated as homogeneous.

Conservatively neglecting radiation attenuation within the pebble itself, the situation of pebbles arranged linearly in a transport pipe can be described as a line source, with the source collapsed to the line passing through the center of each pebble. The linear source strength is a function of the number of pebbles present and the distance between adjacent pebbles; it is strongest for a fixed number of pebbles when they are closest together, which occurs when the quadrants of each of the juxtaposed pebbles are in contact. If the line source is homogeneous, the photon fluence rate attains its maximum value along the line's perpendicular bisector.

Again neglecting attenuation in the pebbles themselves, the case of pebbles arranged on a flat surface can be described by a plane source, where the plane source is that which passes through the center of each pebble. The planar source strength depends upon the number of pebbles present and is strongest when they are the least diffuse. This occurs when the pebbles are arranged in a circle, as close to one another as permitted by the packing factor. If the disc source is homogeneous, then the photon fluence rate is greatest along the perpendicular axis passing through its center.

The possibility of using localized heavy shielding material, lead in particular, was considered. Although the arrangement of the layered absorbers is unknown, it will always be true that there is less secondary radiation produced if the material of lower atomic number is located nearer to the source. Therefore, the opposite case was assumed, so that regardless of the arrangement the results would be appropriate for even the extreme case. For both geometries, the source was assumed to be placed against the wall and the dose rate was calculated for a point directly opposite, on the line along which the source attains its maximum fluence rate. Results of the calculation for both geometries and the two operating conditions of Table 4-7, without lead shielding, are presented in Table 4-8.

Table 4-8 Concrete thickness necessary to achieve specified equivalent dose rate for the given source geometry, without the use of intermediate lead shielding.

	5 mrem/h	50 mrem/h
Line Source Geometry	Normal / Defuel	Normal / Defuel
Ordinary Concrete, 2.35 g/cm ³ density	125 cm / 125 cm	105 cm / 105 cm
Barytes Concrete, 3.60 g/cm ³ density	90 cm / 90 cm	75 cm / 75 cm
Disc Source Geometry	Normal / Defuel	Normal / Defuel
Ordinary Concrete, 2.35 g/cm ³ density	145 cm / 150 cm	125 cm / 130 cm
Barytes Concrete, 3.60 g/cm ³ density	100 cm / 100 cm	90 cm / 90 cm

One building design goal is to not have the walls of the fuel handling room exceed 100 cm in thickness in areas where penetrations (e.g., valve stems) are needed. The results of the calculation indicate that this minimum thickness can be achieved, even without the use of lead, by using special shielding concrete such as barytes. Furthermore, for a given geometry and shielding material, the dose rate from a three day entire core offload that takes place 24 hours after shutdown is only slightly greater than the dose rate generated under normal operating conditions (often, they are equal to within ± 5 cm). It will require little extra in the way of material to shield for the more extenuating circumstance and it is not worthwhile to wait longer than 24 hours before offloading the core.

4.2.4 Spent Fuel Storage Cell Shielding

The spent fuel storage cell (SFSC) shielding was modeled using MCNP5, V1.4 [4.22]. Room dimensions match those supplied by the Mechanical and Plant design team. Sixteen fuel storage canisters are positioned in the cell such that the wall-to-quadrant and quadrant-to-quadrant spacing is equal in the lateral and horizontal directions, with each direction considered separately.

Individual canisters were homogenized in space and time. Spatial homogenization began with the TRISO fuel particle and worked up to the canister. Component properties were weighted by volume so that the mass of each constituent was conserved. Material comprising the canister walls was conservatively neglected and the volume of the canister occupied by the pebbles was determined using the core packing factor (0.60). Homogenization in time was based on the operating procedure that will specify that one canister is to be filled to completion before pebbles are inserted into another canister. Using the normal recirculation interval for a full core, it is determined that it takes about 250 days to fill a single spent fuel canister (683000 pebbles). The radiation source strength from one canister is greatest at the exact moment that the last pebble is inserted, at which time each pebble in the canister has decayed for an average of 125 days.

The radiation field in the SFSC depends strongly upon which canisters are filled, the order in which canister filling is carried out, and the contents of the remaining canisters. It was conservatively assumed that the eight loaded canisters were situated closest together; that is, eight adjacent canisters filled in a 2 x 4 pattern at one end of the spent fuel storage facility and the remaining eight were empty. To remove the variability associated with the order in which the canisters are loaded, the average decay age of all pebbles was assumed to be 125 days.

Sufficient particle simulations were carried out to reduce relative error to an acceptable value. Detectors were placed at various concrete depths and tally multipliers and dose functions were used to determine the point of maximum dose and the concrete thickness required to attenuate the gamma fluence to achieve an acceptable dose. Requisite shielding varies depending upon which wall is under consideration. The thickest shielding dimension is reported in Table 4-9 for two different concrete types.

Table 4-9 Concrete thickness necessary to achieve specified equivalent dose rate around the Modular PB-AHTR SFSC.

	5 mrem/h	50 mrem/h
Ordinary Concrete, 2.35 g/cm ³ density	130 cm	100 cm
Barytes Concrete, 3.60 g/cm ³ density	100 cm	80 cm

The assumptions made in this model were conservative, but not without good reason. It is expected that one canister in the spent fuel storage facility will hold partially burned pebbles during a maintenance outage (the volume of a single canister is sufficient to hold one full core offload). Another canister will be assigned to contain the broken pebbles. Both of these two special canisters will add to the radiation field strength and should be kept in mind during future detailed design for concrete wall thicknesses for radiation shielding. If it is still desired to decrease the concrete wall thicknesses for the SFSC, an operating procedure will need to be drafted that stipulates the location and order in which canisters are filled so as to minimize the fluence rate outside the SFSC. Future detailed analysis for radiation shielding around the SFSC should also consider the possible radiation damage to the rubber components of the seismic base isolators located below the SFSC.

4.2.5 Thermal Decay Heat Generation Rate

Thermal decay heat generation rates were calculated for the interval from zero to five years, which is the time at which it is expected that the spent fuel pebbles can be transferred from canisters within the SFSC to dry cask storage outside of the reactor building. The results of the calculation for a single Modular PB-AHTR fuel pebble are plotted in Fig. 4-6.

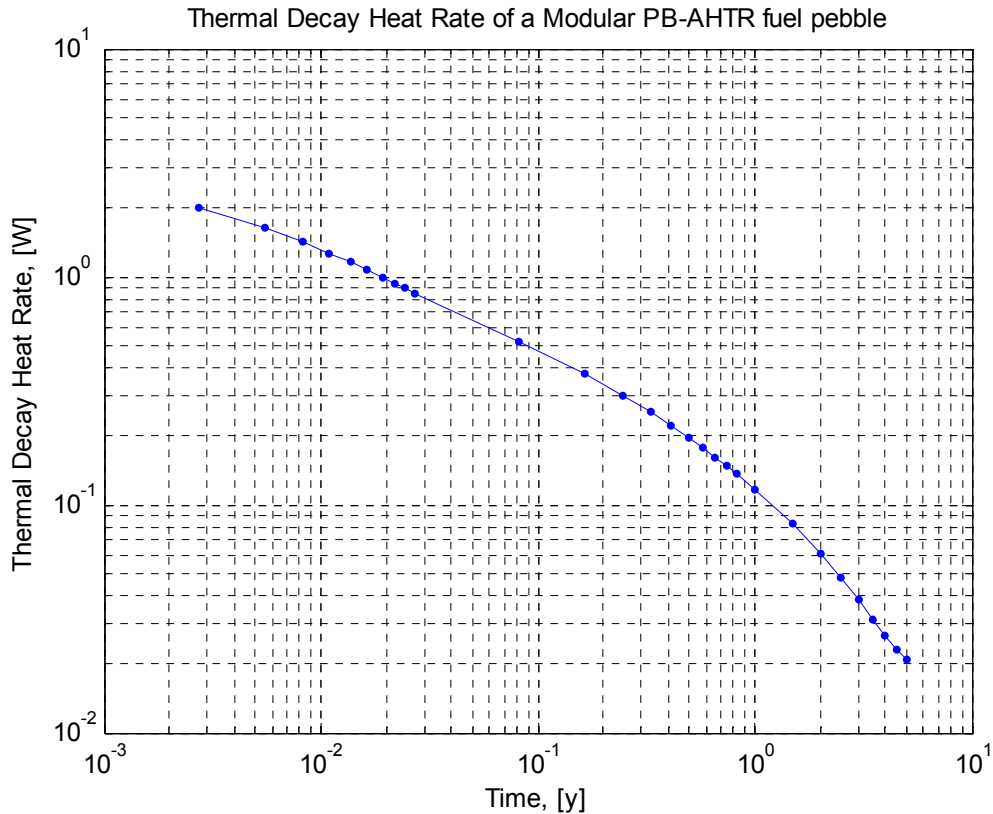


Fig. 4-6 Thermal decay heat rate as a function of time for a single Modular PB-AHTR fuel pebble.

The thermal decay heat rate of a single spent fuel canister at a given time is obtained by summing the thermal decay heat rates from all of the pebbles, each of which was removed from the reactor core at a different time. Functionally, both the number of pebbles present at a given time and the instantaneous thermal decay heat rate are functions of time. The maximum value for the thermal decay heat rate in a spent fuel canister occurs at the moment the last pebble is inserted. For normal operation, the time to fill a single canister is about 250 days; a three day entire core defuel (started after one day of shutdown) fills a single canister in three days with pebbles that have decayed for at least one day each.

Two operating conditions were considered, each characterized by the parameters in Table 4-7. During normal operation, spent pebbles are continuously inserted into a canister until that canister is full. During a maintenance outage, all 630000 partially burned pebbles in the core are loaded into one empty spent fuel canister so that they can be reinserted into the core after the outage is complete. The results are given in Fig. 4-7.

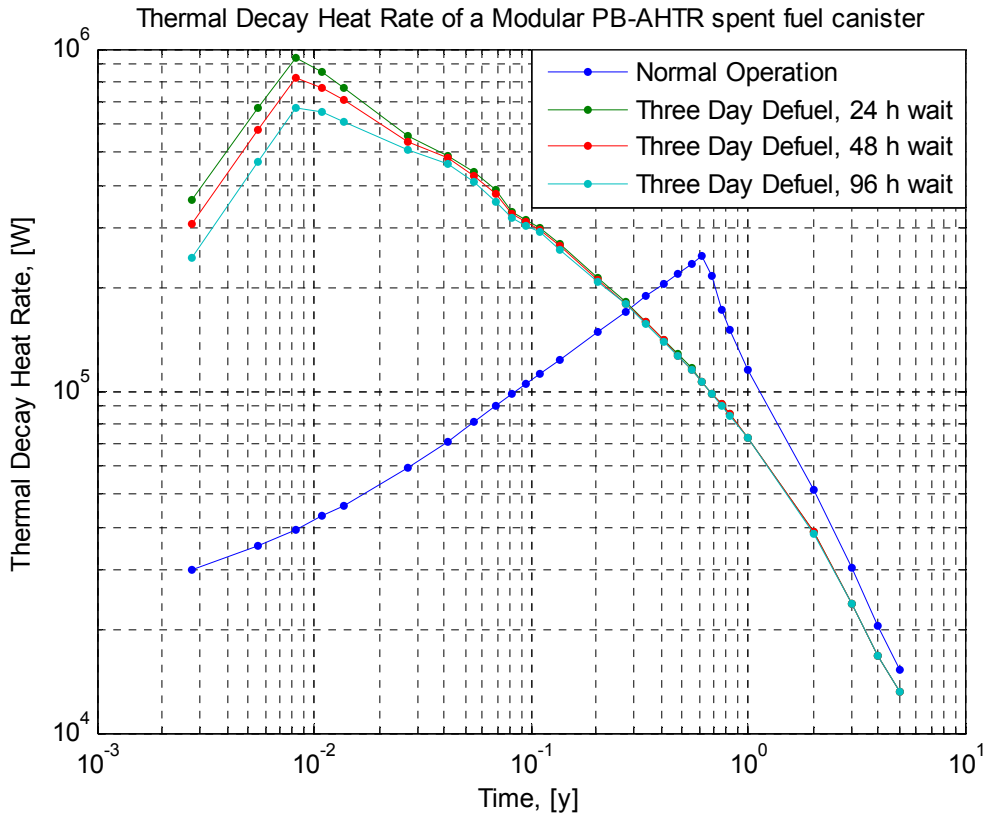


Fig. 4-7 Thermal decay heat rate as a function of time for a single Modular PB-AHTR spent fuel canister loaded under normal operating conditions and during a three day entire core defuel.

4.3. HVAC and Access Control

4.3.1 Introduction and Purpose of Zoning

Regions within the Modular PB-AHTR reactor building are divided into zones according to the level of their potential chemical and radioactive contamination hazard. Beginning with Zone 0 to denote the region of greatest contamination, zone numbers increase with decreasing chemical and radioactive contamination hazard. Zoning is based on the principle that zone pressure should decrease as contamination increases, so that hazardous gaseous material released into a given zone will flow only to zones equipped to handle an even greater hazard and there will be no affect on less restricted zones. Within zones, ventilation flows occur from regions of low potential contamination to regions of higher potential contamination. To monitor environmental releases, all gas exiting the reactor building and turbine hall is directed to an exhaust stack and is continuously monitored.

4.3.2. Definitions of the PB-AHTR Zones

Zone 0. Zone 0 is defined as the primary argon cover gas for the reactor pressure boundary. The argon gas is supplied from the cover gas control system and enters at the control rod drive penetrations in the reactor and through the gas of the Pebble Transfer

System and exits at pump seal bowls to return to the cover gas control system, where it is filtered and can be purged of tritium. All maintenance in Zone 0 is performed remotely. Under accident conditions, the supply and return lines to the cover gas control system are isolated automatically by fail-closed valves.

Zone 1. Zone 1 consists of three separate sub-zones: (1a) the reactor cavity and the intermediate heat exchanger cavities, (1b) the fuel handling area, and (1c) the spent fuel storage cell. Zone 1 operates at a minimum temperature of 550°C, and heat loss to the cavity walls is minimized by a cavity insulation system. Dry nitrogen is used as the gas, which is supplied by the Zone 1 ventilation system and enters at the bottom of the reactor cavity and through the wells of the intermediate heat exchangers and exits at the top of the reactor cavity. Gas flow through Zone 1 is driven by buoyant forces, due to heating of the gas by the reactor vessel. The Zone 1 ventilation system includes a heating system which is used to maintain the minimum temperature under shutdown and defueled condition. All maintenance within Zone 1 is performed remotely. Under accident conditions, the supply and return lines to the Zone 1 ventilation system are isolated automatically by fail-closed valves, and Zone 1 functions as a low-pressure, low-leakage containment.

Zone 2. Zone 2 is made up of the crane room above the refueling deck, the fuel handling area, the intermediate heat exchanger isolation valves and maintenance areas, the primary salt chemistry control system and the cover gas control and Zone 1 ventilation systems. The gas in Zone 2 is HEPA filtered ambient air, which follows a flow path from the reactor high bay space to various other locations within Zone 2, with exhaust ducts located in areas with highest potential contamination. Exhaust flows are also HEPA filtered, and under accident conditions Zone 2 acts as a filtered confinement. Human access is allowed, although security clearance is required and radiation exposures are monitored via the Radiation Control Access system.

Zone 3. Zone 3 comprises the above-grade corridors between the reactor citadel and the three external walls on the reactor building. The fresh fuel storage room is located below-grade in Zone 3. Filtered ambient air serves as the gas for Zone 3; it enters from outside of the building and exits the building at miscellaneous locations. It may be necessary to filter air exiting Zone 3 to lower hazard areas. Zone 3 is a secured access area in which chemical and radiation contamination will be monitored, although it is desired to specify an appropriate air changeover rate so that this requirement is minimized.

Zone 4. Zone 4 is the turbine hall. Filtered ambient air is used as the gas and will flow from the bottom of the turbine hall to the top of turbine hall. Heat generation from the turbomachinery aides gravity driven flow to the exhaust ducts. Zone 4 is human accessible. There is no personnel access from the turbine hall into the reactor building, and thus the turbine hall requires the lowest level of security clearance.

Table 4-10 provides a comparison of the requirements for each zone. The criteria for changeover rates are based on norms used currently in the nuclear industry [4.23]. Volumetric flow rates are those that would have to be produced by the HVAC systems in order to meet the specified changeover rate. The HVAC system (ducts, filters, heaters, coolers, and blowers) for Zone 2 should be designed such that the flow velocity is never

less than 1 m/s to prevent blowback into less contaminated zones and particulate settling [4.23]. Furthermore, considering the large number of HEPA filters that may be required to decontaminate the air in Zone 2, the blowers must generate sufficient head to maintain the minimum flow velocity.

Table 4-10 Modular PB-AHTR reactor building zones.

	Gas	Volume	Pressurization	Changeover Rate	Volumetric Flow Rate
Zone 0 (Red)	Argon	10 m ³	- 3.0 mm to - 6.0 mm H ₂ O	0/h to 1/h	0 m ³ /s to 0.003 m ³ /s
Zone 1 (Yellow)	Dry Nitrogen	3100 m ³	- 2.0 mm to - 5.0 mm H ₂ O	0/h to 10/h	0 m ³ /s to 9 m ³ /s
Zone 2 (Green)	Ambient Air	8400 m ³	- 1.0 mm to - 2.0 mm H ₂ O	6/h to 40/h	14 m ³ /s to 93 m ³ /s
Zone 3 (Blue)	Ambient Air	13600 m ³	- 0.3 mm to - 0.9 mm H ₂ O	6/h to 40/h	23 m ³ /s to 150 m ³ /s
Zone 4 (Purple)	Ambient Air	32400 m ³	- 0.3 mm to - 0.9 mm H ₂ O	6/h to 40/h	54 m ³ /s to 360 m ³ /s

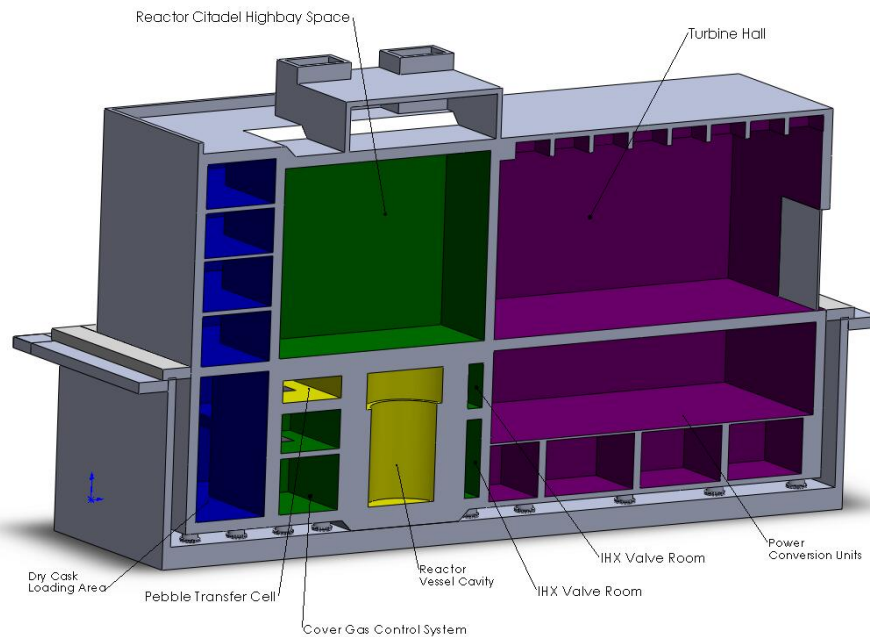


Fig. 4-8 Modular PB-AHTR reactor building zones. Colors correspond to those in Table 4-10. Image courtesy of the Plant and Mechanical design team. For more images of the zones within the Modular PB-AHTR building, the see Chapter 2.

4.4 References

- 4.1 M. Herr, “Defense Programs, Beryllium Good Practice Guide” July 1997.
- 4.2 U.S. Department of Labor: Occupational Safety & Health Administration, “Preventing Adverse Health Effects from Exposure to Beryllium on the Job.”
- 4.3 Niosh Pocket Guide to Chemical Hazards, Department of Health and Human Services, September 2007 pg. 28
- 4.4 Brush Wellman Engineered Materials, Materials Safety Data Sheet – No. M12
- 4.5 Evaluated Nuclear Data File (ENDF) Michal Herman, NNDC, Brookhaven National Laboratory <http://www.nndc.bnl.gov/exfor/endl00.htm> (fig. 1 and 2)
- 4.6 Neutronic and Depletion analysis of the PB-AHTR Massimiliano Fratoni, Ehud Greenspan and Per F. Peterson Global 2007, Boise, Idaho, September 9-13 (fig. 3)
- 4.7 “Radiation detection and Measurement” third edition, Glenn F. Knoll ©2000 John Wiley & Sons, inc.

- 4.8 Lund Nuclear data file, Department of Physics, Lund University, Sweden
<http://nucleardata.nuclear.lu.se/Database/es/>
- 4.9 29CFR1910.120
- 4.10 T.P. Taylor and N.N. Sauer, "Beryllium colorimetric detection for high speed monitoring of laboratory experiments," *Journal of Hazardous Materials*, vol. 93, p. 271, 2002
- 4.11 G. Fukuda, "Vapor Liquid Equilibria of the Ternary Lithium Fluoride-Sodium Fluoride-Beryllium Fluoride System," Doctoral thesis, Spring 2006.
- 4.12 <http://www.lbl.gov/ehs/waste/images/pub-3092/ch3-overview.gif>
- 4.13 Meng-Dawn Cheng, Robert W. Smithwick, III, and Ray Hinton, "Use of Electrically Enhanced Aerosol Plasma Spectroscopy for Real-Time Characterization of Beryllium Particles", Beryllium Sampling and Analysis, ASTM International, August 2006.
- 4.14 Darryl Campling, Bharat Patel, "Sampling and Analysis of Beryllium at JET: Policy Cost and Impact", Beryllium Sampling and Analysis, ASTM International, August 2006.
- 4.15 Kevin Ashley, Michael J. Brisson, and Steven D. Jahn, "Standard Methods for Beryllium Sampling and Analysis: Availabilities and Needs", Beryllium Sampling and Analysis, ASTM International, August 2006.
- 4.16 D. Peterson, Diablo Canyon Power Plant, Personal communication, 21 March 2008.
- 4.17 M. Fratoni, E. Greenspan, and P.F. Peterson, "Neutronic and Depletion Analysis of the PB-AHTR," Proceedings of Global 2007, Boise, Idaho, 9-13 September 2007, pp.856-865.
- 4.18 A.G. Croff, "ORIGEN2: A Versatile Computer Code for Calculating the Nuclide Compositions and Characteristics of Nuclear Materials," Nuclear Technology, Vol. 62, September 1983.
- 4.19 M. Fratoni and P.F. Peterson, U.C. Berkeley Department of Nuclear Engineering, Personal communication, 12 March 2008.
- 4.20 M. Fratoni, U.C. Berkeley Department of Nuclear Engineering, Personal communication, 8 March 2008.
- 4.21 P.F. Peterson, U.C. Berkeley Department of Nuclear Engineering, Personal communication, 20 March 2008.
- 4.22 X-5 Monte Carlo Team, "MCNP - A General Monte Carlo N-Particle Transport Code, Version 5," LANL 2003.
- 4.23 D. Turner, GE Vallecitos Nuclear Center, Personal communication, 9 May 2008.

5. PB-AHTR STRUCTURAL AND SEISMIC DESIGN

The Structural and Seismic Design (SSD) Group studied two primary topical areas for the PB-AHTR design: the structural design of the reactor building for seismic and external event loads, and the response of the reactor pebble bed to seismic accelerations. The following sections review this work

5.1 Introduction - Summary of Design and Interface Requirements

The PB-AHTR uses a seismically base isolated reactor building, which is constructed with approximately half of the building below grade and half above. This places the reactor refueling deck and turbine deck at ground elevation. The physical arrangement of the building emphasized the creation of continuous diaphragms at the roof, refueling and turbine deck, and foundation, along with a larger number of additional diaphragms, to maximize the building's strength and stiffness while minimizing its mass. The turbine hall (Zone 4) and the hallways around the other 3 sides of the reactor citadel (Zone 3) protect the citadel (Zones 0, 1, 2) from external events such as aircraft crash. The design envisions modular construction of the building, where building modules would be factory constructed and then assembled at the reactor site, and would emphasize the use of steel-plate for reinforcing so that the plates can also serve as the forms for pouring concrete. Because the 36-m high building is half the height of a comparable light water reactor or modular helium reactor, it is expected that construction times will be reduced greatly.

The seismic loads on the building are damped by an array of base isolators. These seismic isolators are a composite structure, composed of alternating laminated layers of rubber sheets and thin steel plates that may surround a lead core to provide damping (Figure 5-1).

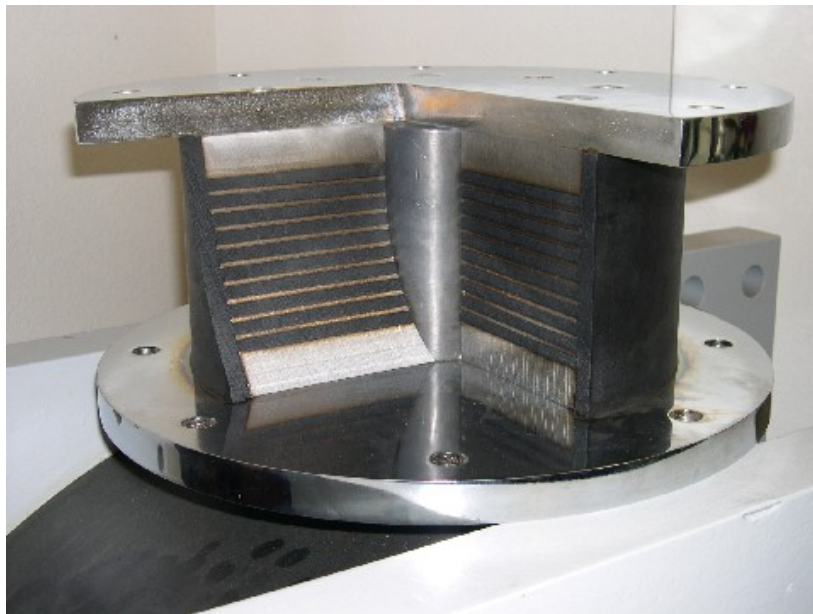


Fig. 5-1 Cross-sectional view of a typical base isolator used for the PB-AHTR building

The base isolators will dampen higher frequencies and make the reactor building oscillate at a lower frequency, reducing damage and impact during an earthquake. The isolators have an approximate total height of one meter and can sustain shear strains of up to 200% of this dimension. A schematic of the base isolator array is shown in Fig. 5-2.

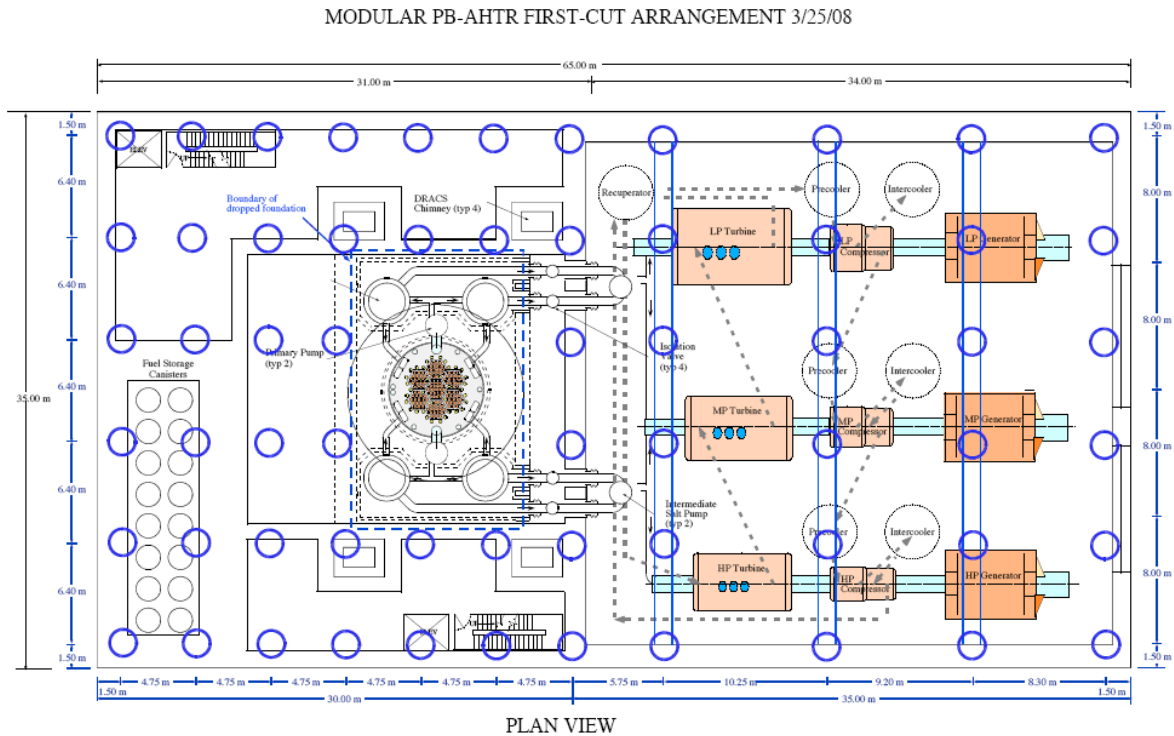


Fig. 5-2 The base isolator array (blue circles).

The final placement of the base isolators was a collaborative effort between the SSD Group and the Plant and Mechanical Design Group. In general, the optimal placing of the base isolators was under the major walls in the reactor building and under ribs crossing under the turbine hall, which help the gravity loads to be distributed on the base isolators.

The PB-AHTR reactor building is designed to respond safely to a variety of external events, including the crash of a large commercial aircraft, such as an Airbus A238 (Fig. 5-3). After an aircraft crash, the physical integrity of the reactor containment boundary (Zones 0, 1, and 2) should be preserved and the capability to shut down the reactor and remove decay heat should be maintained. An analysis was done to estimate the momentum transferred during an aircraft crash and the outer walls of the reactor building and the seismic base isolation system were designed accordingly.

The design of this base isolation system, and the response of the building to aircraft crash, is discussed in greater detail in section 5.2 of this report.



Fig. 5-3: The Airbus A380. This is the largest commercial aircraft being used today.

In the design of pebble-bed reactors, the potential exists that seismic motion could generate motion in the pebble bed, and that expansion or contraction of the bed could cause undesirable reactivity changes. For this reason it is necessary to study the seismic response of pebble beds. Here this was done by constructing a scaled experiment, called the Pebble Seismic Test (PST) experiment. In this experiment, a scaled version of a lower pebble plenum of a PB-AHTR pebble channel assembly in the reactor core was built to investigate the effect of seismic loading on the core. To match the hydrodynamic response of a 3-cm diameter pebble in flibe, 1.25-cm (0.5 in) diameter polyethylene spheres were used with water. The entire PST system is shown in Figure 5-4. Seismic loads were simulated by a test shake table and the displacement of the pebbles was measured to obtain an improved understanding of how the fuel pebble bed would respond to an earthquake. Section 5.3 discusses the experiment design and results in greater detail.

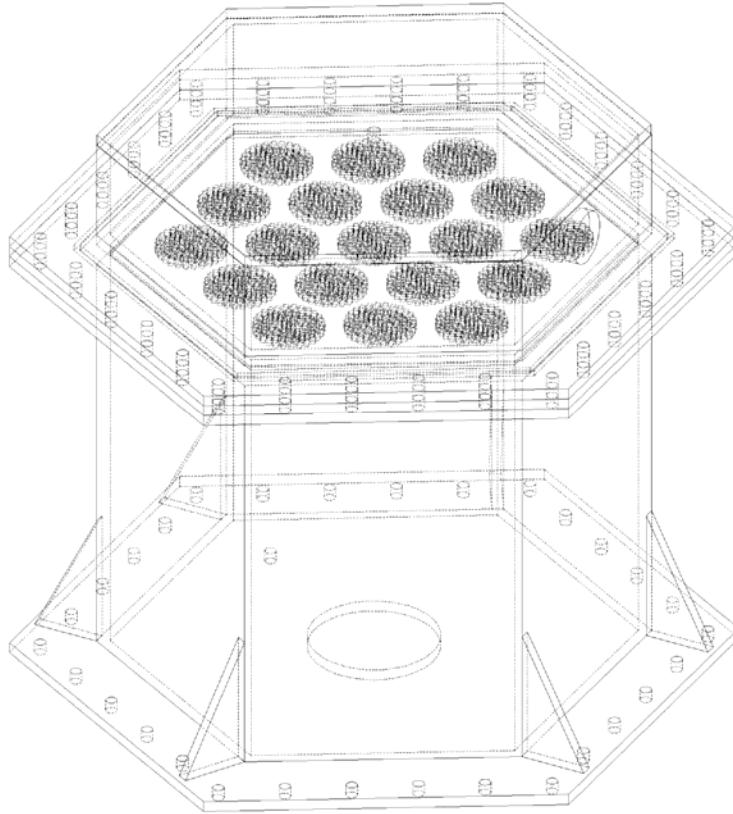


Fig. 5-4 The PST Experimental design.

Overall, the Structural and Seismic Design Group worked to ensure the structural integrity of the reactor building, reactor safety systems, and reactor core under seismic and external event loads.

5.2 Structural Design

5.2.1 Definition of Loading

The PB-AHTR reactor, sphere transfer system, and spent fuel storage canisters contain highly radioactive materials. Therefore we must design the reactor building structure to contain hazardous material and protect safety-related equipment even under extreme loading, including earthquake and aircraft impact events. The reactor and pebble transfer system are located inside a reactor “citadel,” and the spent fuel storage canisters in a below-grade portion of the building next to the citadel. The citadel is surrounded by an external events shield that includes hallways round three of the four quadrants of the reactor citadel, and the turbine hall on the fourth quadrant. The external events shell holds primarily non-safety-related equipment, as well as redundant safety-related equipment such as the three battery power trains, which are located in the three different quadrants of the building. All of these structures and equipment are located on a single base-isolated foundation using rubber base isolators.

5.2.1.1 Seismic Demands

Initial design of the isolators was performed by using response spectrum analysis of the building model. The structure was modeled as a rigid building on an isolation plane with freedom to translate in both horizontal directions and to rotate about the center of mass. A modal analysis of this structure with coupled torsional motion was run. The model was subjected to the Newmark and Hall, median plus one standard deviation, elastic design spectra for 15% damping (as presented in Chopra, 1995). This spectrum was scaled to a peak ground acceleration, PGA, of 0.5g and is reproduced in Figure 5-5.

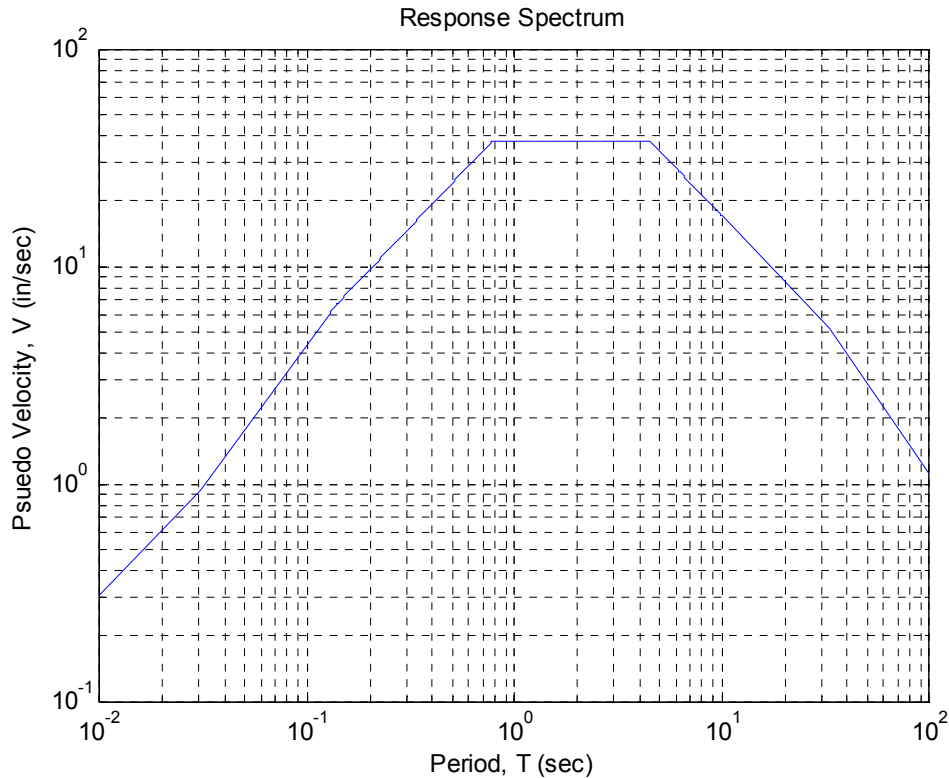


Fig 5-5 Newmark and Hall 0.5g response spectrum.

From this analysis, we first specified the number and size of the isolators which allowed us to find the structural stiffness. Using the calculated period of 3.61 seconds and total structural weight of 56,300 metric tons (123,860 kips) an elastic time history analysis was performed based on the central difference method (presented in Chopra, 1995). The structure was subjected to ground motions scaled to 0.5g in order to ascertain the accelerations and displacements of the isolated reactor during seismic events. The displacements calculated from the time history were checked against a Bispec analysis of the same model and were also used as the input excitations for the PST shake table experiments. These motions, further scaled to 0.1g in order to accommodate the stroke and velocity limitations of the Davis Hall shake table (hence, not design level), are displayed in Figure 5-6. The design level acceleration (0.5 g) was then used subsequently in shake table experiments conducted at the Richmond Field Station.

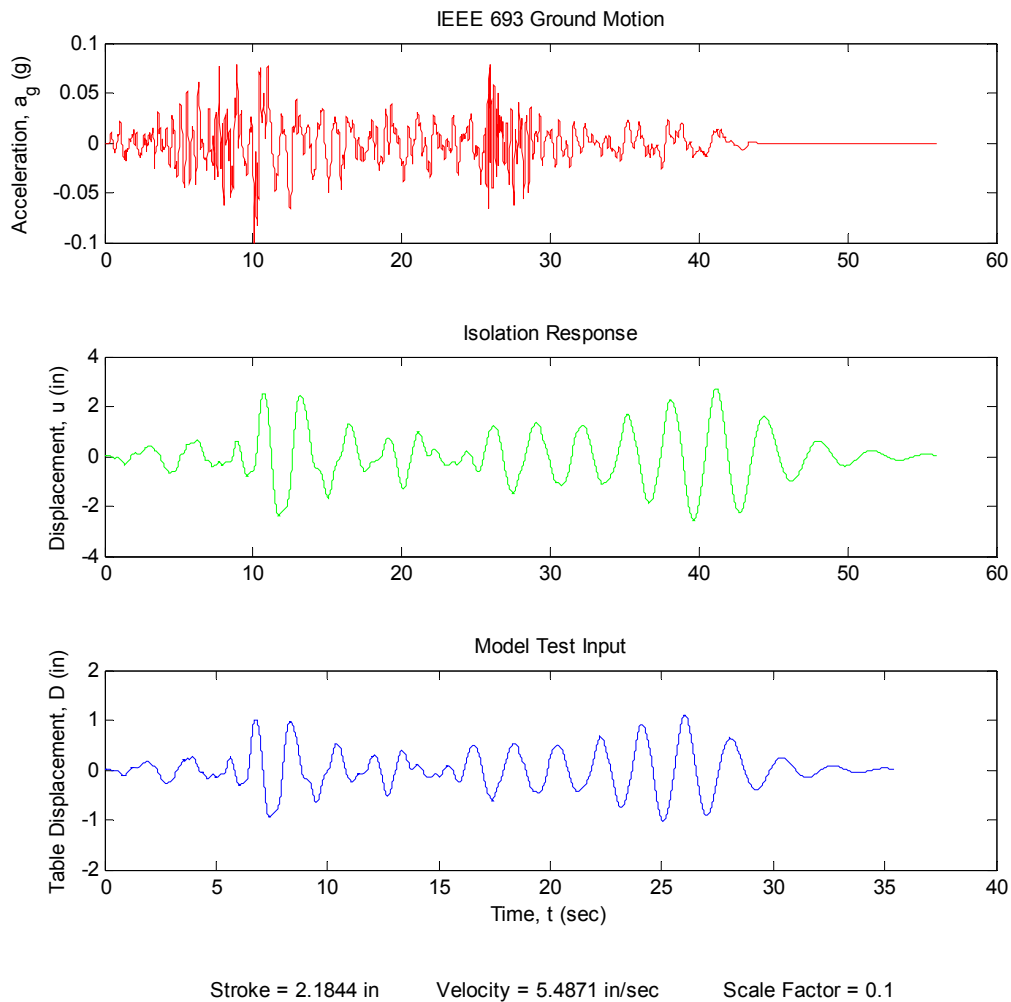


Fig. 5-6 Ground motion, isolator response, and table motion

5.2.1.2 Aircraft Impact Loading

Simulation of an aircraft collision with the above-grade portion of the building external events shell was achieved through a simple momentum conservation calculation, assuming an aircraft mass of 500 metric tons (1,100 kips), impact speed of 200 meters per second (447 miles per hour), and collision time of 0.25 seconds. The assumed aircraft mass is midway between the maximum takeoff weight of a Boeing 747 (440 t) and an Airbus A238 (590 t). With a total base isolated mass of roughly 56,300 metric tons (123,860 kips) and the assumption that the collision is inelastic and delivers its momentum uniformly over the collision time, the acceleration of the building during the collision is 8.0 m/s^2 (0.82 g). The initial structural velocity can be calculated and then converted to a maximum displacement and acceleration by considering the system a single degree-of-freedom system undergoing damped free vibration. From this simple analysis, the maximum isolator displacement was found to be 0.815 meters (32.1 inches). While this simple analysis indicates that the PB-AHTR structure is heavy enough that the

accelerations induced by aircraft crash are acceptable, further design analysis would be needed to study the potential torsional moment on the building and its effect, and the localized inelastic response of the structure in the area where the aircraft contacts the building.

5.2.2 Design of the Base Isolation System

Base isolation systems feature a collection of horizontally flexible devices that decouple the superstructure from the ground undergoing lateral earthquake excitation. In doing so, the fundamental period of the structure is significantly increased, inducing lower spectral accelerations and higher isolation plane displacements. Due to the significant decrease in accelerations transmitted to the superstructure, isolation systems are ideal for use in structures containing relatively heavy, acceleration-sensitive equipment, such as the PB-AHTR reactor vessel.

The most important consideration in selecting a base isolation system for this structure is the unevenly distributed dead load. In the modular PB-AHTR, nearly 60% of the weight is located in the reactor hall, a characteristic that shifts the building center of mass and makes the building susceptible to torsion or twist about a vertical axis under seismic ground motion. Torsional excitation will cause isolators near the perimeter of the building to displace more than the other isolators when the ground motion induces response from the coupled modes. The use of pendulum isolators, which use a sliding bearing on a dished surface and therefore displace vertically when they are deformed laterally, is not practical in a building where torsion is anticipated because differential vertical displacements can be detrimental to equipment as well as the building diaphragms. Therefore, an isolation system that only deforms laterally is the wisest choice for the PB-AHTR.

The base isolation system chosen for this structure is high damping rubber (HDR) bearings. HDR bearings are cylindrical in shape with a cross section that consists of alternating layers of stainless steel and rubber. The inclusion of thin steel layers between rubber layers assures that the bearing deforms laterally in shear instead of bending in a rocking-like motion and adds stability to the bearing. The period of an isolator is a function of its lateral stiffness, K_H , and the gravity load on the isolator, W .

Isolator configurations are limited by the required number of stable isolators and the geometry of the structure itself. In the reactor hall, the base slab immediately below the reactor and IHX cavities was designed to be lower in elevation than the rest of the base slab as a security measure to make physical access immediately below the reactor cavity impossible. Consequently, isolators cannot fit under this lowered area of the foundation slab. Instead the load has to be carried by the isolators on the boundary of the lowered slab. It is for this reason that, as well as the fact that the reactor hall is heavier, that isolators are more closely spaced under the reactor hall. Under the turbine hall the location of isolators was governed by the location where north-south ribs, or walls, could be located without interfering with the cross-over ducts between the turbines and compressors. Hence the horizontal spacing of isolators is not uniform in the turbine hall. The final layout and a summary of design parameters are presented in Table 5.1.

Table 5.1 Summary of Isolator Geometry, Properties, and Response Parameters

Base Isolation Design Summary	
Total Dead Load	$W = 123860 \text{ kips} = 56300 \text{ metric tons}$
Number of Isolators	$n = 62$
Isolator Height	$t = 18 \text{ in} = 0.46 \text{ m}$
Isolator Diameter	$D = 60 \text{ in} = 1.52 \text{ m}$
Rubber Shear Modulus	$G = 100 \text{ psi} = 689.5 \text{ kPa}$
Allowable Bearing Pressure	$p_{\max} = 1500 \text{ psi} = 10.34 \text{ MPa}$
Translational Stiffness	$K_t = 973.89 \text{ k/in} = 17428 \text{ metric tons/m}$
Isolated Period	$T = 3.61 \text{ sec}$
Maximum Displacement	$u_{\max} = 32.38 \text{ in} = 0.82 \text{ m}$
Maximum Shear Strain	$\gamma_{\max} = 180 \text{ \%}$
Maximum Rotation	$\theta_{\max} = 0.0019 \text{ rad}$

5.2.3 Structural Design of Load Bearing Members

The PB-AHTR facility presented in this study is constructed from reinforced concrete members that are arranged in such way so as to be able to withstand earthquake-imposed loads, while maintaining gravity-load carrying capacity and providing protection to the sensitive primary loop components inside the reactor citadel structure. All of the structural components are designed to carry their own weight, a design live load of 4788 Pa (100 psf), and the weight of fixed equipment. In addition, several components are specially designed to provide resistance to lateral loads resulting from earthquake-imposed forces.

Several challenges had to be overcome while carrying out the structural design of these load-bearing members. First, the size of the mechanical components of the power conversion system, particularly the turbines, mandated that large access doors be provided in the east end of the turbine hall for maintenance, hence limiting the arrangement of the main load carrying members. Second, large cranes with a large range of motion are needed for moving the mechanical parts within the turbine hall and reactor room, which limits the placement of vertical/lateral load bearing systems to locations along the turbine and reactor room perimeters. Because of this, the roof in these areas has a large unsupported length, and the gravity load carrying-members in turn are very deep.

The roof configuration of the turbine hall consists of six large concrete beams running in the N-S direction. On top of the beams, there is a 17.8 cm (7") reinforced concrete slab that spans in E-W direction between the six beams and is designed to carry 4788 Pa (100 psf) live load in addition to its own weight 2403 kg/m³ (150 pcf). The load is transferred in the E-W direction to the six 50.8 cm x 152.4 cm (20"x60") beams, which makes this a one-way slab, implying that the slab is experiencing flexure along the axes perpendicular to the beams. The beams then transfer this load to the two 1.5-meter (5-foot) thick concrete shear walls located on the north and south faces of the building, which then distribute it to the foundation, along with loads from the turbine hall crane. The reactor room roof system is designed in similar fashion.

The west end of the building houses many smaller equipment hallways and because the floor spans are not as large, smaller gravity systems are utilized. Live load is supported by 17.8 cm (7") slabs that transfer it to 102 cm x 152.4cm (40"x60") end beams that then carry this load to the columns. The beams and the columns are tied into several systems of frames fixed onto the base mat.

Lateral load resistance is provided by the system of RC shear walls and special moment resisting (SMR) frames. Figure 5-7 shows a simplified building plan outlining major load carrying components. Several cross-sections providing load resistance in the E-W direction are depicted on Figure 5-8. Section A-A consists of a combination of a SMR frame and a large shear wall. Section B-B shows SMR frame, while section C-C is detailed so that the left frame provides some stiffness, while the rest of the components are ductile in E-W direction. In the north-south direction, lateral loads are resisted by two 1.5-meter (5-foot) thick RC walls – one located at the west face of the structure and the other one placed between the reactor and turbine rooms. In addition, two SMR frames are placed – one along the east face of the building and another on the left side of the reactor room, as shown in Figures 5-7, 5-8 and 5-9.

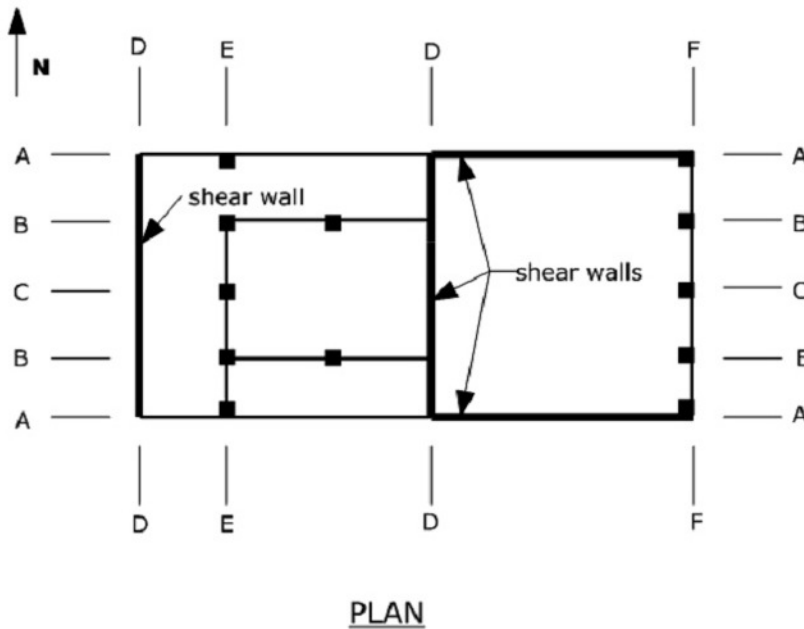


Fig. 5-7 Simplified building plan showing major structural components

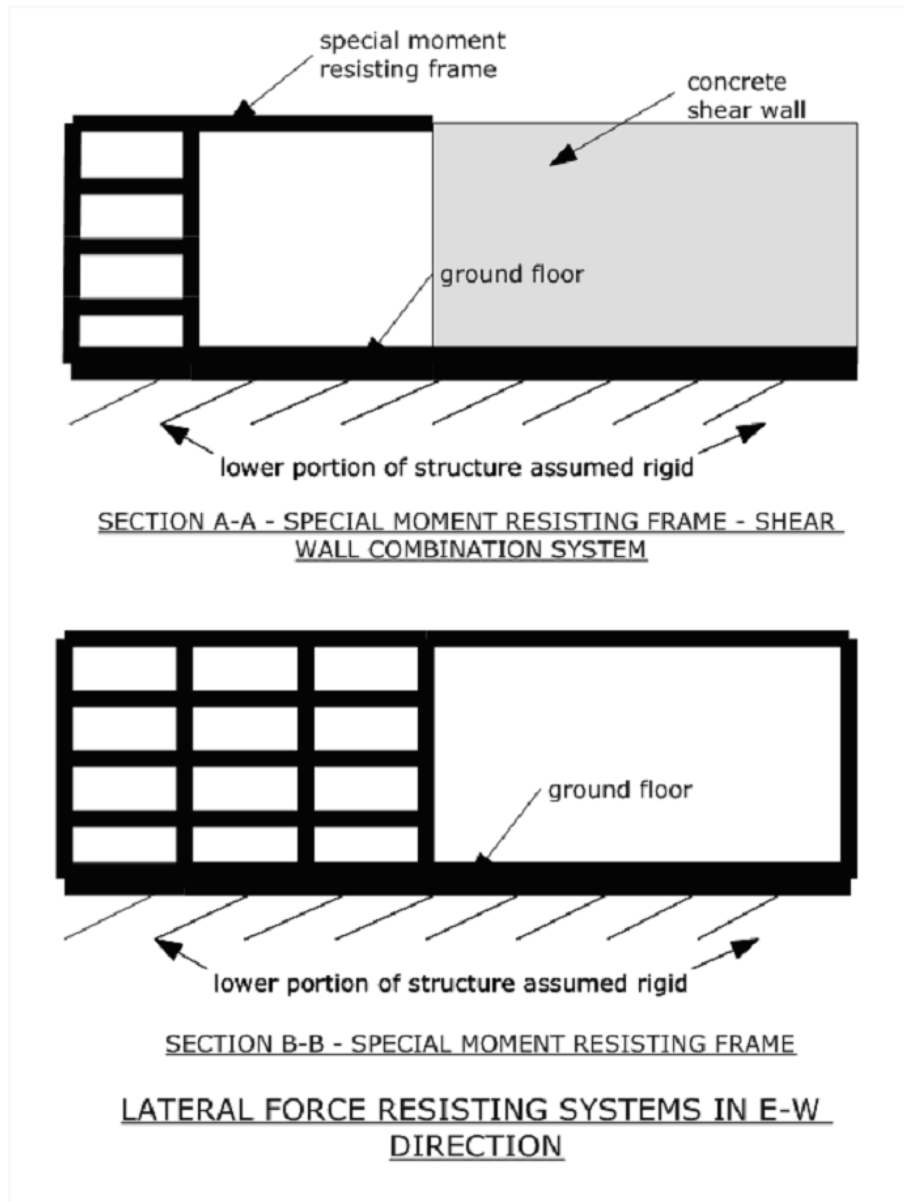


Fig. 5-8 Sketch of typical LFRS systems in East-West direction.

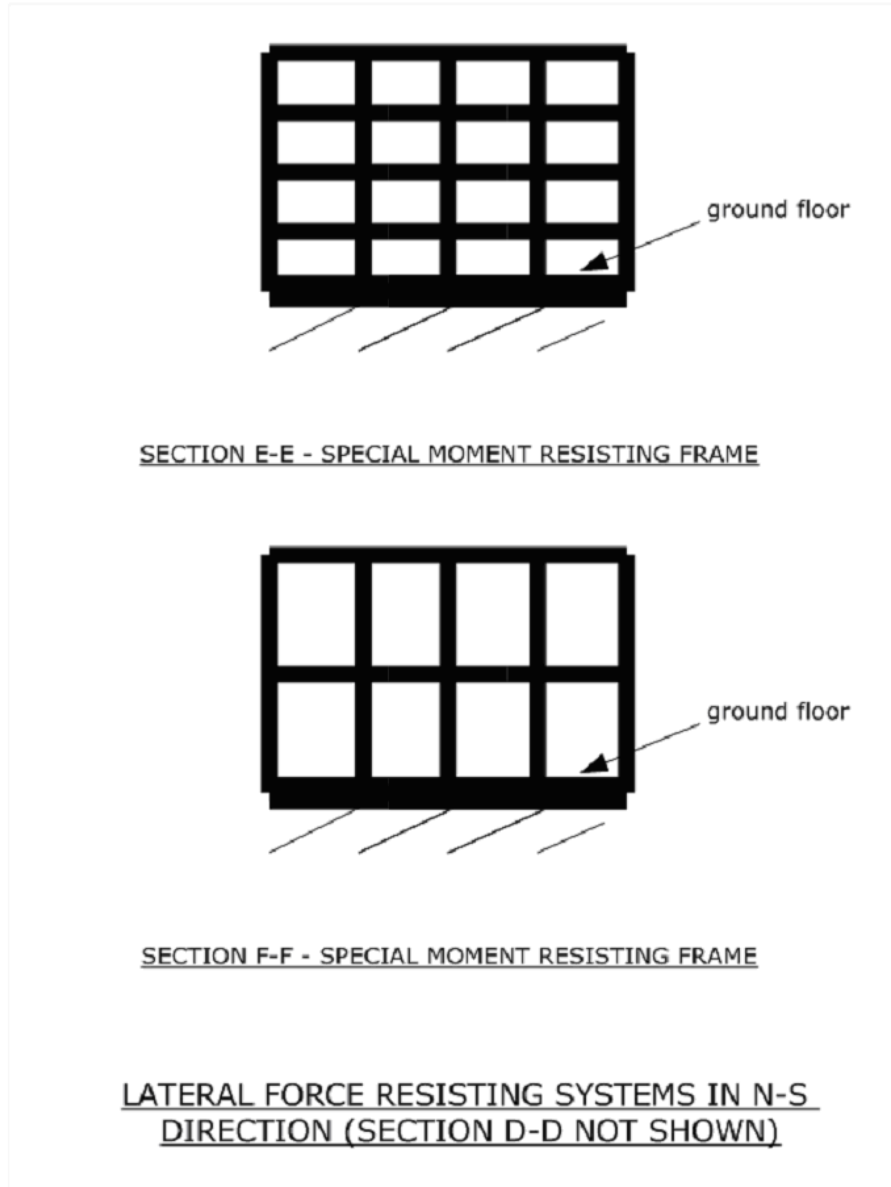


Fig. 5-9 Sketch of typical LFRS systems in North-South direction.

5.3 Pebble Seismic Test (PST) Experiment

5.3.1 Theory and Design

As with any scaled fluid mechanics or heat transfer experiment, the primary goal of the Pebble Seismic Test (PST) experiment is to reproduce dominant phenomena with low distortion. The PST experiment uses reduced height, characteristic length, and dynamic scales to simulate pebble response to seismic acceleration within the seven bottom pebble plenums in the core of the PB-AHTR reactor. In order to determine the correct

proportion to which these scales must be reduced, a dimensional analysis of the pebble bed dynamics and fluid mechanics was done.

A nondimensionalization of the Navier-Stokes equation of motion yields the Reynold's Number (Re), which represents the ratio of the inertial forces to viscous forces within a flow field. Maintaining this ratio allows for the scaled experiment to reproduce transitions from laminar to turbulent flows and wall shear stresses. Equation 5.1 defines the Reynold's Number in which U is the velocity of the flow field, L is a characteristic length and ν is the kinematic viscosity of the fluid. The subscript m refers to the scaled model while p designates the prototypical model.

$$Re_m = Re_p \Leftrightarrow \frac{U_m L_m}{\nu_p L_p} = \frac{\nu_m}{\nu_p} = \frac{\mu_m \rho_p}{\mu_p \rho_m} \quad (5.1)$$

A nondimensionalization of the momentum equation yields the Froude Number (Fr), the ratio of inertial to gravitational forces. Conserving this ratio ensures that gravity forces are properly scaled at interfaces between the liquid, solid, and gas phases.

$$Fr_m = Fr_p \Rightarrow \frac{U_m}{U_p} = \left(\frac{L_m}{L_p} \right)^{1/2} \quad (5.2)$$

The final constraint on the scaled PST experiment requires that the ratio of densities between the fluid and pebbles be maintained in the scaled experiment. This assures that the proper magnitude of buoyant forces is present in the scaled experiment.

Because the PST experiment only serves to reproduce the fluid mechanics of pebble-salt interactions, water was chosen as a suitable room-temperature substitute for the liquid salt. Using the scaling conditions presented above, a reduction in length scale of 40% was used to match the nondimensional parameters. In addition, the density ratio of the flibe to the fuel pebbles can be achieved using commercially available high density polyethylene spheres, which have a density that is 86% of the density of room- As with any scaled experiment, discrepancies do exist between the modeled version and the prototype. Because the coefficient of friction of the graphite pebbles in high temperature salts has yet to be measured, the PST experiment cannot be expected to accurately reproduce the effects of pebble-to-pebble friction in the motion of the pebble bed.

5.3.2 Description of experimental system:

This section describes the PST experiment design.

5.3.2.1 Description of the shake table

Figure 5-10 shows the shake table that was used for the Pebble Seismic Test (PST) experiment. The shake table is located in Davis Hall at U.C Berkeley and measures 38 inches by 48 inches. It can simulate earthquakes with various intensities and accelerations using a computer program to control a hydraulic actuator. The hydraulic piston controls the acceleration of the shake table. The accelerometer shown in this figure was used in this experiment to measure the horizontal acceleration of the PST.



Fig. 5-10 The shake table located in Davis Hall

Figure 5-11 shows the shake table at Richmond Field Station (RFS) that was used for the Pebble Seismic Test (PST) to achieve the design level acceleration of 0.5g.



Fig. 5-11 View of the shake table at the Richmond Field Station (study investigating the seismic response of laboratory equipment). Courtesy of RFS.

5.3.2.2 Description of the acrylic tank

Figure 5-12 shows the design of the hexagonal acrylic tank used in the PST experiment. The PST tank measures .784 m tall and .525 m across from flat to flat. Figure 5-13 shows a picture of this tank mounted on a metal pedestal.

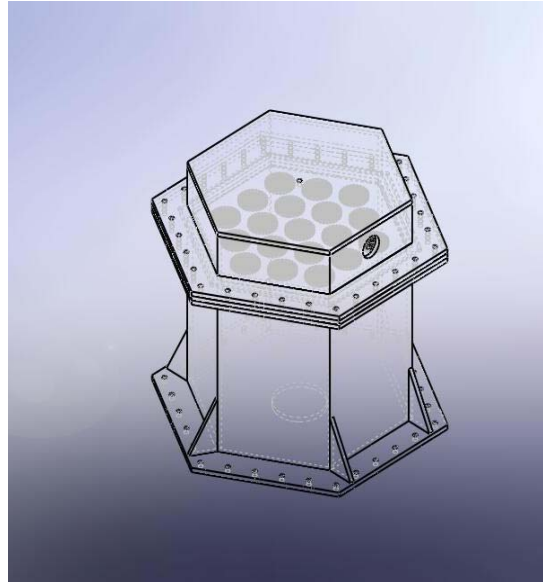


Fig. 5-12 Hexagonal acrylic tank design.



Fig. 5-13 Hexagonal tank mounted on a metal welded pedestal.

5.3.2.3 Description of the filter plate

Figure 5-14 shows the filter plate used in the PST experiment. The plate is designed to simulate the entrance into the pebble channels of a Pebble Channel Assembly and to allow water to circulate uniformly during the experiment. Each of the nineteen holes has a diameter of 7.92 cm, and the hexagonal mesh prevents the pebbles from passing

through the plate into the discharge plenum during pumped operation. The filter plate is secured between the top hexagonal cover and the bottom hexagonal tank.



Fig. 5-14 The PST Filter plate

5.3.2.4 Description of the pump

Figure 5-15 shows the AmeriMerc LLC pump used to circulate water through the PST experiment. Figure 5-16 shows the pump curve for the .75 Hp motor selected for the PST experiment.



Fig. 5-15 FMHP pump [5.3]

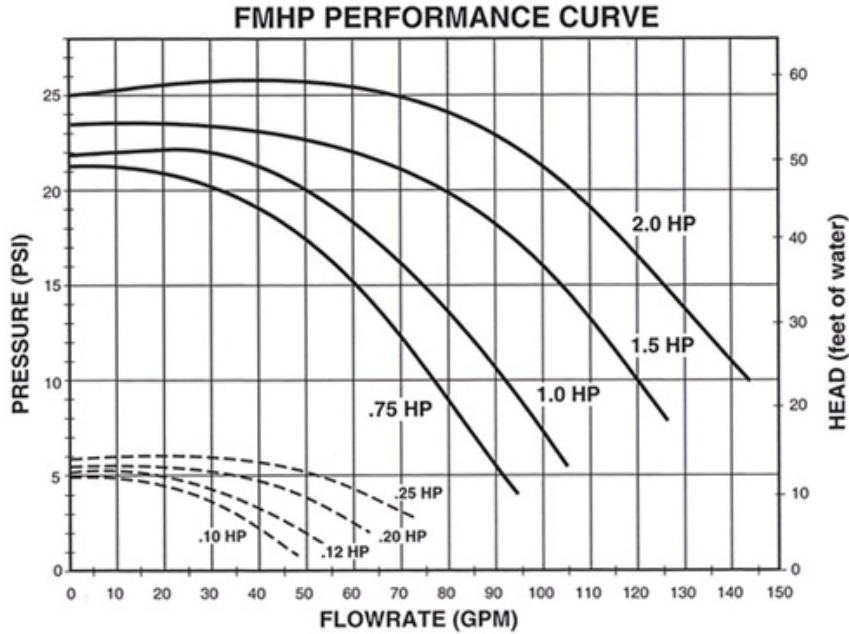


Fig. 5-16 Pump curve for the .75 HP motor. [5.3]

5.3.2.5 Description of the water containment wall

The purpose of the containment wall is to prevent water from reaching the electronic equipment in the event of a leak. The containment wall is made out of wood and lined with a tarp to ensure a waterproof barrier. Figure 5-17 shows a picture of the water containment wall used. This containment wall was not needed for the test done at RFS because the shake table was designed so that nothing is damage in case of a water spill.



Fig. 5-17 Water containment wall with dimension of 3 ft by 4ft by 2 ft.

5.3.2.5 Experimental set up

The acrylic hexagonal tank was bolted to a welded steel pedestal on the shake table and surrounded with the water containment, as shown in Figure 5-18. Approximately 24,500 high density polyethylene plastic balls (pebbles) were loaded inside the hexagonal tank which was then filled with water. The pebbles are 0.5 inches in diameter and less dense than water. A spa pump connected at the bottom of the pedestal was used to circulate water through the hexagonal tank with pebbles inside. Finally, the shake table was accelerated by the hydraulic actuator to simulate an earthquake. A high speed camera was used to track the pebbles and their behavior during the seismic load. Figure 5-19 shows the experimental setup at Richmond Field Station. The pedestal is attached to the shake table using two metal sheets cut from the machine shop.



Fig. 5-18 Pebble Seismic Test Experimental System in Davis Hall.

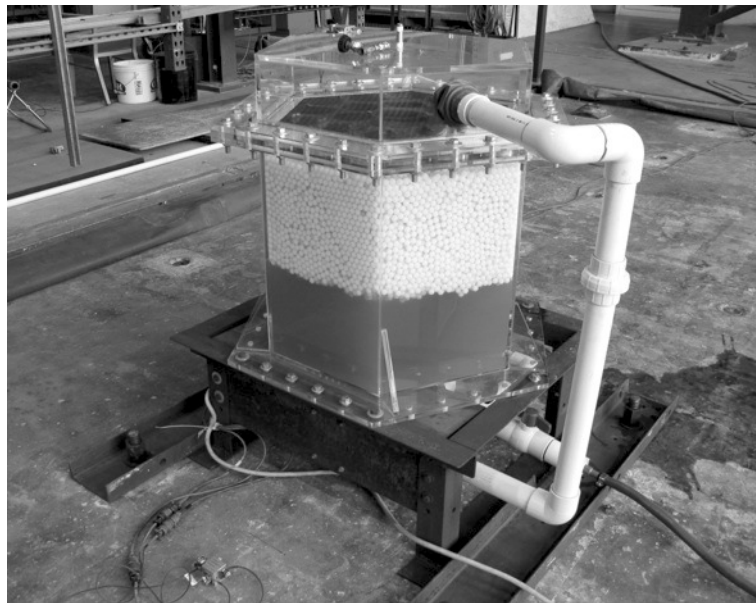


Figure 5-19 Experimental setup of the PST at Richmond Field Station

5.3.3 Results

A static angle of repose experiment was performed using a container filled with water and high density polyethylene plastic balls. The container was tilted at a continuous angle until the bed of pebbles first began to move (Figure 5-18). The angle of repose was measured to be around 25° for the experimental pebbles. Using the angle of repose, the threshold acceleration, the acceleration at which when the pebbles first start moving, was calculated to be about 4.5 m/s² or nearly half the force of gravity. The threshold acceleration provides valuable insight into the intensity and acceleration at which the pebble bed geometry changes could be expected to occur in the PB-AHTR reactor core under seismic loading.



Fig. 5-20 The Static Angle of Repose experiment.

A high speed camera was used to monitor the displacement of the pebbles during the Pebble Seismic Test experiment. Additionally, two accelerometers were attached to the PB-AHTR reactor core to measure the acceleration experienced by the core at bottom and the top of the reactor. The PST experiment was then performed and the acceleration and displacements were recorded as shown in Table 1.

Table 5.2 PST experiment results for pebble displacement without pump circulation in Davis Hall

	w/ base isolation		w/o base isolation			
Peak Amplitude	1 in	2 in	0.2 in	0.5 in	1 in	1.25 in
Peak Acceleration	0.75 g	1.0 g	0.25 g	0.50 g	0.75 g	1.0 g
Displacement	no	no	no	no	yes*	yes*

*Shake table rocked vertically on roller bearings at higher acceleration

5.3.3.1 Discussion and results of the work done at Richmond Field Station

Before the hexagonal tank and the pedestal was placed on pedestal, the 0.75 hp FMHP pump was tested for water circulation. With the pump on, it was observed that the pebbles at the bottom of the bed were bouncing up and down due to the jet entering the bottom of the vessel.

The PST experiment was run with the pump on and with the pump off for four different signals (peak accelerations of 0.25g, 0.50g, 0.75g, 1.0g). After examining the footage from the high speed camera, the signals run at peak accelerations of 0.75g and 1.0g with the pump off do showed some fluidization where minor pebble motion occurred near the bottom of the bed. As seen in Fig. 5-21 for the 1.0g case, the motion in the bed was quite small. No pebble motions were observed for signals run at 0.25g and 0.5g, which is consistent with the results of the static angle of repose measurement.

With the pump on, there was no fluidization in the bed but the pebbles at the bottom of the bed did move up and down due to the hydrodynamic force caused by coolant jet entering the vessel. The fact that no fluidization occurred even at a peak acceleration of 1.0g is consistent with expectations, because with forced circulation the hydrodynamic forces acting on the pebbles are much larger than the buoyancy forces, and the pebbles remain effectively pinned in place.

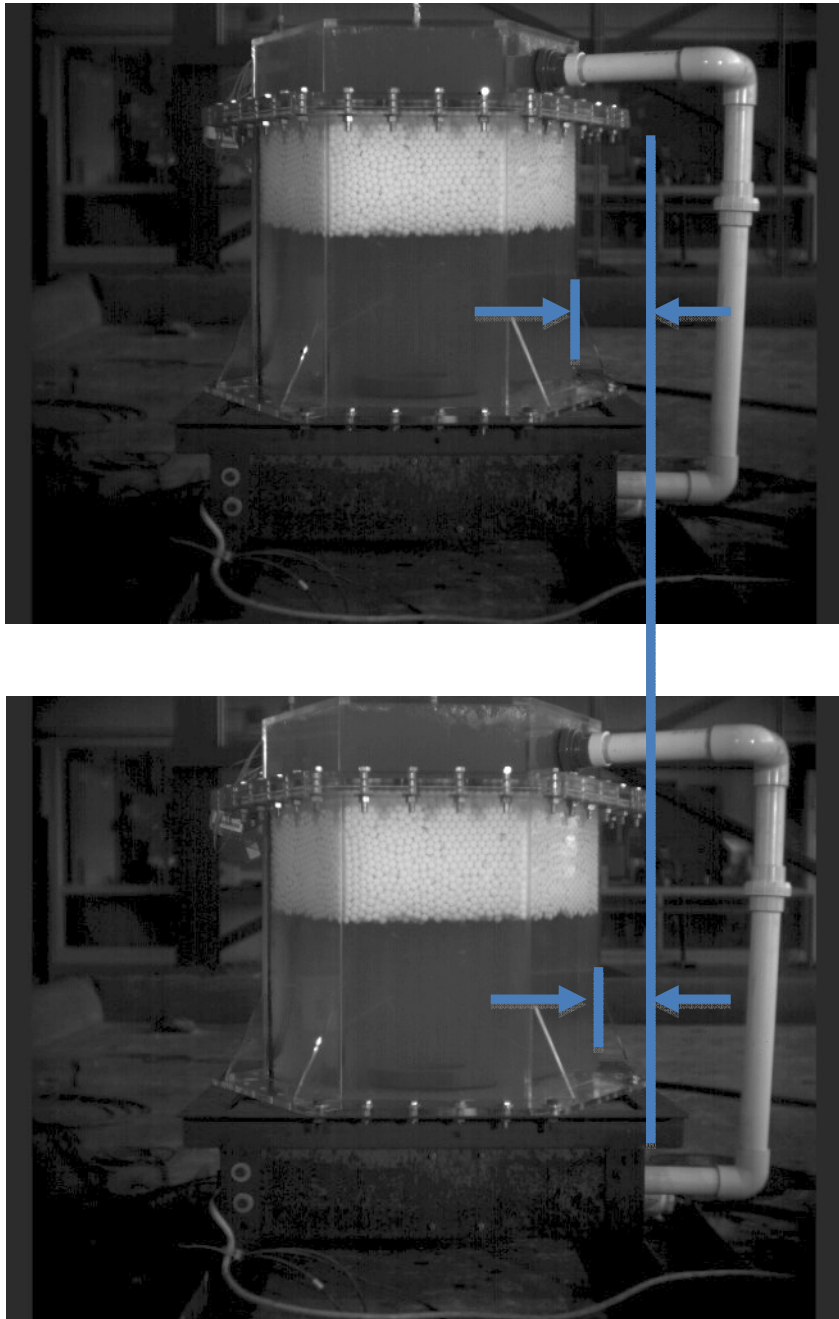


Fig. 5-21 Two frames showing design level peak acceleration 1.0g with pump turned off, resulting in minor pebble motion.

5.5 References

- 5.1 Bardet, Philippe M. and Per F. Peterson. "Options for Scaled Experiments for High Temperature Liquid Salt and Helium Fluid Mechanics and Convective Heat Transfer." Nuclear Technology To Appear.
- 5.2 Bardet, P., J.Y. An, J.T. Franklin, D. Huang, K. Lee, A. Mai, M. Toulouse and P.F. Peterson. "The Pebble Recirculation Experiment (PREX) for the AHTR." Global September 9-13 (2007): 845-851.
- 5.3 "Flo-Master FMCP Aqua Flo Hot Tub Spa Pumps." Flo-Master FMCP. 2008. AmeriMerc. 12 May 2008. < <http://www.amerimerc.com/spa-pump~flo+master-fmcp.htm>>